MEASUREMENTS OF AMMONIA AND NITROUS OXIDE EMISSIONS FROM POTATO FIELDS IN CENTRAL WASHINGTON USING DIFFERENTIAL OPTICAL ABSORPTION SPECTROSCOPY (DOAS), TRACER DISPERSION, AND STATIC CHAMBER METHODS

By

MARY JOY JOSEPHINE M. CAPIRAL

A thesis submitted in partial fulfillment of
the requirements for the degree of

MASTER OF SCIENCE IN ENVIRONMENTAL ENGINEERING

WASHINGTON STATE UNIVERSITY
Department of Civil and Environmental Engineering

MAY 2009

To the Faculty of Washington State University:

The members of the Committee appointed to examine the dissertation/thesis of MARY JOY JOSEPHINE M. CAPIRAL find it satisfactory and recommend that it be accepted.

_____
George Mount, Chair

_____
Brian Lamb

_____
Shelley Pressley

ACKNOWLEDGMENT

I would like to acknowledge and thank all of the people that have helped me in graduate school. First and foremost, I would like to thank my parents for their support, encouragement, and the many sacrifices they have made for me. I would also like to thank my friends and family for their help.

I would like to thank the members in my committee: Dr. George Mount, who is also my advisor, Dr. Brian Lamb, and Dr. Shelley Pressley. They have taught me so much and inspire me to embrace challenges. I cannot forget Dr. Brian Rumburg for teaching me about the DOAS instrument and for being a second brother to me. Thank you so much. I would like to thank the McNair Achievement Program, especially to Dr. Steven Burkett and Dr. Raymond Herrera, for their support and for preparing me for graduate school.

I am grateful to everyone who helped me prepare for and conduct data collection. I would like to thank Robert Gibson for his creativity, hard work, and dedication to the project. Thank you for your friendship and for making fieldwork fun and eventful. Thank you to Gary Held and Kurt Hutchinson of the WSU Engineering Shop for their innovative and quality work. Their talent is inspiring. I would also like to thank Elena Spinei, Gene Allwine, Brandon Little, Mandi Hohner, and Erika Ottenbreit as well as my officemates: Obie Cambaliza, Rasa Grivicke, and Charleston Ramos.

This project was supported by National Research Initiative Competitive Grant from the USDA Cooperative State Research, Education, and Extension Service Air Quality Program. This project would not have been possible without the kindness of Johnson Agriprises, especially Orman Johnson, and AgriNorthwest for allowing us to make measurements in their fields.

MEASUREMENTS OF ATMOSPHERIC AMMONIA AND NITROUS OXIDE EMISSIONS FROM POTATO FIELDS IN CENTRAL WASHINGTON USING DIFFERENTIAL OPTICAL ABSORPTION SPECTROSCOPY (DOAS), TRACER DISPERSION, AND STATIC CHAMBER METHODS

Abstract

by Mary Joy Josephine M. Capiral, M.S.
Washington State University
May 2009

Chair: George Mount

There are limited studies that have measured the magnitude of Nitrogen (N) emissions from intensively managed croplands. In this research, concentrations of ammonia (NH_3) and nitrous oxide (N_2O) from center-pivot irrigated potato fields in central Washington were measured during the 2007 and 2008 growing seasons (June – August). A short-path differential optical absorption spectroscopy (DOAS) instrument that operates in the 200-240 nm wavelength spectral range was used to measure NH_3 concentrations. During some periods, sulfur hexafluoride (SF_6) tracer gas was released from the center of the fields and concentrations were measured along a crosswind sample line downwind of the fields to help characterize local dispersion conditions. A Gaussian plume dispersion model (SIMFLUX) was used, along with the SF_6 tracer data in an inverse approach to estimate NH_3 emission rates. A static chamber flux method was used to measure N_2O emissions with sample analysis via electron capture gas chromatography (ECD-GC). Nitrous oxide flux rates generally peaked between 2.5 and 3.5 hours after irrigation or fertigation. The amount of N lost as N_2O ranged from zero to 12% of the applied N fertilizer which is comparable to documented rates of 0.1 to 8% (Dobbie and Smith,

2003). Measured NH_3 concentrations varied with application status, sprinkler arm location, and wind speed. The highest NH_3 concentrations measured in the summers of 2007 and 2008 were ~34 ppbv and ~112 ppbv, respectively. Both peaks occurred during fertigation, when the sprinkler arm was spraying almost directly towards the DOAS measurement path and winds greater than 1 m s^{-1} were blowing towards the measurement path. Estimated NH_3 flux rates ranged from 9 μg N m^{-2} s^{-1} to 460 μg N m^{-2} s^{-1} for fertigation periods and from 0.6 μg N m^{-2} s^{-1} to 2 μg N m^{-2} s^{-1} for periods of no fertigation or irrigation, which indicates that a significant fraction of NH_3 loss occurs as a result of direct volatilization of NH_3 during fertigation. Overall, the average NH_3 flux during fertigation periods was 10% of N applied as fertilizer.

TABLE OF CONTENTS

LIST OF FIGURES

LIST OF TABLES

LIST OF FIGURES

LIST OF TABLES

Dedication

This thesis is dedicated to my mother and father for their unconditional love and support.

CHAPTER 1

INTRODUCTION

1.1 Motivation and Research Objectives

The increasing use of synthetic Nitrogen (N) fertilizers has led to an altered nitrogen cycle and a doubled amount of fixed N entering the biosphere (Vitousek *et al*., 2000). There are uncertainties in the magnitude of N emissions from various sources, including intensively managed croplands. Up to 50% of the applied N to croplands can be lost, with gaseous emissions being the dominant N loss mechanism (IFA, 2001).

Excess emissions of NH_3 and N_2O can have negative effects on human health and the environment. Ammonia reacts rapidly with both sulfuric and nitric acids in the atmosphere to form fine particles, which cause health problems, reduce visibility, cause acid deposition, and perturb the earth's radiation balance (Pandis, 1995). Nitrous oxide is a potent greenhouse gas which ranks just below carbon dioxide (CO_2) and methane (CH_4) in global warming concerns (EPA, 2006). Due to the impacts on the environment and human health, it is important to quantify and understand the factors that control NH_3 and N_2O emissions.

In this research, concentrations of NH_3 and N_2O from potato fields in central Washington (WA) were measured during the 2007 and 2008 growing seasons (June – August). A short-path differential optical absorption spectroscopy (DOAS) instrument that operates in the 200-240 nm wavelength spectral range was used to measure NH_3 concentrations. During some periods, sulfur hexafluoride (SF_6) tracer gas was released from the center of the fields and concentrations were measured along a crosswind sample line downwind of the fields to help characterize local dispersion conditions. A Gaussian plume dispersion model (SIMFLUX) was used, along with the SF_6 tracer data in an inverse approach to estimate NH_3 emission rates. Nitrous oxide fluxes

were measured using a static chamber method and samples were analyzed using a gas chromatograph equipped with an electron capture detector. The overall goals for this work are to improve our understanding of the loss of N gases from croplands and to account for the impact of these emissions upon regional air quality and global climate change.

This thesis is presented in six chapters. In the remainder of Chapter 1, the research location is described. In Chapter 2, literature describing the sources, controlling factors, and measured rate of N_2O and NH_3 emissions are reviewed. In Chapter 3, the measurement techniques used for measuring N_2O and NH_3 concentrations and the methods for estimating the flux rates are presented. Chapter 4 is a manuscript which summarizes the results in terms of NH_3 and N_2O concentration and emission patterns. Chapter 5 provides an analysis of errors. Finally, Chapter 6 provides conclusions from this research and possible future work.

1.2 Research Location Description

In central WA, approximately 62,000 hectares of cropland are used to grow more than 4.33 million tons of potatoes (data from 2005) (Liu *et al.,* 2007). Information on NH_3 and N_2O emissions from the potato fields in the area are scarce making this a viable area of study. Potato crops are managed with high inputs of water and N fertilizers. The soil properties, climate, and management practices in the area promote N_2O and NH_3 losses from croplands. In section 1.2.1, the location of the measurement site will be discussed. The soil properties and climate as well as the management practices for the research location will be presented in sections 1.2.2 and 1.2.3, respectively.

1.2.1 Location Background Information

The potato fields used for this project are located approximately 16 miles east of Othello, WA, US. Summer 2007 measurements were conducted at potato field 19-7, shown in Figure 1.1 (N 46° 46.166', W 118° 58.099'). Summer 2008 measurements were conducted at potato field 25-1, shown in Figure 1.2 (N 46° 45.659', W 118° 52.357'). These fields were preferred over others because they were relatively flat and they were far from other potentially interfering sources of NH_3 and N_2O. Fields of grass seed, alfalfa, and wheat, which are not typically managed with high inputs of N fertilizers, surrounded the two potato fields. Fields 19-7 and 25-1 were planted with ranger russet potatoes and with premier russet potatoes, respectively. The crop rotation for both fields is grass seed - wheat - potatoes.

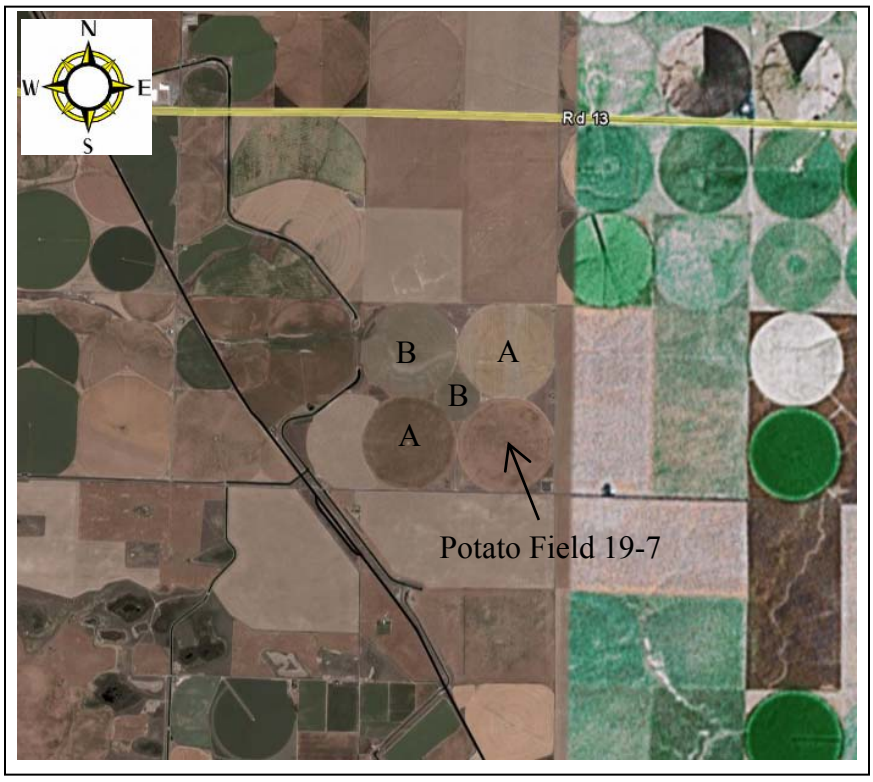

Figure 1.1: Aerial view of the potato field in central WA used for measurements in summer 2007 (Figure adapted from GoogleEarth). Surrounding the field were grass seed (A) and alfalfa (B) fields which are not typically managed with high amounts of N fertilizers.

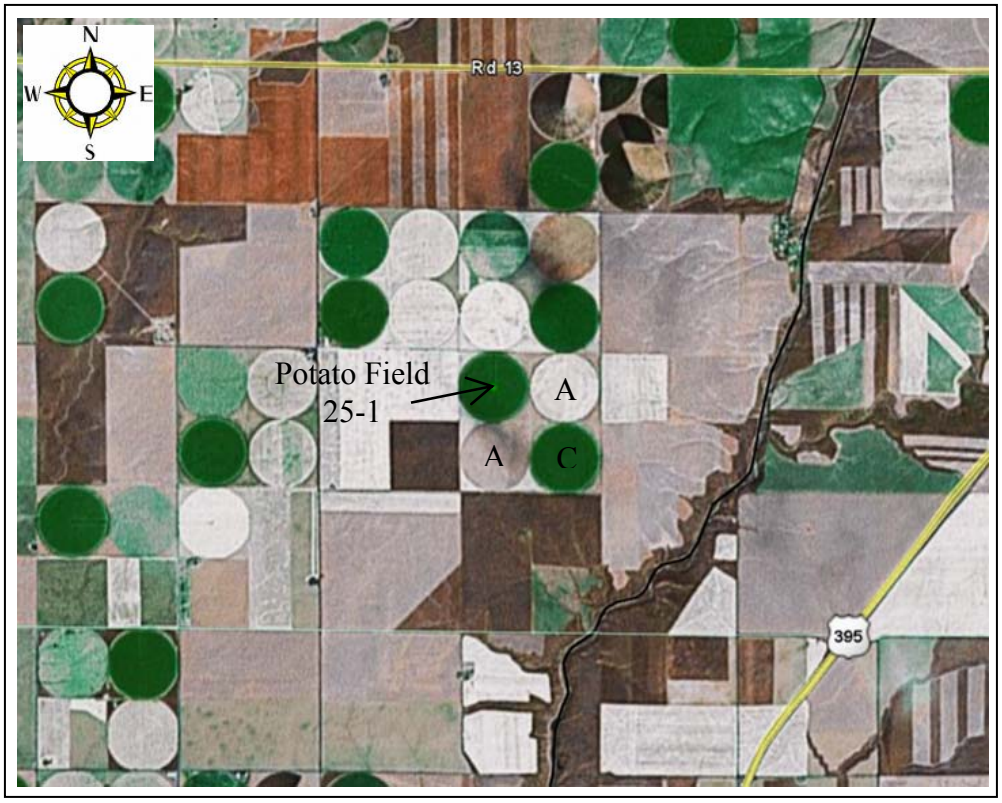

Figure 1.2: Aerial view of the potato field used for measurements in summer 2008 (Figure adapted from GoogleEarth). Surrounding the field were grass seed (A) and wheat (C) fields, which are not typically managed with high amounts of N fertilizers.

1.2.2 Soil Properties and Climate

Quincy fine sand soils are dominant in the region, where anaerobic conditions are easily maintained for long periods of time. The surface soil has a bulk density of 1.24 Mg per m^3. The soil porosity and pH are 0.53 and 6.6, respectively.

The growing period is characterized by lack of cloud cover, high daytime temperatures, and cool nights. The average annual rainfall is 150 mm so the crops are highly dependent on irrigation. As a result, crops are generally irrigated five out of seven days per week and often above the rate necessary for crop growth.

1.2.3 Management Practices

In winter, field preparation included deep ripping and disk plowing of the soil and ground rig fumigation. Deep ripping and disk plowing were conducted to break up traffic-induced or naturally occurring compaction layers and to increase soil moisture. In addition, potassium (K) and phosphorous (P) were applied.

In the spring, a chisel chopper was used to loosen and plant (seed) the soil. A rod weeder was used to kill weeds before plant emergence. Between two to six weeks after planting, the potato plants emerged from the ground and irrigation (application of water only) began. The plants began to grow tubers a few weeks after emergence. A dense, green canopy from approximately June to August was maintained. Heavy N fertilizer application began in early July. The potatoes were harvested during the first weeks of October, depending on the type of potato planted.

Water and N fertilizer were applied to the potato fields using a center-pivot irrigation system. In the center-pivot irrigation system, sprinklers were positioned over the crop canopy and along the length of connected pipe segments. The pipe segments were supported by trusses and mounted on wheeled towers. The sprinkler system rotated in a circular pattern and was fed with water or water with N fertilizer from the pivot point at the center of the field.

The timing and rate of irrigation and fertigation (application of water with N fertilizer) varied from day to day and from each field, under the discretion of the farmer. The type of fertilizer used for both fields was UAN solution 32, which contained 25% nitrate-N, 25% ammonium-N, and 50% urea-N. There were two rates for sprinkler rotation; 12 degrees clockwise (cw) per hour and 18 degrees cw per hour. For days of NH_3 measurement, 2.7 kg of N

was applied per acre per full 360° rotation. When pesticides were being applied, the sprinkler arm rotated 30 degrees cw per hour.

CHAPTER 2

LITERATURE REVIEW

2.1 The Nitrogen Cycle

The N cycle describes the movement of different forms of N species between the atmosphere, biosphere, and geosphere. Nitrogen is essential for all life forms on Earth since it is an important component of DNA, RNA, and proteins, the building blocks of life. About 20% of the global N is in sedimentary rocks, and is not readily available to organisms. The Earth's atmosphere is the major reservoir of N and is composed of 78% diatomic nitrogen (N_2) (Galloway *et al*., 2004). Most organisms cannot use N in the form of N_2 due to the strong triple bond that binds the two N atoms together.

The form usable by most organisms is reactive N (Nr), which includes all biologically active, photochemically reactive, and radiatively active N compounds. Reactive N compounds include inorganic reduced forms of N, such as NH_3 and ammonium (NH_4^+). Inorganic oxidized forms of N, such as nitrogen oxides ($NO + NO_2 = NO_x$), nitric acid (HNO_3), nitrous oxide (N_2O), nitrate (NO_3^-) and organic compounds, such as urea, amines, proteins, and nucleic acids, are also included.

Diatomic N (N_2) can be naturally converted to Nr in two ways: biological fixation and high-energy natural events. In biological fixation, symbiotic bacteria and free-living bacteria convert N_2 into Nr. Only about 10% of the Nr produced through this process is emitted into the atmosphere (Galloway *et al*., 1998). High-energy natural events, such as lightning strikes and forest fires, can break the strong triple bond that binds the atoms of N_2. The resulting individual N atoms combine with molecular oxygen to form NO. Production of Nr through high-energy

natural events occurs only at the global rate of 3 to 10 Tg N $year^{-1}$ (Prather *et al*., 2001 as cited in Galloway *et al*., 2001).

Human activities, mainly the production and use of synthetic N fertilizers and burning of fossil fuels, during the past century have altered the N cycle. The amount of fixed N that enters the biosphere has doubled (Vitousek *et al*., 2000). In 1913, the Haber-Bosch process, which describes the formation of NH_3 by combining N_2 and hydrogen in high temperature and pressure, was discovered. The NH_3 formed is used to make fertilizer, which has led to increased agricultural productivity. It is predicted that by 2020, the current global production of synthetic N fertilizer of 80 Tg $year^{-1}$ (1 Tg = 10^{12} g) will increase to 134 Tg $year^{-1}$ (Vitousek *et al*., 2000).

The second main cause of human-fixed N is the burning of fossil fuels in automobiles, power generation plants, and industries. During the combustion of fossil fuels, N is emitted to the atmosphere as a waste product (NO) from either the oxidation of atmospheric N_2 or organic N in the fuel. One study predicts that production of NO_x from fossil fuels will more than double in the next 25 years, from about 20 Tg $year^{-1}$ to 46 Tg $year^{-1}$ (Vitousek *et al*., 2000).

2.2 Human Health and Environmental Impacts

The human alteration of the N cycle has consequences. Excess emissions of NH_3 and N_2O negatively impact the environment and human health. Ammonia reacts rapidly with both sulfuric and nitric acids in the atmosphere to form fine particles or aerosols (Pandis, 1995). Human exposure to aerosols negatively impact human health. Long-term exposures (months to years) cause deterioration of lung function and development of chronic bronchitis (EPA, 2003). Short-term exposures (hours to days) aggravate lung diseases and increases susceptibility to respiratory infections (EPA, 2003). Aerosols also reduce visibility in regional and urban areas

and perturb the earth's radiation balance (Pandis, 1995). In addition, deposition of NH_3 can lead to eutrophication and acidification of ecosystems (EPA, 2007).

Nitrous oxide is a potent greenhouse gas. The global warming potential (GWP) is a measure of how much a given mass of greenhouse gas contributes to global warming relative to the same mass of carbon dioxide (IPCC, 2007). The Intergovernmental Panel on Climate Change (IPCC) reports that the GWP of N_2O over a 100 year period is 310 (IPCC, 2007). Despite its low atmospheric concentration, N_2O ranks just below carbon dioxide and methane in importance. Due to their impacts to the environment and human health, it is important to quantify and understand the factors that control NH_3 and N_2O emissions.

2.3 Sources of Nitrous Oxide (N_2O)

2.3.1 Natural Sources

Natural sources of N_2O are primarily from bacterial breakdown of N in soils and oceans through the microbial nitrification and denitrification. Tropical soils emit approximately 6.3 Tg of N_2O annually (IPCC, 1995). Of this, about 75% comes from wet forest soils and 25% comes from dry savannas. Temperate soils, including forest soils and grasslands, emit approximately 3.1 Tg of N_2O annually (IPCC, 1995). Tropical and temperate soils generally have different levels of nutrients, with tropical soils often being phosphorous limited while temperate soils are generally N limited. As a result, added N emissions tend to result in greater N_2O emissions in tropical soils than in temperate soils. Oceans produce approximately 4.7 Tg of N_2O $year^{-1}$ (EPA, 2006).

2.3.2 Anthropogenic Sources

According to the U.S. Greenhouse Gas Emissions Inventory, the estimated total N_2O emission in the U.S. in 2006 was 367.9 Tg CO_2 Equivalent (Eq.), with an uncertainty range from 352.2 to 449.3 Tg CO_2 Eq. (EPA, 2008). Table 2.1 lists sources of N_2O emissions in the U.S. and their contributions.

Table 2.1: U.S. Nitrous Oxide Emissions by Source (Tg CO_2 Equivalents) (adapted from U.S. Greenhouse Gas Emissions Inventory, 2008)

Source	**Year**				
	1990	**1995**	**2000**	**2003**	**2006**
Agricultural Soil Management	269.4	264.8	262.1	247.3	265.0
Mobile Combustion	43.5	53.4	52.5	42.3	33.1
Nitric Acid Production	17.0	18.9	18.6	15.4	15.6
Stationary Combustion	12.8	13.4	14.6	14.3	14.5
Manure Management	12.1	12.8	13.7	13.6	14.3
Wastewater Treatment	6.3	6.9	7.6	7.7	8.1
Adipic Acid Production	15.3	17.3	6.2	6.3	5.9
N_2O from Product Uses	4.4	4.6	4.9	4.4	4.4
Forest Land Remaining Forest Land	0.5	0.6	2.2	1.2	2.8
Composting	0.4	0.8	1.4	1.6	1.8
Settlements Remaining Settlements	1.0	1.2	1.2	1.5	1.5
Field Burning of Agricultural Residues	0.4	0.4	0.5	0.4	0.5
Municipal Solid Waste Combustion	0.5	0.5	0.4	0.4	0.4
Total	**383.4**	**395.6**	**385.9**	**356.4**	**367.9**

Agricultural soils account for a large portion of N_2O emissions (265.0 Tg CO_2 Eq. in 2006) (EPA, 2008). The application of synthetic N fertilizer and livestock manure to croplands and pasture directly increase the amount of N in the soil, which can be converted into N_2O. Indirect addition of N_2O to soils occurs when applied fertilizer or manure volatilizes to NH_3 and is re-deposited onto the soil as particulate NH_4^+, nitric acid, and NO_x. Also, runoff and leaching of applied N to ground water and surface waters indirectly adds N_2O to soils.

Nitrous oxide emissions from livestock manure and urine also occurs through nitrification and denitrification. The amount of N_2O produced depends on the composition of the manure and urine, the type of bacteria present, and the amount of oxygen and liquid present. Emissions of N_2O from manure management were estimated at 14.3 Tg CO_2 Eq. for the year 2006.

Nitrous oxide emissions also result from the reaction that occurs between N and oxygen during fossil fuel combustion. The type of fuel and pollution control device used as well as the maintenance and operating practices affect the amount of N_2O emitted. Catalytic converters on vehicles can promote the formation of N_2O, although the latest technical modifications to converters are addressing this problem. From 1990 to 2006, N_2O emissions from mobile combustion decreased by 24 percent. The total N_2O emission from mobile combustion was 33.1 Tg CO_2 Eq. in 2006 (approximately 9 percent of total U.S. N_2O emissions).

Nitric acid production accounts for 15.6 Tg Eq. CO_2 for N_2O emissions in 2006 while adipic acid production accounts for 5.9 Tg CO_2 Eq. Nitric acid is used for production of synthetic fertilizers, adipic acid, and explosives.

Wastewater treatment plants are another anthropogenic source of N_2O emissions, where human sewage and other household wastewater end up. Nitrous oxide emissions result from both nitrification and denitrification of the N present in the wastewater, usually in the form of urea, ammonia, and proteins. Wastewater treatment plants account for 8.1 Tg Eq. CO_2 of N_2O emissions.

2.4 Factors that Affect N_2O Emissions

There are many factors regulating the loss of N_2O from croplands to the atmosphere. Section 2.4.1 will discuss the role of nitrification and denitrification in N_2O emissions. In section 2.4.2, the role of crop management will be discussed.

2.4.1 Nitrification and Denitrification Rates

The microbial process of denitrification and nitrification are the major sources of N_2O emission from the soil. Nitrification is the biological oxidation of ammonium (NH_4^+) to nitrite (NO_2^-) or nitrate (NO_3^-) under aerobic conditions and N_2O is a byproduct of nitrification (Seinfeld and Pandis, 1998). In denitrification, which is the bacterial process of converting nitrate (NO_3^-) to dinitrogen (N_2) and N_2O under anaerobic conditions, N_2O is an intermediate (Seinfeld and Pandis, 1998). Nitrification rates are relatively uniform throughout a field while denitrification rates vary temporally and spatially (IFA, 2001). Various factors control whether nitrification or denitrification dominates in the production of N_2O.

Haverkort and MacKerron (2000) and the International Fertilizer Industry Association (IFA) (2001) have summarized the factors that affect nitrification and denitrification in crop production. They concluded that in most soils, nitrification depends on the amount of NH_4^+ and oxygen in the soil as well as the soil pH and temperature. The amount of NH_4^+ in the soil is derived from either mineralization of organic matter or from applied N fertilizer. Nitrification activity is generally suitable for pH levels between 4 to 8, and at high pH values (pH > 8) it may be inhibited due to toxic effects to the bacteria. When the soil temperature is above 4 °C, nitrification activity is favorable and is optimized when the soil temperature is between 20-40 °C. The factors that control nitrification are not the same for denitrification.

Denitrification depends on soil components such as the availability of organic carbon (C), oxygen, and NO_3^-. Organic compounds, such as organic C, serve as electron donors and are sources of bacterial cellular material for denitrification activity. As soil oxygen content decreases, denitrification activity increases since anaerobic conditions are required for both synthesis and activity of the enzymes involved in the denitrification process. Denitrification rates generally increase linearly with NO_3^- concentrations up to 40 mg L^{-1}, while at relatively high NO_3^- concentrations denitrification is independent of NO_3^- concentration.

Similar to nitrification, the soil pH controls bacterial denitrification activity. Under acidic conditions (pH < 7), denitrification rates are slower than in alkaline conditions (IFA, 2001, Haverkort and MacKerron, 2000). In contrast to nitrification, soil temperature does not control denitrification activity because soil denitrifiers are adapted to and are capable of growing under a wide range of temperatures (Haverkort and MacKerron, 2000).

Other controlling factors for denitrification include the presence of decomposing organic matter and the magnitude of NH_3 volatilization. The presence of decomposing soil organic matter and plant litter produces anaerobic areas where high denitrification rates occur. NH_3 volatilized from applied fertilizer can be re-deposited onto the soil, indirectly affecting the availability of N for nitrification or denitrification (Haverkort and MacKerron, 2000).

2.4.2 Management Practices

Various agricultural management activities affect N_2O emissions from soils. Such activities include the application of nitrogen and excessive water and soil tillage. Nitrogen inputs to the soil, such as N fertilizer, animal manure, and crop residues, increase the amount of N available for nitrification and denitrification. Thus, N_2O emissions may increase with the N application rate. The production of N_2O is also related to the timing of fertilizer application.

When NH_4^+-based fertilizers are applied to the soil under conditions suitable for nitrification activity without any competition from plant uptake, N_2O emissions are likely to increase (IFA, 2001). This is also true when NO_3^--based fertilizers are applied to soil under conditions suitable for denitrification activity.

Soil moisture is another factor since the soil moisture content affects the diffusion of oxygen through the soil. The rate of N_2O emission increases as the water-filled pore space (WFPS) in the soil increases. High N_2O emissions have been observed when the WFPS is between 60 and 90%, when the production of N_2O is dominated by denitrification (Dobbie *et al.,* 1999, IFA, 2001, Flessa *et al.,* 2002). High water content may result from heavy rain or excessive rates of irrigation. Below 60% WFPS nitrification, an aerobic process, is the dominant process for the production of N_2O (IFA, 2001).

Also, localized spatial variations in micro-relief (such as ridges and furrows or raised beds) or in water infiltration rates due to compaction, can result in localized wet spots. Usually, greater N_2O emission rates occur from tractor-compacted furrows than from ridges due to a greater reduction of air-filled pore space (Flessa *et al.,* 2002, Smith *et al.,* 1997). Flessa *et al.* (2002) measured mean WFPS values of 61% for tractor compacted inter-rows, 49% for uncompacted inter-rows, and only 30% for ridges for the growing period of potato fields in Germany.

Soil tillage may induce enhanced organic N mineralization (IFA, 2001). Soil tillage is typically conducted during planting and harvesting of root/tuber crops, and is the process of digging up the soil for the purpose of incorporating plant residues and/or fertilizer, seedbed preparation, weed control, and soil and water conservation. Soil tillage affects the gas diffusivity within the soil and the water and air holding capacity of the soil pores.

2.4.3 Other Factors

Soil properties, such as soil texture, affect N_2O emissions. Fine-textured soils hold water more tightly because they have more capillary pores within aggregates than sandy soils. Thus, in fine-textured soils, anaerobic conditions are easily maintained for longer periods of time (IFA, 2001).

Gas diffusion also has an influence on emissions of N_2O since before being emitted to the atmosphere, the N_2O gas must first diffuse through the soil pores. High soil water content, impeded drainage, soil compaction, fine soil texture, and soil surface sealing can all limit gas diffusion through the soil. Haverkort and MacKerron (2002) state that high denitrification activity may be present in soils that are close to saturation, but the emission of N_2O from the soil can be low. Thus, anaerobic conditions promote denitrification but limits gas diffusion.

2.5 Emission Rates of N_2O

The increase in atmospheric N_2O concentration of two to three percent every year is well documented but the sources of the increase are not (Vitousek *et al*., 2000). Nitrous oxide emissions from agriculture are typically reported as an emission factor (EF), which is the amount of N_2O emitted as a percentage of the N fertilizer applied. A default mean EF of 1.25 ± 1% of the N fertilizer applied was adopted by the Intergovernmental Panel on Climate Change (IPPC) in 1997 (Bouwman, 1996). This default EF is based on experiments that were at least 1 year in duration. The default EF is a general approximation and is independent of the specific crop type, region, environment, and management practices. Documented EF values range from 0.1 to 7.8% (Dobbie and Smith, 2003). The use of the default mean EF value is highly uncertain since there are extremely high spatial, temporal, inter-annual, and crop type variability in N_2O emissions.

Dobbie *et al*. (1999) measured N_2O emissions from intensively managed fields of ryegrass, winter wheat, potatoes, broccoli, and oilseed rape in Scotland. The fields of grassland, winter wheat, potato, and oilseed rape were treated with ammonium nitrate fertilizer. An ammonium nitrate/ammonium/phosphate/urea fertilizer mix was applied to the broccoli fields. Nitrous oxide fluxes varied widely throughout the year at all sites and also between sites. Emissions from the winter wheat, barley, and oilseed rape fields (0.2 to 0.7 kg N_2O per 100 kg applied N; EF: 0.2 to 0.7%) were consistently lower than emissions from the fields of grassland, potato, and broccoli (0.3 to 5.8 kg N_2O per 100 kg applied N; EF: 0.3 to 5.8%). Daily fluxes were as high as 1.2 kg N_2O hectare^{-1} day^{-1} and annual emissions ranged from 0.3 to 18.4 kg N_2O hectare^{-1} year^{-1}. At all sites, fluxes generally increased sharply after N-fertilizer additions and gradually decreased with time. All of the reported emission rates were obtained from flux measurements using chambers.

Flessa *et al.* (2002) reported mean N_2O emissions of 1.6 and 2.0 kg hectare^{-1} for the 1997 and 1998 growing periods (end of May to September) of two adjacent potato fields in Germany. The fields were applied with 75 and 37 kg N hectare^{-1} for 1997 and 1998, respectively, resulting in EF values of 2.1% and 5.4%. Flessa *et al.* obtained these emission rates from flux measurements made by automated gas sampling chambers.

Haile-Mariam *et al.* (2008) reported N_2O losses of 0.5% (0.55 kg N hectare^{-1}) of applied fertilizer (112 kg N hectare^{-1}) in corn fields and 0.3% (0.59 kg N hectare^{-1}) of 224 kg N hectare^{-1} applied fertilizer in potato fields in central Washington during the 2005 and 2006 growing seasons. The fields were applied with urea-ammonium-nitrate (UAN) solution (32% N) through a center pivot irrigation system. The fields were under sweet corn–potato rotation. Aerobic soil

conditions dominated, with soil WFPS ranging from 0.50–0.63 m^3 m^{-3}. Gas samples were collected using static chambers.

2.6 Sources of Ammonia (NH_3)

Global sources of NH_3 emissions and their estimated contributions and uncertainty range are listed in Table 2.2. Oceans are the major natural source of NH_3 emissions. Ammonia will volatilize from seawater at a rate that depends on the atmospheric NH_3 concentration, water salinity, and temperature (Bouwman *et al*., 1997). Another natural source of NH_3 is soils under natural vegetation. Ammonia is emitted by organisms within the soil that breakdown organic matter.

Table 2.2: Global Contributions of Atmospheric NH_3 Sources in 1990 (Bouwman *et al*., 1997)

Source	**NH_3-N emission (Tg $year^{-1}$)**	**Uncertainty Range (Tg N $year^{-1}$)**
Oceans	8.2	3-16
Soils under natural vegetation	2.4	0-10
Animal excreta	21.7	10-30
Synthetic fertilizer use	9.0	4.5-13.5
Crops and decomposition of crops	3.6	1.4-5.0
Biomass burning	5.9	3.9-7.7
Human excreta	2.6	1.3-3.9
Fossil fuel combustion, including aircraft	0.1	0.0-0.2
Industrial processes	0.2	0.1-0.3
Total	**53.6**	**40-70**

Agriculture contributes between 55% and 95% of the anthropogenic NH_3 emissions (McGinn and Janzen, 1997). Animal excreta are a major source, and there are two reaction pathways for NH_3 formation. One reaction pathway is the reaction of urea in urine with urease in the manure or soil to form liquid ammonia-N (NH_3 and NH_4^+):

$$CO(NH_2)_2 + 2H_2O \Rightarrow (NH_4)_2CO_3 \Leftrightarrow 2NH_4^+ + CO_3^{2-} \qquad 2.1$$

Ammonia emissions from urine deposited in natural areas are lower than from high density areas where animals are domesticated. The second reaction pathway is the microbiological anaerobic breakdown of organic N. Increasing human population, and therefore increasing food demand, has led to more domesticated animals and increased NH_3 emissions (Vitousek *et al.,* 1997). Ammonia emissions also result from sprinkler application of dairy lagoon slurry from milking cows (Rumburg *et al.*, 2006).

Application of synthetic fertilizer to croplands is another anthropogenic source of NH_3 emissions. Up to 50% of the applied N to croplands can be lost through gaseous emissions, leaching, runoff, or erosion. Generally, the dominant N loss processes are through gaseous emissions, mainly from volatilization of NH_3 and denitrification (IFA, 2001). Ammonia emissions can come from both soil and crop foliage. Ammonia emissions from soil depend on factors such as soil properties (i.e. soil pH, water content, and porosity). From crop foliage, the emissions depend on the plant developmental stage and a compensation point of atmospheric NH_3, below which vegetation acts as a source and above which vegetation acts as a sink (Lemon and van Houtte, 1980 as cited in McGinn and Janzen, 1997). Other factors such as the type and quantity of fertilizer applied and meteorological factors (i.e. wind speed, temperature, and precipitation) affect NH_3 emissions from soil and crop foliage.

Another source of NH_3 is from human breath, sweat, and waste. Emissions of NH_3 from treatment systems of human waste result from anaerobic degradation and are not well studied (Bouwman *et al*., 1997).

Incomplete combustion of fossil fuels also produces NH_3 emissions. Information on NH_3 emissions from fuel combustion is scarce and associated with large uncertainties (Bouwman *et al*., 1997). The use of emission controls in car engines to reduce NO and NO_2 emissions has led

to increased NH_3 emissions. Vehicles with three-way catalytic converters emit more NH_3 than cars with no emission controls (Bouwman *et al*., 1997). The combustion of coal and natural gas and industrial processes (i.e. production of explosives) also contribute to NH_3 emissions.

2.7 Regulating Factors of NH_3 Emission

There are many factors regulating the loss of NH_3 from soil-plant systems to the atmosphere. Section 2.7.1 will discuss factors that affect NH_3 emissions from the soil. In section 2.7.2, the factors that affect NH_3 emissions from the crop foliage will be discussed.

2.7.1 NH_3 Emissions from Soil

Emissions of NH_3 from soils result from biological degradation of organic compounds and are dependent on the following factors: the transformations of the total ammonicial N (TAN) in the soil, which include NH_3-N + NH_4^+-N, the soil properties, climatic factors, management practices, and the partial pressure between the atmosphere and the soil.

The NH_4^+ in the fertilizer applied can be bacterially nitrified to nitrate (NO_3^-), converted to NH_3, or remain as NH_4^+ (Bouwman and Bouman, 2002). Ammonium will be in equilibrium with NH_3 depending upon the pH of the solution, as shown in the following reaction:

$$NH_3 + H_2O \leftrightarrow NH_4^+ + OH^- \qquad 2.2$$

Soil properties such as soil pH, moisture content, infiltration rate, and cation exchange capacity (CEC) affect the rate of NH_3 volatilization from the soil to the atmosphere. Ammonia volatilization increases with increasing pH; the greatest NH_3 volatilization occurs when the soil pH is greater than 7.5 (Liu *et al*., 2007). From 0 to 30 % soil water content, the amount of NH_3 emission increases with increasing moisture due to the inability of the NH_3 molecules to displace water molecules (IFA, 2001). When the soil water content increases from 30 % to 100 %, NH_3

emissions decrease due to dissolution of NH_3 in the soil (IFA, 2001). The CEC is the capacity of a soil for ion exchange of positively charged ions between the soil and the soil solution. The lower the CEC, the more likely it is for NH_3 volatilization to occur (Bouwman and Bouman, 2002; Haverkort and MacKerron, 2000).

Climatic factors, such as wind speed and temperature, also affect NH_3 volatilization from the soil. Increasing wind speed promotes more rapid transport of NH_3 away from the water or soil to the atmosphere (Bouwman and Bouman, 2002; Haverkort and MacKerron, 2000). As soil temperature increases, the relative proportion of NH_3 to NH_4^+ increases while the solubility of NH_3 in water decreases (Bouwman and Bouman, 2002). Ammonia emissions may also increase as conditions of stress caused by crop disease, pests, and/or adverse weather conditions, such as drought, occur (Heckathorn and DeLucia, 1995 as cited in Bouwman *et al*., 1997).

The method and rate of fertilizer application can have a significant effect on the amount of NH_3 loss from fertilizer applications. Generally, applications that effectively bury the fertilizer (i.e. banding) result in lower NH_3 loss (IFA, 2001, Potter *et al.,* 2001). While the effect of fertilizer application type is fairly well understood, studies conducted on the effect of N fertilizer application rate and the amount of NH_3 volatilization show conflicting results (IFA, 2001). Some studies reveal higher NH_3 volatilization rates at high N application rates while other studies show the opposite result.

The type of fertilizer applied influences the emissions of NH_3 since different types of fertilizer contain various percentages of N. When urea fertilizer is applied to very moist soils, the urea is hydrolyzed by the enzyme urease to produce a mixture of NH_3, NH_3^+, and bicarbonate (HCO_3^-) by the following reaction (Sommer *et al.,* 2004):

$$CO(NH_3)_2 + 2H_2O \leftrightarrow NH_3 + NH_4^+ + HCO_3^- \qquad 2.3$$

The rate at which urea is hydrolyzed is related to urease activity, the availability of water, the pH of the solution, and temperature. The rate increases as water content and pH increases. Soil urease activity is optimized when the soil pH is between 8 and 9. The rate of urea hydrolysis also increases as temperature increases.

Ammonia volatilization is also driven by the atmospheric NH_3 concentration, and occurs when atmospheric NH_3 concentration is lower than the NH_3 concentration in the soil, liquid, or intercellular air space of the plant leaves (Bouwman and Bouman, 2002).

2.7.2 NH_3 Emissions from Crop Foliage

Plant leaves are another source of NH_3 emissions. Dissolved NH_3 and NH_4^+ can be found in the water film, also known as the apoplastic solution, in the mesophyll cell walls of plant leaves. The amount of NH_3 and NH_4^+ dissolved depends on the plant developmental stage, climate, fertilization, and the difference between the atmospheric NH_3 concentration and the NH_3 concentration in the leaves (Sommer *et al.*, 2004). Ammonia will be emitted from a leaf if the leaf NH_3 concentration is greater than the atmospheric NH_3 concentration and NH_3 will be absorbed by the leaf in the reverse situation. Another source of NH_3 emission is decomposing potato tops and other plant residues. Generally, NH_3 volatilization increases with moisture, temperature, and N content of plant residues.

2.8 Emission Rates of NH_3

Agriculture is the largest source of global NH_3 emissions. Up to 50% of the applied N to croplands can be lost with gaseous emissions being the dominant N loss mechanism (IFA, 2001). There is a great deal of uncertainty in the magnitude of NH_3 emissions from various croplands. There are many factors that affect the emission rates and only a limited number of studies on the

emissions are available. A standard emission rate of 2.5 kg N hectare^{-1} year^{-1} has been used for all agricultural crops when compiling global emissions inventories, which contains a high degree of inaccuracy (Bouwman *et al*., 1997). Current U.S. emission estimates are based upon European measurements, which are not representative of actual farming practices in the U.S.

The IFA (2001) reports that there is a clear difference between measurements carried out in the fields and those performed inside laboratories. In addition, the measurement method used and the location where the measurements are made significantly affects the emission rates while the crop type is less significant (IFA, 2001). The average NH_3 emission rates from grass are generally 20 and 10% lower than from upland crops (croplands with no standing water throughout the growing season; i.e. corn and potato fields) and flooded systems, respectively (IFA, 2001).

The IFA (2001) report has grouped NH_3 volatilization rates from upland crops by fertilizer type applied. Using micrometeorological techniques, the reported NH_3 loss from broadcast applied UAN fertilizer ranges from 8% to 18%, with an average of 15%. Broadcast application typically involves spreading dry fertilizer over the soil surface. Using dynamic flow chambers, the reported NH_3 loss varies from negligible to 45%. For the potato fields used for this study, UAN fertilizer was applied using a center-pivot irrigation system. From upland crops applied with ammonium bicarbonate, an NH_3 loss rate of 21% was measured in a field study using static chambers. Higher NH_3 loss rates (as high as 30 to 70%) were measured in a laboratory study using dynamic flow chambers. From calcium ammonium nitrate applications, NH_3 loss rates of up to 6% were reported from laboratory studies and much lower rates from field studies. Both the laboratory and field studies used dynamic flow chambers. Ammonia losses from upland crops applied with urea range from 15 to 20%. This range comes from

various measurement techniques including chambers with and without forced flow, micrometeorological techniques, and wind tunnel measurements.

Studies have shown that the magnitude of NH_3 emissions resulting from decomposition of crop residue depends on the N content in the residue (McGinn and Janzen, 1997). In a study on perennial ryegrass herbage, 10% of the NH_3 applied was emitted to the atmosphere from herbage with 29.8 mg N g^{-1} of leaf biomass, and no losses from herbage with 9.2 mg N g^{-1} leaf biomass. In another study, 14% of the N applied was emitted into the atmosphere for a legume green manure (McGinn and Janzen, 1991). In the U.K., it is estimated that volatilized N losses by grassland decomposition accounts for 2.7% of the total N emissions in agriculture (Whitehead and Lockyer, 1989 as cited in McGinn and Janzen, 1997). Measured NH_3 emissions from decomposing sugar beet leave, potato tops, and field beam straw range from 0.9 to 3.7% of the N content (Sommer *et al*., 2004).

Little information is known on NH_3 volatilization losses in potato fields. The potato plant's N uptake efficiency under current best management practices is approximately 65% (Lang *et al.,* 1999) with a mean of 40% (Balasubramanian *et al.,* 2004). Measured NH_3 emission rates from barley, wheat, and oilseed rape canopies range from 1 to 15 kg hectare^{-1} year^{-1} while measured NH_3 emissions from sugar beet leaves and potato shoots ranged from 8.6 to 12.6 kg N hectare^{-1} year^{-1} (Sommer *et al*., 2004).

CHAPTER 3

METHODOLOGY

This chapter describes the methods used for measuring N_2O and NH_3 concentrations and for determining flux rates from the potato fields. Mixing ratios of N_2O were measured using gas chromatography (GC) and flux rates of N_2O were estimated using a static chamber method. A short-path differential optical absorption spectroscopy (DOAS) instrument was used to measure concentrations of NH_3 along a path downwind of the fields. Sulfur hexafluoride (SF_6) was released from a point source from the center pivot of the fields to simulate NH_3 plume dispersion and to calibrate a Gaussian plume model (SIMFLUX). SIMFLUX was then used in an inverse modeling approach to estimate flux rates of NH_3 from the fields. Data were collected at potato fields in central WA, near Othello.

3.1 Measurement of N_2O

A disjunct eddy accumulation (DEA) system was used in summer 2006 for measurement of N_2O fluxes. In operation, air samples are partitioned into updraft and downdraft reservoirs over some averaging period based on the sign of the vertical velocity (Turnipseed *et al*., 2008). The total flux is related to the concentrations in the updraft and downdraft reservoirs. It was found that N_2O flux measurements with the DEA were below detection limits and so a static chamber method was then used for the summers of 2007 and 2008. For more information on the DEA system, refer to Turnipseed *et al*. (2008).

3.1.1 Static Closed Chamber Method and Flux Rate Calculation

Fluxes of N_2O were measured using a static closed chamber method (Hutchinson and Mosier, 1981). Chambers were installed between potato plant rows and sampled according to USDA-ARS GRACEnet (Greenhouse gas Reduction through Agricultural Carbon Enhancement network) protocols (USDA-ARS, 2003; www.GRACEnet.usda.gov). Each chamber used consisted of a base and a lid. Chamber bases were made from 30.5 cm inner diameter x 15 cm high polyvinyl chloride (PVC) cylinders. The bases were inserted 10 cm into the soil and at least 24 hours prior to sampling to allow for stabilization. The chamber lids (30.5-cm inner diameter by 7.5 cm high) were made from PVC caps and included a 2.54 cm sampling port, a built-in vent tube, and an internal 12-V DC 60 mm fan. The built-in vent tube prevented pressure perturbations by maintaining atmospheric pressure inside the chamber. The fan ensured sufficient gas mixing within the chamber for homogeneous gas concentrations and better simulated mass transfer from the soil to the atmosphere.

The approximate locations of the chambers are shown in Figure 3.1. The dashed blue lines and the solid red lines represent the road that lead to the center of the field used in summer 2007 and summer 2008, respectively. The wheel tracks of the sprinkler system are represented by the dashed gray concentric circles. The numbers in blue and red are chambers used in summer 2007 and summer 2008, respectively. Chambers 1, 2, 10, 11, 12, and 13 were placed near the dirt road that led to the center of the fields. Chambers 3, 4, 7, 8, and 14 were placed along the south edge of the fields. Chambers 5 and 6 were placed along the 4th wheel track, near the dirt road. Chamber 9 was placed approximately 10 m south of the dirt road, between the edge of the field and the 1st wheel track.

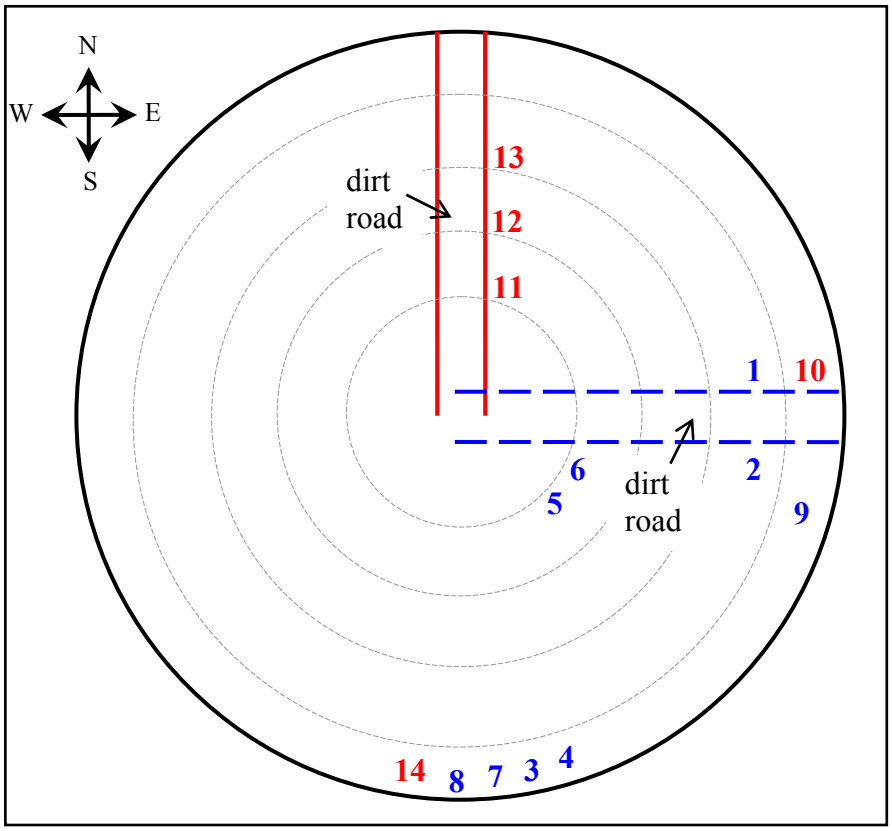

Figure 3.1: Locations of the chambers used for N_2O flux measurements. Blue marks represent the field in 2007, and red marks represent the field in 2008.

Air samples (about 30 ml) from within the chambers were collected every 15 minutes over a period of 1 hour after covering the chambers. After the first 1 hour of sampling, the chamber was uncovered for 30 minutes before the second hour of sampling began. Typically, a total of 4 hours of sampling was conducted for each chamber. To calculate the flux of N_2O, linear regression and the following calculation was used:

rate of change of N_2O concentration inside chamber (ppm/min) or (10^{-6} L N_2O gas/ (L total gas*min))	X	chamber volume (L)	÷	chamber surface area (m^2)	=	10^{-6} L N_2O/ (m^2*min)

3.1

The gas flux values were converted from a volumetric basis to a mass basis.

3.1.2 Advantages and Disadvantages of using the Chamber Method

The advantages of using the chamber method is that chambers are relatively inexpensive, easy to build, install, and remove, and have low detection limits. The disadvantages of using chambers include the inability to account for environmental conditions (i.e. winds) and disturbance to the soil which can easily occur when installing chamber bases. In addition, the method is labor intensive. Five air samples are needed to calculate one flux rate value. Chamber bases need to be installed at least 24-hours prior to sampling to minimize soil disturbance and root damage. Careful planning of sampling time is necessary to ensure that the measurements are made immediately after spraying of water or water with N fertilizer by the sprinkler system. Finally, numerous chambers are needed to capture the variability of N_2O flux rates through the field due to heterogeneity of the soil.

3.1.3 Sample Analysis

Gas sampling was performed 0 to 6.5 hours after fertigation and irrigation events. Analysis of air samples for N_2O concentration was conducted using a Hewlett-Packard 5890 Gas Chromatograph (GC) with an Electron Capture Detector (ECD). An ECD is best for analysis of compounds containing halogens and nitro groups (Poole and Poole, 1991). An Alltech Porapak Q (80/100) column was used and kept isothermal at 40 °C. The carrier gas was 95% Argon (Ar) and 5% methane (CH_4). The GC flow rate ranged from 24.5 to 25.5 standard cubic centimeters per minute (sccm) and was maintained using an Alltech Digital Flow Check Flow Meter. A 777 ppbv N_2O ± 10% (Scott-Marrin) standard was analyzed multiple times during each sampling day. All samples were analyzed within one day of collection since tests showed decreased concentrations (~25% reduced) from syringes analyzed after 24 hours.

3.2 Measurement of NH_3

3.2.1 Differential Optical Absorption Spectroscopy (DOAS)

Spectroscopy is the study of the interaction between radiation and matter as a function of wavelength (λ). Gas molecules absorb radiation if the radiation can electronically excite or change the vibrational or rotational energy of the molecule. A short-path differential optical absorption spectroscopy (DOAS) technique was used to measure NH_3 emissions from the potato fields. The DOAS technique avoids the NH_3 adhesion problem (Mount *et al*., 2002) that is common with in-situ methods using inlets and sampling tubes.

The DOAS technique measures the spectroscopic molecular absorption of trace gases over an open atmospheric path. Using Beer's Law, which relates the amount of light absorbed to the number of molecules in the measurement path length, the concentration of NH_3 can be calculated. Beer's Law states that there is a logarithmic dependence between the transmissivity of light through a substance and the product of the absorption coefficient of the molecule and the distance the light travels through the material. Beer's Law can be expressed as:

$$T = I(\lambda)/I_o(\lambda) = \exp^{-\sum \sigma i(\lambda) L N i} \qquad 3.2$$

T - transmissivity;

λ - wavelength [nanometers];

$I(\lambda)$ - light intensity in the presence of absorbers [counts];

$I_o(\lambda)$ - light intensity without absorbers [counts];

$\sigma_i(\lambda)$ - absorption cross-section of the i^{th} absorber expressed in [cm^2];

N_i - concentration of the i^{th} absorber [molecules cm^{-3}];

L - distance that the light travels through the material or the path length [cm].

The subscript "i" in the summation refers to any particular atmospheric specie that absorbs at the wavelength region of measurement and the sum occurs over all species that can absorb at wavelength λ. As a result, it is important to know all of the atmospheric species that absorb over the wavelength region measured and to account for them in the analysis. The DOAS instrument used for this project operates in the 200-240 nm wavelength range. In this wavelength range, atmospheric species NH_3, nitric oxide (NO), and sulfur dioxide (SO_2) absorb (Mount *et al.,* 2002). The absorbances of NO and SO_2 are very low (below the detection limit) in the potato fields so they were not accounted for in the data analysis (Mount *et al.*, 2002).

In addition to other gas species that absorb in the wavelength region measured, other atmospheric processes contribute to the measured spectrum and must be accounted for. Rayleigh scattering is wavelength dependent and describes the scattering of light by small molecules such as dinitrogen (N_2) and oxygen (O_2) which makeup about 98% of the atmosphere. As the wavelength decreases, the amount of scattering increases. For Rayleigh scattering, the ratio of the diameter of the scattering particle to the wavelength of measurement is much less than 1 and is computed using the following equation:

$$x = 2\pi r/\lambda \qquad 3.3$$

x - size parameter

r - characteristic dimension of the scattering particle;

λ - wavelength of the light.

Rayleigh scattering occurs when $x << 1$. The Rayleigh scattering cross-section is computed from the Pendorf equation (Pendorf, 1957):

$$\sigma_R(\lambda) \approx \sigma_{RO} \cdot \lambda^{-4} \qquad 3.4$$

where $\sigma_{RO} \approx 4.4 \times 10^{-16}$ cm^2 nm^4 for air.

Mie scattering (clouds and aerosols) occurs when the particles causing the scattering are larger than the wavelengths of radiation in contact with them. Similarly, Mie scattering can be modeled as an absorption cross-section. The cross-section for Mie scattering depends on the particles causing the scatter, but is typically given by $\lambda^{-1.6}$. Since NH_3 absorption is being measured in the mid-ultraviolet range (below the atmospheric cutoff of 290 nm) the solar spectrum does not need to be accounted for, a major benefit of measuring in this spectral region. Accounting for Rayleigh and Mie scattering, Beer's law becomes the following:

$$I(\lambda)/I_o(\lambda) = \exp[(-\sum\sigma i(\lambda)LNi) + \varepsilon R(\lambda) + \varepsilon M(\lambda)] \quad 3.5$$

3.2.2 Instrument Description

Two versions of the instrument were used for NH_3 measurements. Details of the instrument used in summer 2007 are described in Mount *et al*. (2002). In this section, a brief description of the original instrument will be presented, followed by a description of the revised instrument.

A schematic diagram of the original DOAS instrument used for summer 2007 measurements is shown in Figure 3.2 and a picture of the instrument housing, which was a small trailer, is shown in Figure 3.3. A 150 W xenon (Xe) high-pressure emission lamp (source region of 0.5 mm, Hamamatsu Corp. model L2273) is used as a light source and is located at the side of the optical path of the primary mirror. The light from the Xe lamp is directed onto the 1st folding mirror, which then directs the light onto a f/5 parabolic primary mirror. The primary mirror is 40 cm in diameter, coated with aluminum (Al) and magnesium fluoride, and was made by Colorado Precision Optics. Only an annulus of 6 cm of light is illuminated onto the primary mirror since there is a second folding mirror that is located between the primary mirror and the 1st folding mirror which blocks part of the beam.

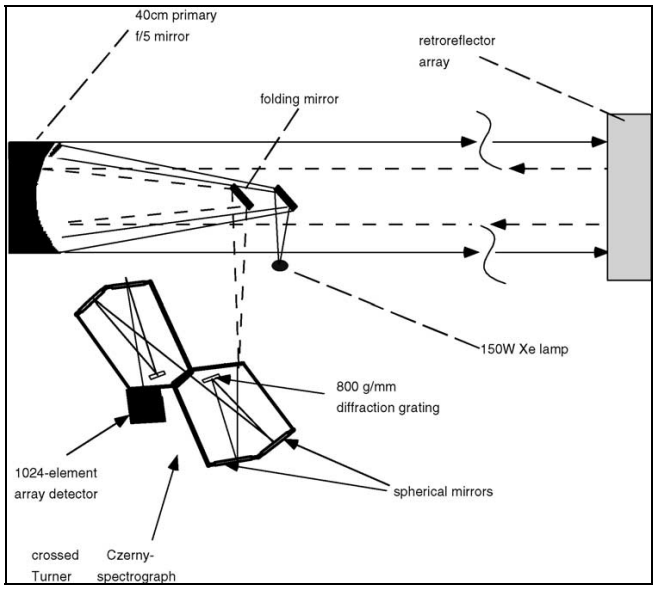

Figure 3.2: Schematic drawing of the original DOAS instrument showing the optical light path from the Xe lamp to the Reticon detector (Figure adapted from Mount *et al.,* 2002).

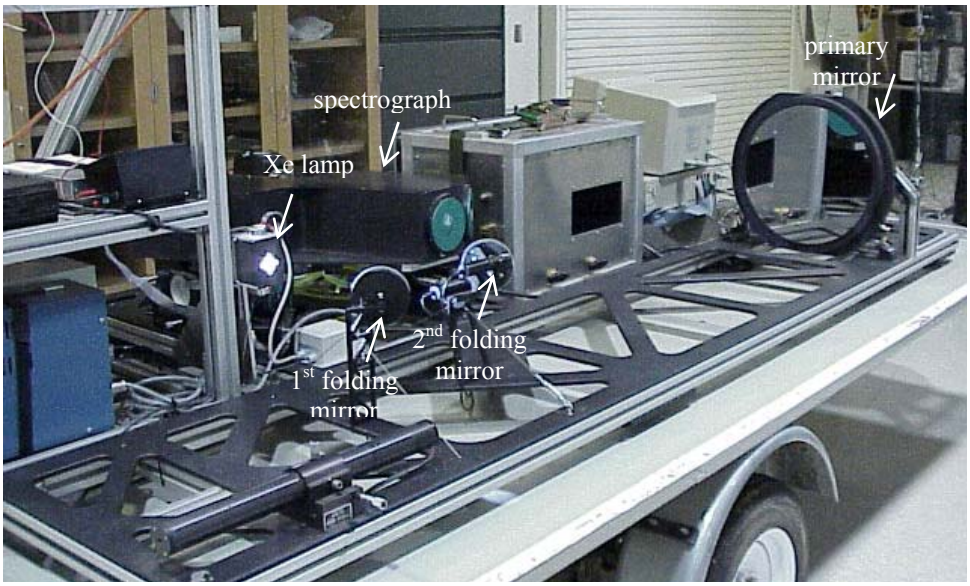

Figure 3.3: The original DOAS instrument housing (cover removed), which was a trailer (Figure adapted from Mount *et al.,* 2002).

From the primary mirror, the annulus of light is directed towards a set of four large retro-reflectors or a set of thirty-seven small retro-reflectors mounted on a tripod. Each of the four big retro-reflectors is 12.7 cm in diameter, and each of the small retro-reflectors is 9 cm in diameter. All are coated with Al and magnesium fluoride for protection. The retro-reflectors were obtained from Melles Griot Inc. The light from the retro-reflectors is displaced and returned to the primary mirror. The light is then intercepted by the second folding mirror, which directs the light towards the slit of a double crossed Czerny–Turner spectrograph. The focal length of the telescope optical system is 200 cm.

Inside the spectrograph, the light hits the 1st collimating mirror to make the rays parallel before it is reflected to a diffraction grating. The grating breaks the light up into its constituent colors. From the grating, the light travels to the 1st focusing mirror and then enters another entrance aperture. Once again, the light passes through a 2nd set of collimating mirror, grating, and focusing mirror. The spectrographs were double-crossed to reduce scattered light. The detector used for the original DOAS instrument was a homebuilt Reticon silicon photodiode array with 1024 pixels with each pixel 25 μm wide and 2.5 mm high. Spectral coverage was about 60 nm and spectral resolution was about 0.6 nm.

The original DOAS instrument had several limitations. The computer used to control the system was a Macintosh IIfx, which has been long discontinued. In addition, transporting the trailer to and into an agricultural field was laborious. Pulling the trailer had to be done carefully because the optics, detector, and other parts of the instrument are delicate and there were insufficient mountings to absorb the shock. In the field, the slightest movements of the trailer (e.g. heating and expansion of the tires) would result in loss of signal due to misalignment.

During the undertaking of this project, several parts of the DOAS instrument were revised from the prototype version used at the WSU dairy including the instrument housing, telescope and its light feed, and the detector. The revised DOAS instrument is more compact than the original instrument. The optics setup of the revised instrument is similar to the setup of the original instrument but the spectrograph is placed below instead of to the side of the 2nd folding mirror and the primary mirror. The primary mirror (made by Stevens Optical) is only 32 cm in diameter instead of 40 cm, which allows for a more compact design. The light reflected from the retro-reflectors is returned to the primary mirror and then is intercepted by the 2nd folding mirror, which directs the light downward to a 3rd folding mirror. The 3rd folding mirror directs the light into the entrance slit of the spectrograph. The angle of this third folding mirror is manually tilted in two axes by small motors so that peak light intensity can be directed into the spectrograph entrance slit. The f/number of the optical system is the same as the one used in the original instrument. A schematic diagram and a picture of the revised DOAS instrument are shown in Figure 3.4 and 3.5, respectively.

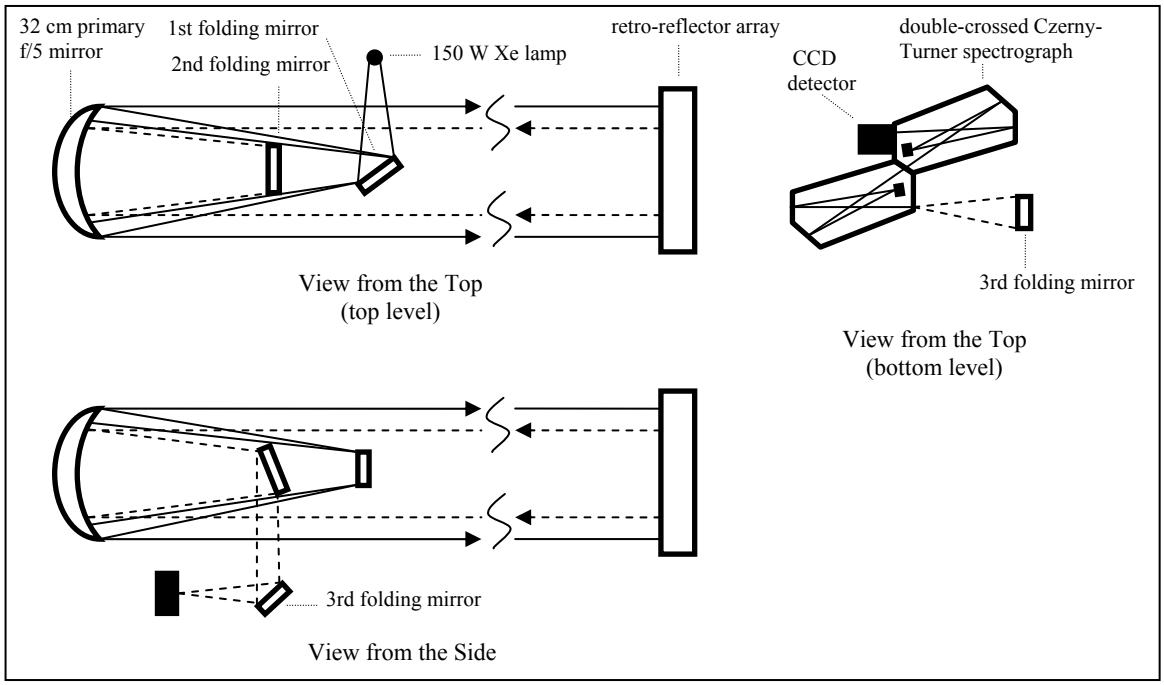

Figure 3.4: Schematic drawing of the revised DOAS instrument showing the optical light path from the Xe lamp to the CCD detector. The top figures illustrate a view from the top of the instrument, the bottom figure shows the view from the side.

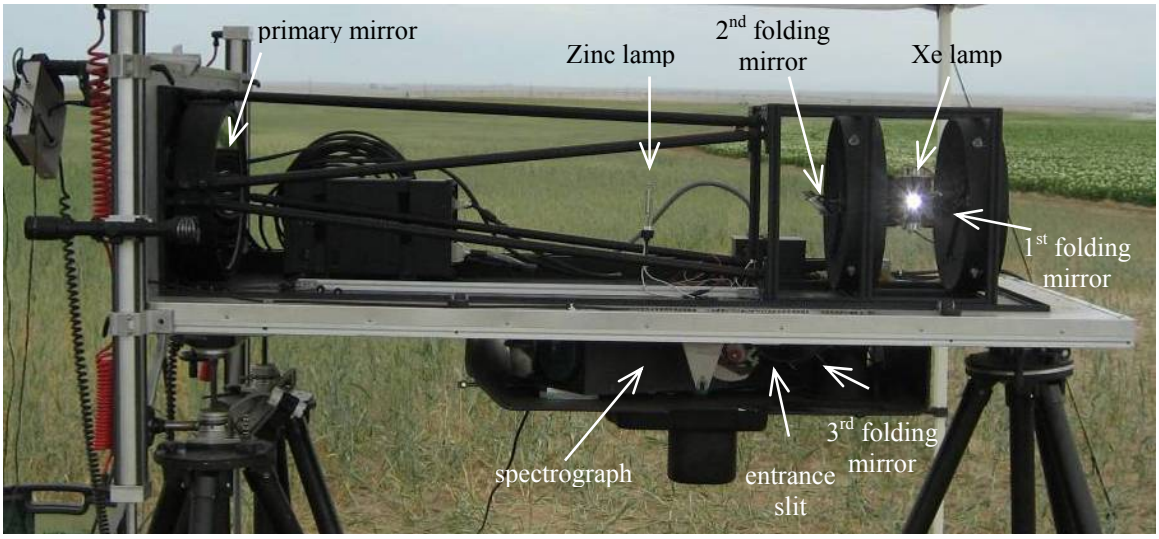

Figure 3.5: The revised DOAS instrument with the cover removed.

The detector used in the revised instrument is a Princeton Instruments charge coupled device (CCD) detector system (spec-10:400B) with 400 pixels x 1340 pixels, with each pixel 19.4 μm wide and 19.4 μm high, and the spectral direction in the long direction. More details regarding the CCD detector can be found on the Princeton Instruments website under products-spectroscopy cameras-Spec-10-CCD. The WinSpec Spectroscopy Software version 2.5.16.5 was used for data collection. This software is compatible with Windows. A PC laptop was used for control of the system.

The main optics of the revised version are assembled on a 1.82 m by 0.85 m bench which is loaded in the back of a pickup truck. A special canopy was designed to house all of the necessary equipment (instrument, retro-reflectors, generator, etc.) for transport purposes. Two bicycle tires are attached to the sides of the instrument in order to maneuver the system in the field. A winch and two removable ramps are used to load the instrument into the back of the pickup truck. The instrument canopy rides on a set of six inflatable tires to increase stability during transportation and help absorb shock. Figure 3.6 shows a picture of the revised instrument housing.

Figure 3.6: The new housing (a pickup truck canopy) for the DOAS instrument, which is used for transporting the instrument.

To set up, the instrument is winched down the ramps. Four air jacks are attached to the corners of the instrument bench. The air jacks lift the instrument off the ground and the instrument is placed on three tripods. Unloading and set up of the instrument can be accomplished by three or more people and typically takes several hours. Aligning and fine tuning of the instrument to the retro-reflectors takes an additional several hours. Figure 3.7 is a picture of the revised DOAS instrument when it is setup for taking measurements.

Figure 3.7: The revised DOAS instrument when it is setup for taking measurements.

3.2.3 Advantages and Disadvantages of the DOAS Technique

Use of the DOAS technique for measuring NH_3 concentrations has many advantages over traditional in-situ measurements (Mount *et al.,* 2002). Ammonia adheres to surfaces, such as inlet tubes and sampling cells, and the use of the DOAS technique eliminates this problem. Results depend only on the quality of the independently measured cross-sections of the species and the algorithm used for data analysis (Mount *et al.,* 2002). Finally, the DOAS technique can measure several gas species simultaneously (i.e. NO, SO_2, NH_3 for the wavelength region used).

The DOAS technique also has disadvantages. First, it is limited to molecular species that have spectrally structured absorption cross-sections in the wavelength region of the measurement. In addition, the DOAS technique is limited to times of good visibility. Rain and snow make measurements impossible due to the strong attenuation in the UV-Visible region. Lastly, the DOAS technique is labor intensive because the instrument must be monitored on an hourly basis to keep the instrument properly aligned.

There are many uncertainties associated with solving the Beer's Law equation (eq. 3.3). $I(\lambda)$ and $I_o(\lambda)$ are generally not measured over the same path since the I_o measurement should not have any of the measured species in it. This negatively affects the spectral residual analysis. Changes in the instrument, such as lamp output, may occur due to changes in temperature and pressure that occur between measurement of $I(\lambda)$ and $I_o(\lambda)$. Generally these changes are very low frequency in spectral occurrence and so do not affect the analysis.

Table 3.1: DOAS instrument characteristics

Reticon Detector	
pixel size	25 μm wide x 2.5 mm high
CCD Detector	
pixel size	20 μm x 20 μm
Spectrograph	
focal length	375 cm
Telescope	
focal length (original system)	200 cm
focal length (revised system)	160 cm
Xe Lamp	
output power	150 W
arc length spot size	0.5 mm
wavelength range	185-2000 nm
average life	3000 hrs
output fluctuation	1%
Other	
path length	~250 m
detection limit:	
2007 data (original system)	5 ppbv
2008 data (revised system)	10 ppbv
spectral coverage	200-240 nm

3.2.4 Data Collection

Data was collected using the Reticon detector in the summer of 2007 and using the new CCD detector in the summer of 2008. The instrument was aligned towards the retro-reflectors so that the return signal counts were maximized. The integration time, which depends on the path length, was varied so that the maximum count rate was about 30,000 to 40,000 counts per integration time. Spectra were co-added so that data was averaged over five minute intervals.

Before taking actual measurements the electronic noise (dark spectra) of the instrument system was measured by placing a black slide in front of the entrance slit of the spectrograph and using the same settings as for the actual spectra. Changes in detector temperature caused changes in dark spectra. As a result, dark spectra measurements were also taken about every hour and were co-added and averaged. The average dark spectra were subtracted from the actual spectra measured (when the slide was removed). A zinc (Zn) emission lamp was placed in front of the entrance slit every hour to provide a strong spectral line fiducial at 213.9 nm. The Zn fiducial line was centered at a chosen pixel.

3.2.5 Limitations on Data Collection

Time was a major limitation for collection of data. Measurements had to be taken during the short potato growing season. The farmers who owned the fields would often make sudden changes to the fertigation and irrigation schedules. This would be due to uncontrollable changes in the weather, the crop's reaction to the fertigation and/or irrigation, and the amount of fertilizer and/or water available. Data collection was prohibited during times of chemigation (i.e. herbicides and/or pesticides) application because of health concerns.

Problems with the instrument were encountered in the field. Changes to the DOAS instrument were implemented without being fully tested (e.g. the replacement of the detector) before being used for data collection. High outside air temperature caused a significant problem with the CCD detector. The internal cooler of the CCD detector could not keep the detector cold enough when the outside air temperature was above ~24 °C. This problem was anticipated but not enough testing was performed prior to going to the fields and so a solution was initiated in the field. At the potato field near Othello, WA, the average outside air temperature during the afternoon was always above ~24 °C and even occasionally reached above 37 °C. An external radiator was used with cooling lines running through an ice bath in order to keep the detector running. However, variations in the dark current were sufficiently uncontrollable that the dark subtractions could not always be performed correctly.

3.2.6 Limitations on Data Quality

Analysis of the optical arrangement in January 2009 showed the focal position of the spectrograph was incorrect, which resulted in loss of light (signal). Lower signal to noise ratio (s/n) resulted in lower precision. However, this should not have affected the actual determinations of molecular concentration when sufficient NH_3 was present. It was also discovered that the mirrors within the spectrograph were not properly aligned and this resulted in a degraded spectral resolution. The crude temperature regulation of the CCD detector caused major problems with dark subtraction and overall had a significant negative effect on the measurement.

Figure 3.8 is a plot of the CCD Detector quantum efficiency (QE) with respect to wavelength. The QE, which is a measure of the detector's electrical sensitivity to light, in the wavelength region used (200 to 240 nm) was below 10%, which resulted in lower s/n ratio.

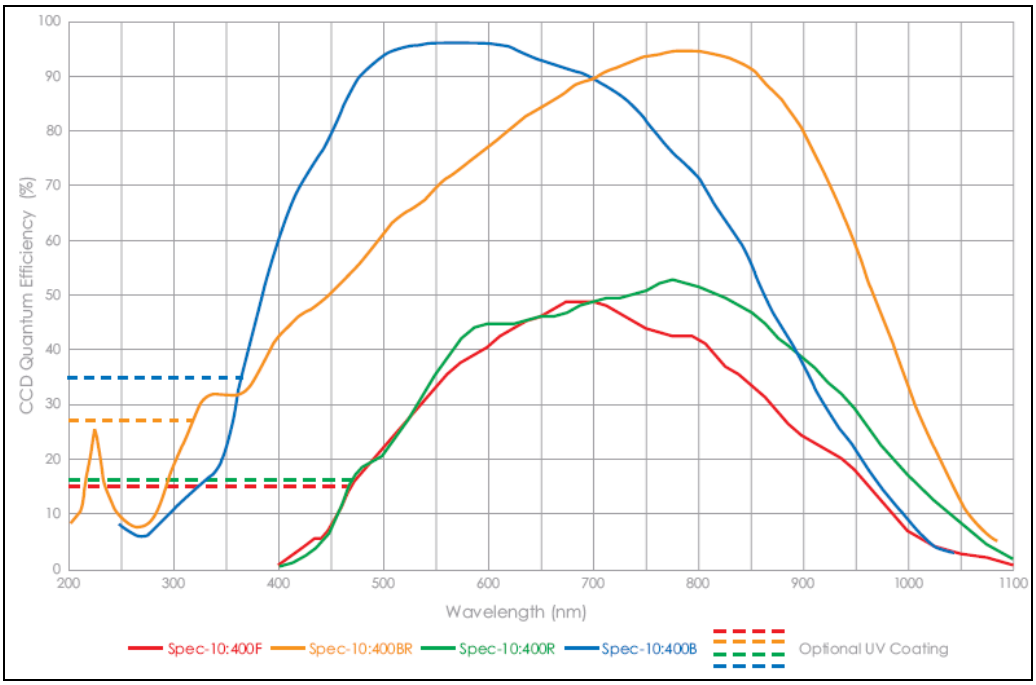

Figure 3.8: Quantum Efficiency (QE) of the CCD Detector (Model Spec-10:400B (blue line)) with respect to wavelength (figure adapted from Princeton Instruments Spec-10 Datasheet, www.princetoninstruments.com/products/speccam/spec10/dsheet.aspx).

The detection limit of the instrument depends on the magnitude of the spectral residuals of the data, which is the remainder of the spectral ratio of I and I_o after removal of the known absorbers (NH_3) as well as the spectrum of Mie and Rayleigh scattering. The residual spectrum should be random noise, but this level of precision is never reached due to systematic errors in the removal of the spectral signatures, detector temperature problems, and changes in the spectral structure of the Xe lamp. The original DOAS instrument was sensitive to a few ppbv of NH_3 while the revised version is only sensitive to at best 10 ppbv of NH_3.

The revised instrument can clearly be improved with more testing and modifications. Problems for our field work were accentuated by time constraints due to the late completion of the modified instrument, resulting in insufficient testing before using at the fields. The optical problems with the spectrograph resulted in degraded performance, but it was decided not to change this once the data collection was started. The main effects caused a degradation of s/n

and precision. Problems in the design of the telescope and feed optics were corrected part way through the experiment to increase the collection of light and significantly reduced the integration time.

3.2.7 Data Analysis

To convert the absorbance of NH_3 given by Beer's law to concentration, a nonlinear least squares fitting method was used. The method fits the pattern of the cross-section of each gas molecule that absorbs in the wavelength range used to the natural logarithm of the ratio of I/ I_o. In this case, only the cross-section of NH_3 was used since the absorbances of NO and SO_2 were found to be very low.

Figure 3.9 shows the cross-section spectra of NH_3 in the mid UV spectral region. This shows the ability of NH_3 to absorb light as a function of wavelength. For summer 2007 measurements, three absorption lines were used to reduce the data. For the summer 2008 data, only two absorption lines were used (wavelength range: 199nm to 207nm).

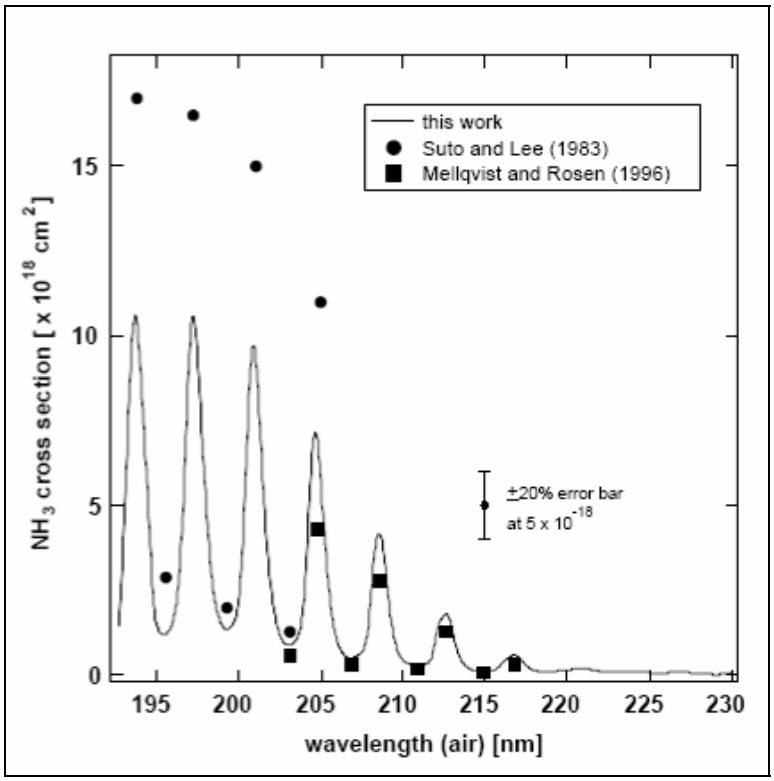

Figure 3.9: Ammonia absorption cross-section.

In addition to the cross-section spectra of NH_3, the nonlinear least squares algorithm accounts for the spectral pattern of Rayleigh and Mie scattering as well as the shift and stretch of the two spectra being ratioed. Shift and stretch in the spectra can result from displacement of the grating and detector as well as temperature changes experienced by the spectrograph. The method minimizes the spectral residual of patterns in the data after removal of the molecular spectra signatures.

Data analysis is conducted in two steps. First, a relative I_o, containing NH_3 features, was chosen from the measurement data (same-day) and used for initial data reduction. The NH_3 concentration for each measurement period was then calculated relative to the I_o chosen. The actual NH_3 concentration was then determined by reducing the relative I_o with an absolute I_o, a spectra with no NH_3 features taken in the laboratory.

3.2.8 Characterization of Dispersion Conditions using Tracer Studies

During some measurement periods, SF_6 tracer gas was released from the center of the fields and concentrations measured along a crosswind sample line downwind of the fields to help characterize local dispersion conditions. To conduct tracer studies, SF_6 was released as a continuous point source from ground-level at the center pivot of the field. The SF_6 release rates ranged from ~0.6 to ~0.7 L min^{-1}. Air flow was maintained using a 1.00 SLPM Tylan mass flow controller (S/N AA9605027) and a Tylan RO-32 control box. A BIOS International DryCal DC-Lite Flow Meter was used check flow rates. Sulfur hexafluoride is ideal for tracer studies because it is inert, concentrations can be measured with satisfactory accuracy at very low concentrations, and ambient concentrations of SF_6 are negligible. Even though SF_6 has a higher molecular weight (146.06 g mol^{-1}) than NH_3 (17.03 g mol^{-1}), the effect of this is negligible since turbulent diffusion is the dominant transport mechanism (Kaharabata *et al.,* 2000).

Positioned downwind of the source were Trace Gas Automated Profile System (TGAPS) sample lines and syringe samplers. TGAPS is an automated sampling and analysis system, which continuously measures 5-minute averaged concentrations of SF_6 at seven different locations. The system draws air through 7 long inlet lines positioned along the length of the DOAS measurement path and air from these inlets is pumped into a set of seven 10-L Tedlar bags. While one set of 7 bags collects air samples, a second set of 7 bags is analyzed. During analysis, air from each bag is drawn to a continuous SF_6 analyzer (Flaherty *et al*., 2007). Between the sample analysis and collection, the Tedlar bags are evacuated completely to ensure that the bags are "clean" for the next sampling period.

Air samples were also collected using programmable, battery-operated syringe samplers. Each syringe sampler contains 12 syringes, which sequentially collect 30-minute averaged air

samples. Each syringe sampler is enclosed in an aluminum case, which serves to protect the 12-syringe unit inside. A sealed compartment inside the syringe sampler houses the electronics, stepper motors, and clock. Krasnec *et al*. (1984) provides a complete description of the syringe samplers used. The syringe samplers were also deployed along and beyond the DOAS measurement path downwind of the field and tracer release to provide a measure of plume width.

A GC equipped with an ECD and coupled with an electronic integrator was used to measure SF_6 concentrations. The air samples were combined with hydrogen (H_2) and then passed through a packed bed of palladium catalyst, which converted the oxygen (O_2) in the air to water (H_2O). Then, the air passed through a nafion tube with a countercurrent flow of N_2 to remove the H_2O from the sample stream. The sample stream was then passed to the ECD, where voltage changes due to the SF_6 in the stream provided the signal for concentration. See Benner and Lamb (1985) and Flaherty *et al*. (2007) for additional information about this type of detector system. Calibration was performed using 1005 pptv, 1625 pptv, and 1462 pptv Scott-Marrin Inc. calibration gases (certified accuracy ±5%). All samples were analyzed within a day of collection.

3.2.9 Field Setup

Figure 3.10 is a diagram of the field setup. Southwest winds are predominant in the central WA region. Thus, the DOAS instrument measurement path (path from the spectrograph to the retro-reflectors) was setup outside the edge on the northeast quadrants of the potato fields to capture the NH_3 plume as it traveled along the wind trajectory. Path lengths varied from ~150 to ~250 m.

Tracer sample lines and syringe samplers were set up along the DOAS measurement path and extended over a distance of 800 m so that ideally the entire plume of SF_6 would be captured. More details on how the dispersion studies were conducted will be provided in section 3.3.2.

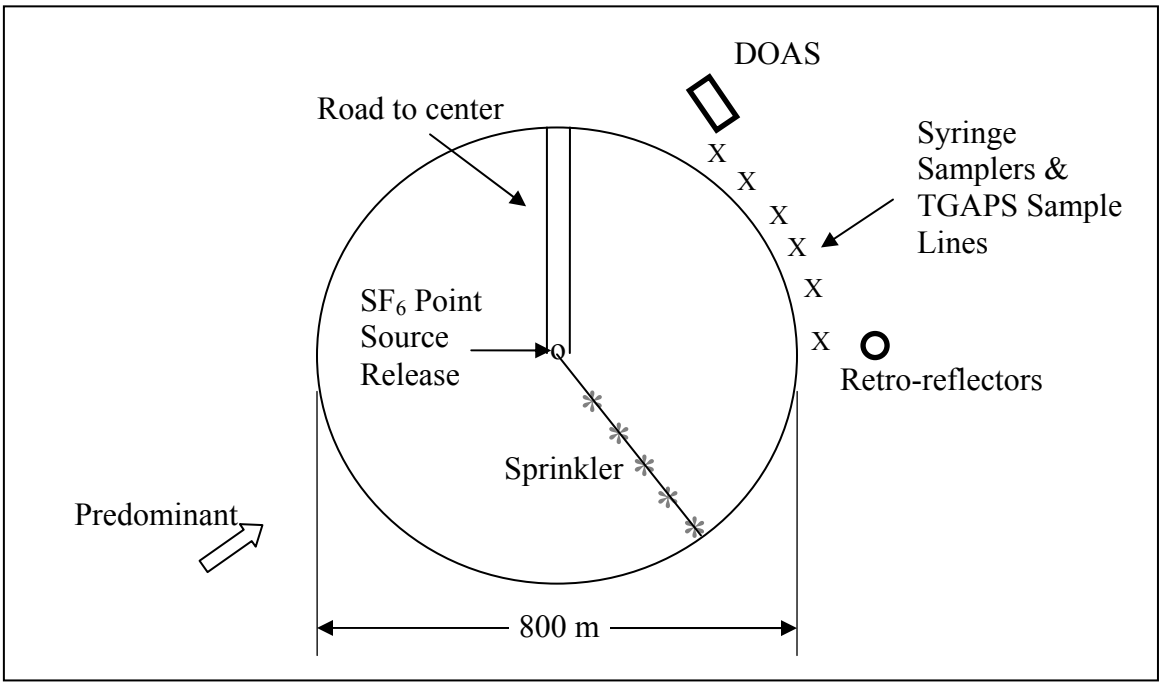

Figure 3.10: Diagram of the field setup.

The only source of electrical power was at the center of the fields. As a result, instruments used in the fields (i.e. DOAS instrument) were powered using portable generators. A storage building with power located nearby was used to power other instruments such as the N_2O GC.

3.3 Measurement of Meteorological Variables

Meteorological information such as wind velocity, wind direction, and air temperature were measured using a sonic anemometer at 10 Hertz frequency. Soil moisture and temperature were measured using CS515s Water Content Reflectometers and copper/constantan

thermocouples (Campbell Scientific Inc.), respectively. Campbell Scientific CR10 data loggers were used to record data. Leaf stomatal conductance was measured using Decagon Devices Hand Held Leaf Porometer.

3.4 Determining Emission Rates of NH_3

A Gaussian plume dispersion model (SIMFLUX) was used with an inverse approach to estimate NH_3 emission rates. The first part of this section will present the basis of the Gaussian plume dispersion equation (section 3.4.1) and in section 3.4.2, the details of SIMFLUX will be presented.

3.4.1 The Gaussian Plume Dispersion Equation

The Gaussian plume dispersion model is useful for measuring the impacts of air pollutant sources on air quality. After a release, individual particles move according to velocity fluctuations which are random, resulting in a random distribution in each coordinate system. The result of this random distribution is that the plume contains more particles near the center of mass while fewer particles are present at increasing distances from the center of mass. It is reasonable to assume a Gaussian concentration distribution based on measurements of typical plumes and for ease of mathematical computation.

For a continuously emitting point source strength (Q) in grams per second (g s^{-1}) at an effective height (h) in meters above the ground, the concentration C at a receptor location x, y, and z in grams per cubic meter is given by the equation:

$$C(x,y,z) = \frac{Q}{2\pi\sigma_y\sigma_z u} e^{\frac{-y^2}{2\sigma_y{}^2}} \left[e^{\frac{-(z-h)^2}{2\sigma_z{}^2}} + e^{\frac{-(z+h)^2}{2\sigma_z{}^2}} \right] \qquad 3.6$$

where x is the downwind distance of the receptor from the source in meters (m), y is the crosswind distance in meters, z is the height of the receptor above the ground in meters, u is the wind speed in meters per second, and σ_y and σ_z are the horizontal and vertical diffusion coefficients, respectively, in meters. A complete general overview of the Gaussian plume equation is discussed by Hanna *et al*. (1982).

Requirements for the Gaussian dispersion models are homogeneous turbulence, uniform flow, no loss of pollutants, and steady state conditions (Arya, 1999). In addition, mean wind speed is required to be larger than the standard deviations of turbulent velocity fluctuations, so that the upstream or longitudinal diffusion can be neglected. Thus, significant wind shears, inhomogeneous turbulence, and weak winds make the theoretical basis of Gaussian dispersion modeling invalid. Finally, the methods for obtaining certain input parameters used in the Gaussian plume dispersion equation are also subject to many assumptions and constraints. Such critical parameters are the diffusion coefficients, σ_y and σ_z, since they describe the shape of the plume as it travels along in the mean wind direction. Various methods (Martin, Briggs, Taylor, and Draxler) for determining σ_y and σ_z were compared with actual data obtained from a series of SF_6 tracer dispersion studies conducted in the potato fields. A comparison of the various methods is included in Appendix A.

3.4.2 SIMFLUX

A Gaussian plume model (SIMFLUX) was used in an inverse method to estimate NH_3 emission rates. SIMFLUX uses a dense array of point sources to calculate the dispersion of emissions from point, line, and area sources. It is a versatile model because it is applicable for a wide range of area source configurations. Each potato field was modeled as an array of individual point sources at 1 m spacing. Howard *et al.* (1996) evaluated the effect of the length

of the spacing between each point source and found that the best model results occurred when the spacing between source points are less than one standard deviation of the lateral dispersion at any receptor location for the appropriate stability class.

Ammonia emission rates were back-calculated using observed NH_3 concentrations. The DOAS measurement path was modeled as a line of point receptors, approximately 400 m downwind from the center of the fields and at 1 m spacing. All measured variables, including wind speed and wind direction, were measured using a sonic anemometer at 10 Hz frequency and were input into the Gaussian plume equation. Analytical equations that represent the Pasquill-Gifford diffusion curves were employed for estimating the vertical and horizontal dispersion (Martin, 1976). For the results on the comparison of various sigma methods to be used in SIMFLUX, see Appendix A. The contribution from each point source was summed to estimate the concentration at each downwind receptor. An emission rate (Q) of 1 g s^{-1} $point^{-1}$ was first used for all point sources and then adjusted until predicted NH_3 concentrations at the point receptors match observed concentrations.

Howard *et al*. (1996) discovered that significant errors result if a receptor is placed too far crosswind from the plume centerline. As a result, only flux rates calculated from periods that captured the shape of the Gaussian plume were considered to be valid. The percent of plume captured for each 30-min sampling period was calculated by determining the ratio of the area of the plume measured and the area of the entire plume predicted.

CHAPTER 4

Measuring Gaseous Losses of Nitrogen from Potato Fields in central Washington

Mary Capiral, Shelley Pressley, Brian Rumburg, George Mount, Brian Lamb

Department of Civil and Environmental Engineering

Washington State University

Pullman, Washington 99164-2910

to be submitted to

Atmospheric Environment

4.1 Abstract

There are limited studies that have measured the magnitude of Nitrogen (N) emissions from intensively managed croplands. In this research, concentrations of ammonia (NH_3) and nitrous oxide (N_2O) from potato fields in central Washington were measured during the 2007 and 2008 growing seasons (June – August). A short-path differential optical absorption spectroscopy (DOAS) instrument that operates in the 200-240 nm wavelength spectral range was used to measure NH_3 concentrations. During some periods, sulfur hexafluoride (SF_6) tracer gas was released from the center of the fields and concentrations were measured along a crosswind sample line downwind of the fields to help characterize local dispersion conditions. A Gaussian plume dispersion model (SIMFLUX) was used, along with the SF_6 tracer data in an inverse approach to estimate NH_3 emission rates. A static chamber flux method was used to measure N_2O emissions with sample analysis via electron capture gas chromatography (ECD-GC). Nitrous oxide flux rates generally peaked between 2.5 and 3.5 hours after irrigation or fertigation. The amount of N lost as N_2O ranged from zero to 12% of the applied N fertilizer which is comparable to documented emission factor values of 0.1 to 8% (Dobbie and Smith, 2003). Measured NH_3 concentrations varied with application status, sprinkler arm location, and wind speed. The highest NH_3 concentrations measured in the summers of 2007 and 2008 were ~34 ppbv and ~112 ppbv, respectively. Both peaks occurred during fertigation, when the sprinkler arm was spraying almost directly towards the DOAS measurement path and winds greater than 1 m s^{-1} were blowing towards the measurement path. Estimated NH_3 flux rates ranged from 9 μg N m^{-2} s^{-1} to 460 μg N m^{-2} s^{-1} for fertigation periods and from 0.6 μg N m^{-2} s^{-1} to 2 μg N m^{-2} s^{-1} for periods of no fertigation or irrigation, which indicates that a significant fraction

of NH_3 loss occurs as a result of direct volatilization of NH_3 during fertigation. Overall, the average NH_3 flux during fertigation periods was 10% of N applied as fertilizer.

4.2 Introduction

The increasing use of synthetic nitrogen (N) fertilizers has led to an altered N cycle and doubled amount of fixed N entering the biosphere (Vitousek *et al.*, 2000). There are uncertainties in the magnitude of N emissions from various sources, including intensively managed croplands. Up to 50% of the applied N to croplands can be lost, with gaseous emissions being the dominant N loss mechanism (IFA, 2001). It is important to quantify and understand the factors that control ammonia (NH_3) and nitrous oxide (N_2O) emissions because they pose negative effects to human health and the environment. Ammonia reacts rapidly with both sulfuric and nitric acids in the atmosphere to form fine particles, which cause health problems, reduce visibility, cause acid deposition, and perturb the earth's radiation balance (Pandis, 1995). Nitrous oxide is a potent greenhouse gas which ranks just below carbon dioxide and methane in global warming concerns.

In this research, emissions of NH_3 and N_2O from potato fields in central Washington (WA) were measured during the 2007 and 2008 growing seasons (June – August). A short-path differential optical absorption spectroscopy (DOAS) instrument (Mount *et al*., 2002) that operates in the 200-240 nm wavelength range was used to measure NH_3 concentrations. During some measurements, sulfur hexafluoride (SF_6) tracer gas was released from the center of the fields and concentrations were measured along a crosswind sample line downwind of the fields to help characterize local dispersion conditions. A Gaussian plume dispersion model (SIMFLUX) was used, along with the SF_6 tracer data, in an inverse approach to estimate NH_3 emission rates. A static chamber flux method was used to measure N_2O emissions with sample analysis via electron capture gas chromatography (ECD-GC).

The data collected will help improve CropSyst, a one-dimensional process-oriented model developed to simulate gaseous N emissions from various crop fields (Stockle, 1994). CropSyst is aimed to assist farmers in better management practices. The data will also improve NH_3 emission estimates in the AIRPACT-3 regional air quality forecast system (Chen *et al*., 2008; http://www.lar.wsu.edu/airpact-3/).

4.3 Materials and Methods

4.3.1 Description of Research Location

Field studies were conducted in 2007 and 2008 to characterize trace gas fluxes from potato fields near Othello, Washington, US. Two fields were chosen based on their flatness (for ease of setting up the DOAS instrument) and to maximize the distance from other interfering sources of NH_3 and N_2O. Fields of grass seed and wheat, which are not typically managed with high inputs of N fertilizers, surrounded the two potato fields. The crop rotation for both fields was grass seed - wheat - potatoes. The field used in summer 2007 was planted with ranger russet potatoes and the field used in summer 2008 was planted with premier russet potatoes.

Field preparation included deep ripping and disk plowing of the soil and ground rig fumigation during winter. Deep ripping and disk plowing were conducted to break up traffic-induced or naturally occurring compaction layers and to increase soil moisture. In addition, potassium (K) and phosphorous (P) were applied. In the spring, a chisel chopper was used to loosen and plant (seed) the soil. A rod weeder was used to kill weeds before plant emergence. Between two to six weeks after planting, the potato plants emerged from the ground and irrigation (application of water only) began. The plants began to grow tubers a few weeks after emergence. A dense, green canopy from approximately June to August was maintained. Heavy

N fertilizer application began in early July. The potatoes were harvested during the first weeks of October, depending on the type of potato planted.

A center-pivot irrigation system that rotated in a clockwise fashion was used for irrigation and fertigation (application of water with N fertilizer). The timing and rate of irrigation and fertigation varied from day to day and between the two fields, under the discretion of the farmer. The type of fertilizer used was UAN solution 32, which contains 25% nitrate-N, 25% ammonium-N, and 50% urea-N. During days of N_2O and NH_3 measurements, 2.7 kg of N was applied per acre per full 360° rotation. There were two rates for sprinkler rotation: 12 deg hr^{-1} and 18 deg hr^{-1}. For calculations of the N fertilizer application rates, see Appendix C (section C.1). Table 4.1 summarizes the schedule and rate of irrigation, fertigation, and chemigation (application of pesticides) for all days of NH_3 measurement.

Table 4.1: Schedule and rate of application for days of NH_3 measurement

Date/Time (PDT)	Application Status	Rate of Sprinkler Rotation (deg hr^{-1})
12 am on 7/07/07 to 6 am on 7/10/07	Fertigation	12
6 am on 07/10/07 to 6 pm on 07/10/07	Nothing	--
6 pm on 7/10/07 to 3 pm on 7/17/07	Fertigation	12
3 pm on 7/17/07 to 3 am on 07/18/07	Chemigation	30
3 am on 07/18/07 to 5 am on 07/19/07	Fertigation	12
5 am on 07/19/07 to 4 pm on 07/19/07	Nothing	--
5 am on 7/22/08 to 5 am on 7/24/08	Fertigation	18
5 am on 7/24/08 to 5 am on 7/25/08	Nothing	--
5 am on 7/25/08 to 5 am on 7/27/08	Fertigation	18
5 am on 7/27/08 to 5 am on 7/28/08	Nothing	--
5 am to 7:30 am on 7/28/08	Fertigation	18
7:30 am to 4 pm on 7/28/08	Irrigation	18
4 pm on 7/28/08 to 4 am on 7/29/08	Irrigation	12
after 4 am on 7/29/08	Nothing	--

The growing period was characterized by clear skies, high daytime temperatures, and cool nights. The average rainfall in the area was 150 mm so the potato plants were highly dependent on irrigation. Quincy fine sand soils are dominant in the fields, where anaerobic conditions are easily maintained for long periods of time. The measured bulk density of the surface soil (0–10 cm) was 1.24 Mg m^{-3}. The soil porosity and pH were 0.53 and 6.6, respectively.

4.3.2 Field Setup

Figure 4.1 is a diagram of the field setup. Southwest winds were dominant. Thus, the DOAS measurement path (path from the spectrograph to the retro-reflectors) was setup along the northeast edge of the potato fields to capture the NH_3 plume as it traveled along the wind trajectory. Path lengths varied from ~150 to ~250 m. Dispersion studies were conducted to characterize local dispersion conditions. Sulfur hexafluoride was used as a tracer gas and was released as a point source at the center of the fields. The trace gas analytical profile system (TGAPS) and syringe samplers were set up along the DOAS measurement path and extended over a distance of 800 m so that ideally the entire plume of SF_6 would be captured.

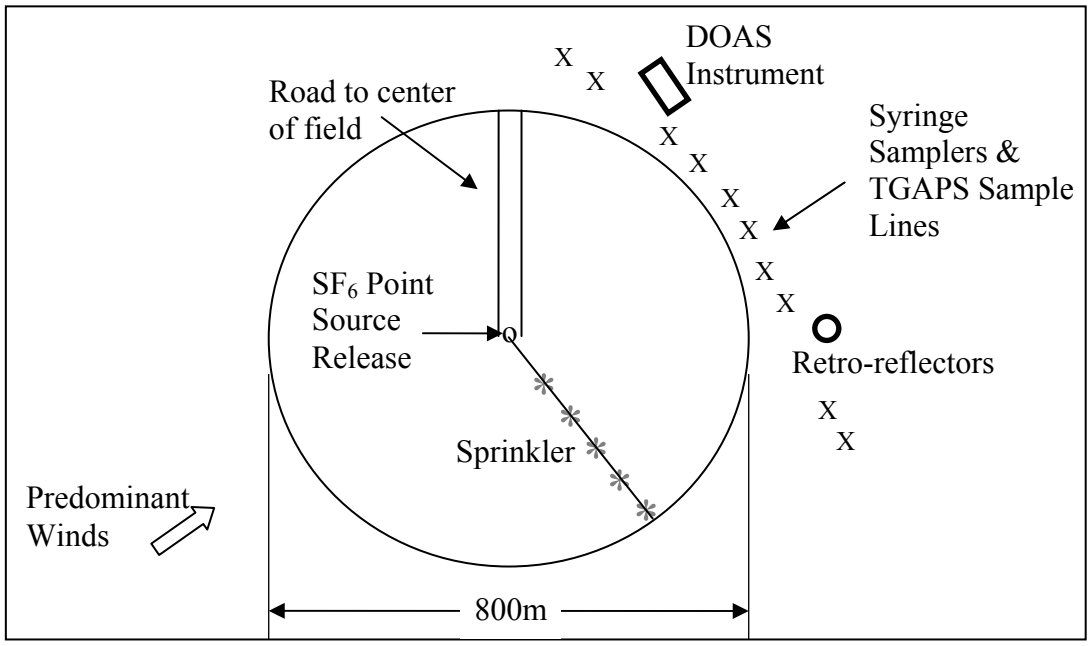

Figure 4.1: Diagram of the field setup

4.3.3 Measurement of Nitrous Oxide Concentrations and Flux Rates

Fluxes of N_2O were measured using the static closed chamber method (Hutchinson and Mosier, 1981). Chambers were installed between potato plant rows and sampled according to USDA-ARS GRACEnet (Greenhouse gas Reduction through Agricultural Carbon Enhancement network) protocols (USDA-ARS, 2003; www.GRACEnet.usda.gov). Chamber bases were made from 30.5 cm inner diameter x 15 cm high polyvinyl chloride (PVC) cylinders. The bases were inserted 10 cm into the soil and at least 24 hours prior to sampling to allow for stabilization. Chamber lids (30.5 cm inner diameter and 7.5 cm high) each contained a built-in vent tube, an internal fan, and a sampling port.

Air samples (about 30 ml each) from within the chambers were collected every 15 minutes over a period of 1 hour after covering the chambers. Gas sampling was performed 0 to 6.5 hours after fertigation and irrigation events. A Hewlett-Packard 5890 GC (Hewlett Packard, Palo Alto, CA) with an isothermal (40 °C) Alltech Porapak Q (80/100) column and an Electron Capture Detector (ECD) was used for analysis of air samples for N_2O concentrations. The carrier gas was 95% Argon (Ar) and 5% methane (CH_4). The GC flow rate ranged from 24.5 to 25.5 standard cubic centimeters per minute (sccm) and was maintained using an Alltech Digital Check Flow Meter. A 777 ppbv ± 10% (Scott-Marrin) N_2O standard was analyzed multiple times each day to determine analytical uncertainties. All samples were analyzed within a day of collection and approximately 10% of all the samples were reanalyzed during each analytical period for QA/QC purposes. Nitrous oxide flux rates were calculated using the slope of the gas concentration over time within the chamber as described by Hutchinson and Mosier (1981).

Table 4.2 summarizes the dates, time periods, and application status for all days of N_2O flux measurement. Nitrous oxide flux rates measured on days of no irrigation or fertigation were found negligible and are not included in the table.

Table 4.2: Summary of chamber measurements

Date	Time (PDT)	Application Status	Chamber No.
7/09/07	1 pm to 2 pm	water w/ N fertilizer	1, 2
7/11/07	8:45 am to 9:45 am	water w/ N fertilizer	4
7/11/07	1:45 pm to 2:45 pm	water w/ N fertilizer	5, 6, 7, 8
7/17/07	9:15 am to 2:45 pm	water w/ N fertilizer	9
6/20/08	12:10 pm to 5:10 pm	water only	10
6/21/08	9:45 am to 3:15 pm	water only	11, 12, 13
7/22/08	9:45 am to 3:15 pm	water w/ N fertilizer	14

4.3.4 Measurement of Ammonia

Atmospheric NH_3 concentrations were measured using an open path DOAS instrument. The instrument measures the photo-absorption of NH_3 in the mid-ultraviolet from 200 to 240 nm, and consists of the following parts: a 150 W Xenon lamp as a (UV) light source, a telescope to beam the UV light into the measurement path, retro- reflectors to direct the light back towards the telescope, optics to focus the light onto a spectrograph, a double crossed Czerny-Turner spectrograph, and a detector (Mount *et al*., 2002). For measurements made in summer 2007, the instrument was housed in a trailer and contained a multiplexing detector (Reticon). Details are described in Mount *et al*. (2002). A revised configuration of the instrument was used in the summer 2008 measurements, which is more compact, easier to maneuver in the fields, utilizes a charge coupled device (CCD) detector, and employs a PC laptop for control of the system (instead of a Macintosh IIfx used for the original version). A schematic and picture of the revised DOAS instrument are shown in Figures 4.2 and 4.3, respectively.

The optics setup is similar to the setup of the original instrument but the spectrograph is placed below instead of to the side of the second folding mirror. In addition, the primary mirror is only 32 cm in diameter (instead of 40 cm) which allows for a more compact design. The revised system uses a Princeton Instruments CCD detector system (spec-10:400B) with 1340 x 400 array (pixel size of 19.4 μm square).

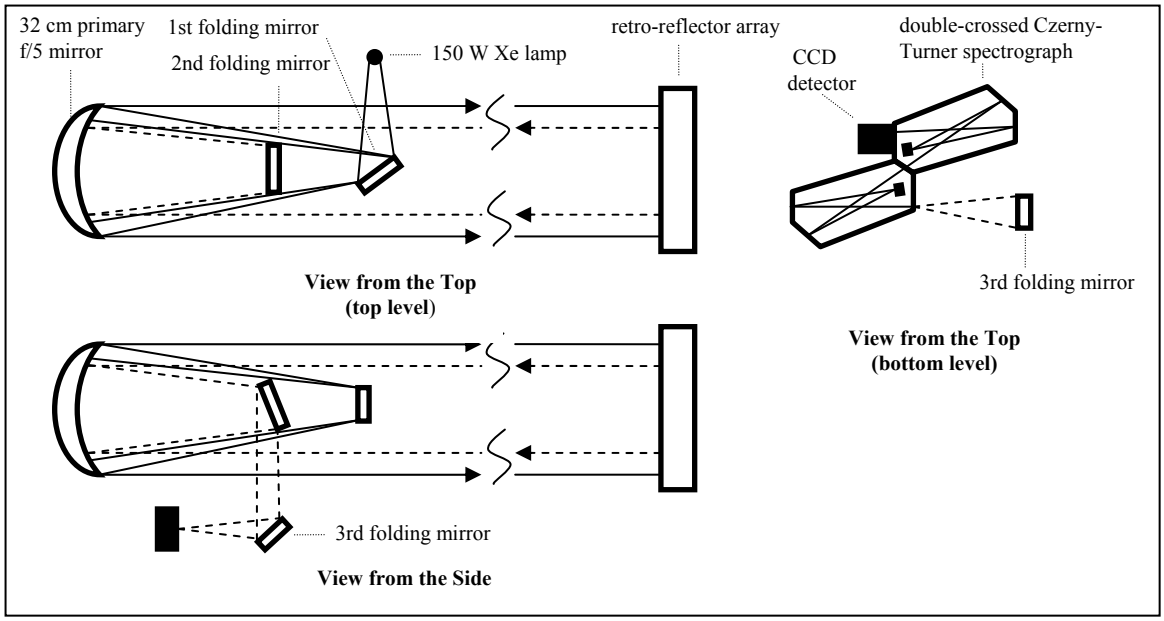

Figure 4.2: Schematic drawing of the revised DOAS instrument showing the optical light path from the Xe lamp to the CCD detector.

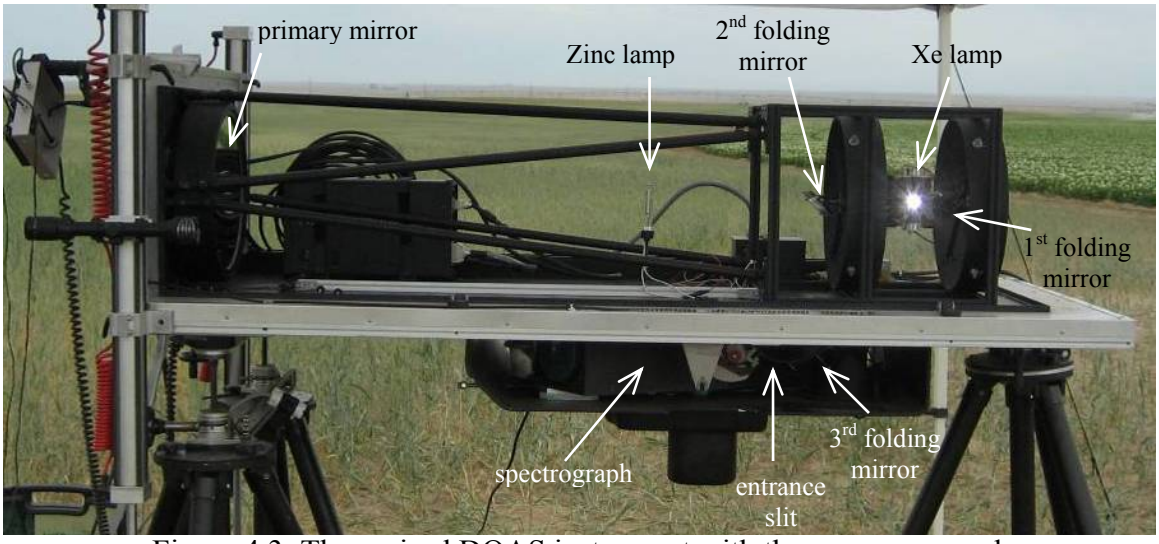

Figure 4.3: The revised DOAS instrument with the cover removed.

During data collection, the instrument was aligned towards the retro-reflectors so that the return signal counts were maximized. The integration time, which depends on the path length, was varied so that the maximum count rate was about 30,000 to 40,000 counts per integration time. Spectra were co-added so that data were averaged over five minute intervals. Electronic noise (dark spectra) of the instrument system was measured every hour, co-added and averaged, and subtracted from the actual spectra measured. A zinc (Zn) emission lamp was placed in front of the entrance slit every hour to provide a strong spectral fiducial at 213.9 nm. A nonlinear least squares fitting method, which accounts for Rayleigh and Mie scattering as well as the shift and stretch of the spectra, was used for data analysis.

4.3.5 Sulfur Hexafluoride Tracer Studies

During some NH_3 measurements, SF_6 tracer studies were conducted to help characterize local dispersion conditions. Sulfur hexafluoride is ideal for tracer studies because it is inert, its concentration can be measured with satisfactory accuracy at very low concentrations, and ambient concentrations of SF_6 are negligible. Even though SF_6 has a higher molecular weight (146.06 g mol^{-1}) than NH_3 (17.03 g mol^{-1}), the effect of this is negligible since turbulent

diffusion is the dominant transport mechanism (Kaharabata *et al.,* 2000). Pure SF_6 was released from a single point at the center of the fields at rates ranging from ~0.6 to ~0.7 L min^{-1}. Sulfur hexafluoride concentrations were measured at several points along and beyond the DOAS integration path using a Trace Gas Automated Profiling System (TGAPS) and portable syringe samplers. The total length covered by the TGAPS sampling locations and syringe samplers was greater than 800 m, which was typically long enough to capture background concentrations outside of the plume. Continuous 5-minute average concentrations of SF_6 were measured through TGAPS sample lines at 7 locations. For more information on the TGAPS system, refer to Flaherty *et al.* (2007). Programmable and battery-operated syringe samplers measured 30-minute average SF_6 concentrations. All samples were analyzed using a HP 5890 GC with an ECD detector coupled with an electronic integrator (Benner and Lamb, 1985). Scott-Marrin (Riverside, CA) SF_6 standards with ±5% certified accuracy were used for calibration of the GC.

4.3.6 Inverse Gaussian Plume Model (SIMFLUX) for Estimating Ammonia Flux Rates

A Gaussian plume dispersion model (SIMFLUX) (Howard *et al.,* 1996) was used in an inverse approach to estimate NH_3 emission rates. For fertigation periods, the sprinkler arm was modeled as an array of point sources in a rectangular area (10 m by 400 m). For periods of no fertigation or irrigation, the entire potato field was modeled as an array of point sources in a circle (400 m radius). The DOAS measurement path was modeled as a line of point receptors. All point sources and receptors were spaced 1 m apart. Measured variables, including wind speed and wind direction, were input into the Gaussian plume equation. Analytical equations (Martin, 1976) that represent the Pasquill-Gifford diffusion curves provided the best match for the tracer studies conducted and, thus, were employed for estimating the vertical and horizontal dispersion. The contributions from each point source were summed to estimate the concentration

at each downwind receptor. Ammonia flux rates were calculated from the average predicted NH_3 concentration based upon a point source release of 1 g s^{-1} $point^{-1}$ and the measured DOAS NH_3 concentration.

A set of criteria was developed to determine which periods of NH_3 measurements were suitable for estimating NH_3 flux rates using SIMFLUX. Only periods associated with wind speeds greater than 1 m s^{-1}, mean winds pointed towards the DOAS measurement path, wind direction standard deviations less than 30 degrees, and measured NH_3 concentrations greater than the detection limit of 10 ppbv for 2008 and 5 ppbv for 2007 were used. For periods of low wind speeds and high variation in wind direction, the theoretical basis of the Gaussian plume dispersion model becomes invalid (see Figure C.16 in Appendix C for determination of cutoff values).

Howard *et al*. (1996) discovered that significant errors result if a receptor is placed too far crosswind from the plume centerline. As a result, only periods that captured a significant portion of the NH_3 plume were used for estimation of flux rates. For each measurement period, SIMFLUX was used to determine the plume width along the extended DOAS measurement position. The portion of the NH_3 plume captured was calculated by determining the ratio of the area of the plume measured and the area of the entire plume predicted.

4.3.7 Measuring Meteorological Variables

Meteorological information such as wind velocity and air temperature were measured using a sonic anemometer at 10 Hz frequency located near the DOAS instrument. Soil moisture and temperature were measured using Campbell Scientific Inc. CS515s Water Content Reflectometers and copper/constantan thermocouples, respectively. Campbell Scientific CR10 data loggers were used to record data. Leaf stomatal conductance was measured using Decagon

Devices Hand Held Leaf Porometer. The water filled pore space (WFPS) was calculated as the ratio of the volumetric water content and soil porosity.

4.4 RESULTS

4.4.1 Nitrous Oxide Flux Rates

The key factors affecting N_2O emissions from the potato fields were soil WFPS, soil temperature, and time after fertilizer application. Figure 4.4 is a plot of all measured N_2O flux rates as a function of time after the sprinkler has passed for irrigation and fertigation periods. Individual plots for 7/17/07, 6/20/08, 6/21/08, and 7/22/08 (days when at least 4 hours of sampling were conducted per chamber) can be found in Figures B.1, B.2, B.3, and B.4 in Appendix B. As shown in Figure 4.4, N_2O flux rates ranged from zero to 120 μg N_2O m^{-2} s^{-1} and from zero to 290 μg N_2O m^{-2} s^{-1} immediately after irrigation and fertigation periods, respectively. The average N_2O flux rate for all measurements was 74 μg N_2O m^{-2} s^{-1} with a standard deviation of 73 μg N_2O m^{-2} s^{-1} and a median of 55 μg N_2O m^{-2} s^{-1}. The average N_2O flux rate after fertigation was 97 μg N_2O m^{-2} s^{-1} (standard deviation of 92 μg N_2O m^{-2} s^{-1}, median of 61 μg N_2O m^{-2} s^{-1}). The average N_2O flux rate after irrigation was 53 μg N_2O m^{-2} s^{-1} (standard deviation of 42 μg N_2O m^{-2} s^{-1}, median of 45 μg N_2O m^{-2} s^{-1}). Generally N_2O flux rates peaked between 2.5 to 3.5 hours after passing of the sprinkler arm. As expected, the maximum measured N_2O flux rate occurred during fertigation since the N inputs to the soil increased the amount of N available for nitrification and denitrification.

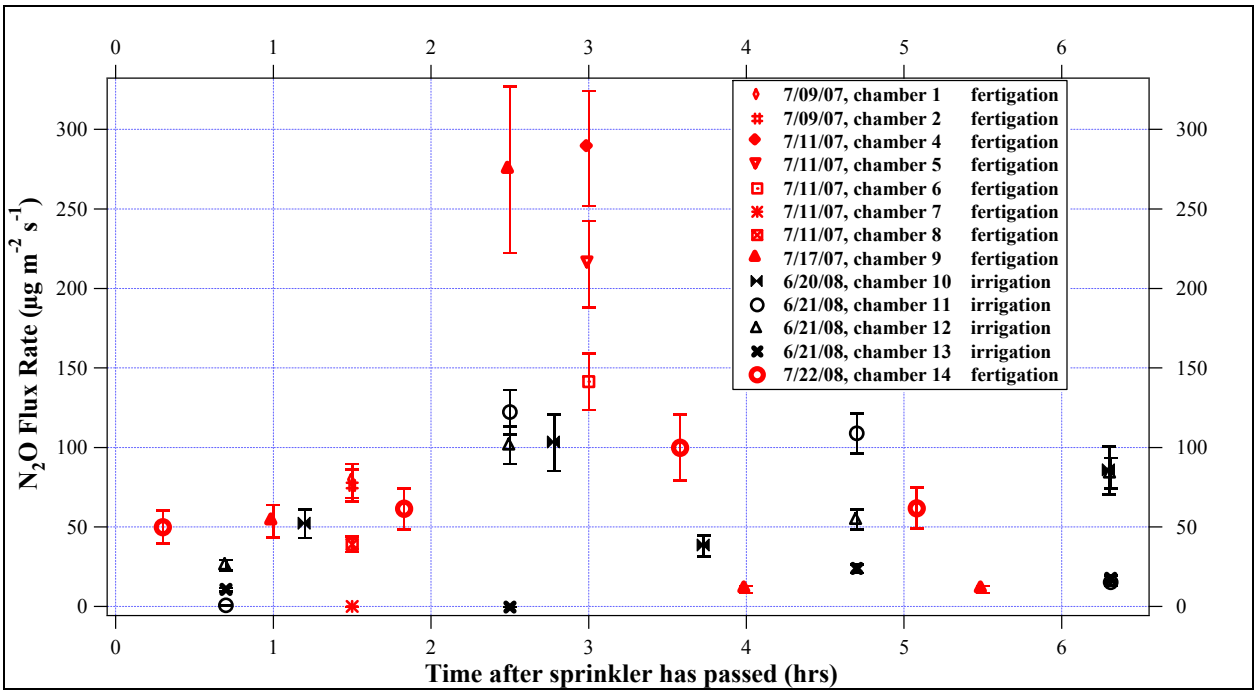

Figure 4.4: Nitrous oxide flux rates as a function of time after the sprinkler has passed (hrs) with water only (black) or water w/ N fertilizer (red).

Nitrous oxide flux rates as a function of soil surface temperature and soil WFPS are plotted in Figures 4.5 and 4.6, respectively. The soil WFPS ranged from 68% to 87%, and soil surface temperatures ranged from 14 °C to 29 °C. The greatest N_2O flux rate occurred when the soil surface temperature was 19 °C and the soil WFPS was 73%. Fertigation and irrigation events combined with the ability of the fine-textured soil to hold water tightly resulted in anaerobic soil conditions, thus allowing denitrification activity to occur. There was no clear trend in N_2O flux rates as a function of soil surface temperature since soil denitrifiers are adapted to and capable of growing under a wide range of temperatures (Haverkort and MacKerron, 2000).

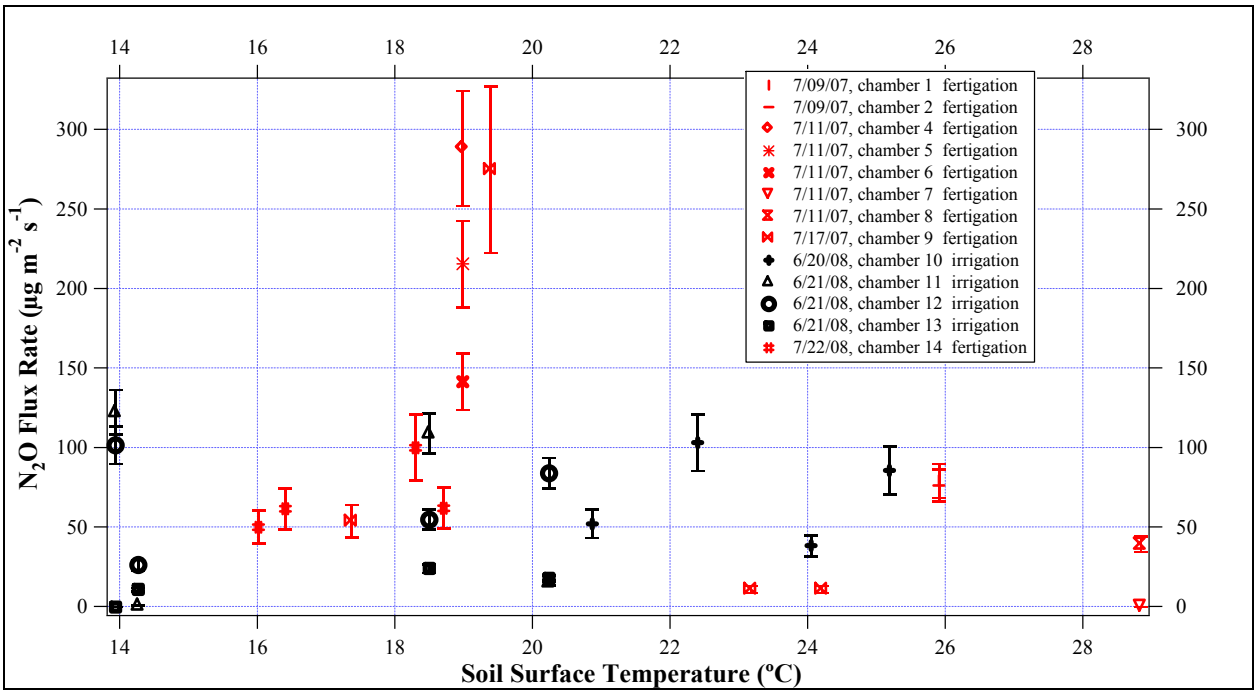

Figure 4.5: Nitrous oxide flux rates as a function of soil surface temperature. The gray and red data points represent periods of irrigation and fertigation, respectively.

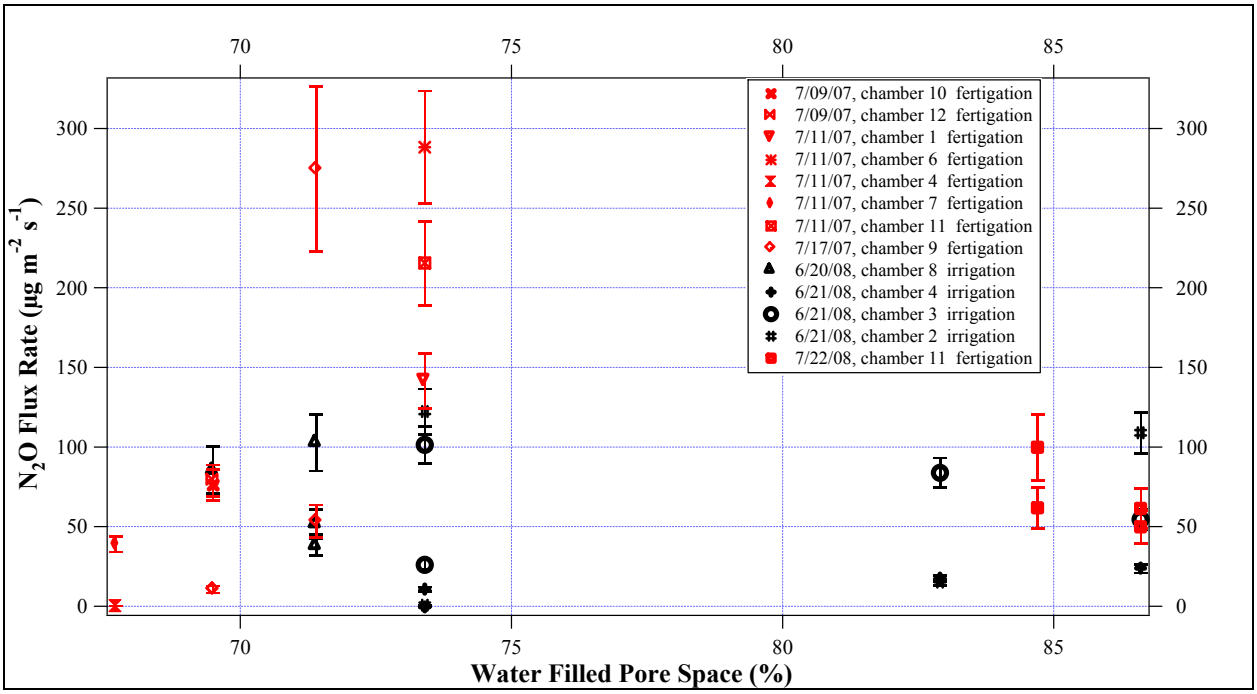

Figure 4.6: Nitrous oxide flux rates as a function of soil WFPS. The black and red data points represent periods of irrigation and fertigation, respectively.

Table 4.3 contains N_2O flux rates for fertigation periods with the corresponding fertilizer application rate and the amount of N lost. The amount of N lost as a function of amount applied ranged from zero to 12%, with a mean of 4%, which is comparable to documented emission factor (EF) values of 0.1 to 8% (Dobbie and Smith, 2003). The standard deviation was 3.9% and the median was 2.2%. Although denitrification activity was the main driver for observed N_2O fluxes, the bulk soil may not have been entirely anaerobic. Aerobic conditions may occur at the base of the plants where it is less compacted.

Table 4.3: Percent of N lost for days of N fertilizer application

Date	Chamber #	Fertilizer App. Rate ($\mu g\ N\ m^{-2}\ s^{-1}$)	N_2O Flux Rate ($\mu g\ N\ m^{-2}\ s^{-1}$)	% N Lost
7/9/2007	1	780	25	3.2
	2		24	3.1
7/11/2007	4		92	11.8
	5		68	8.8
	6		45	5.8
	7		0	0
	8		12	1.6
7/17/2007	9	780	17	2.2
			87	11.2
			3.4	0.44
			3.4	0.44
7/22/2008	14	1170	16	1.3
			19	1.7
			32	2.7
			20	1.7

4.4.2 Ammonia Concentrations

Measurements from 12:30 pm on 7/26/08 to 4:00 am on 7/27/08 (PDT) provide a good example of measured NH_3 concentrations. Figure 4.7 is a time-series plot of measured NH_3 concentrations, wind speed, wind direction, air temperature, and soil temperature (measured 8 inches below the surface). Figures 4.8 to 4.9 are polar plots illustrating the measured NH_3 concentrations as a function of sprinkler arm rotation angle (marked with circles) and wind

direction (marked with squares). Each polar plot shows the relationship between the location of the sprinkler arm relative to the DOAS measurement path and the magnitude of the measured NH_3 concentrations. Additional time-series plots and polar plots for the rest of the data can be found in Appendix C (Figures C.1 to C.15). Only NH_3 concentrations above the DOAS instrument detection limit (5 ppbv for 2007 and 10 ppbv for 2008) are shown in the polar plots.

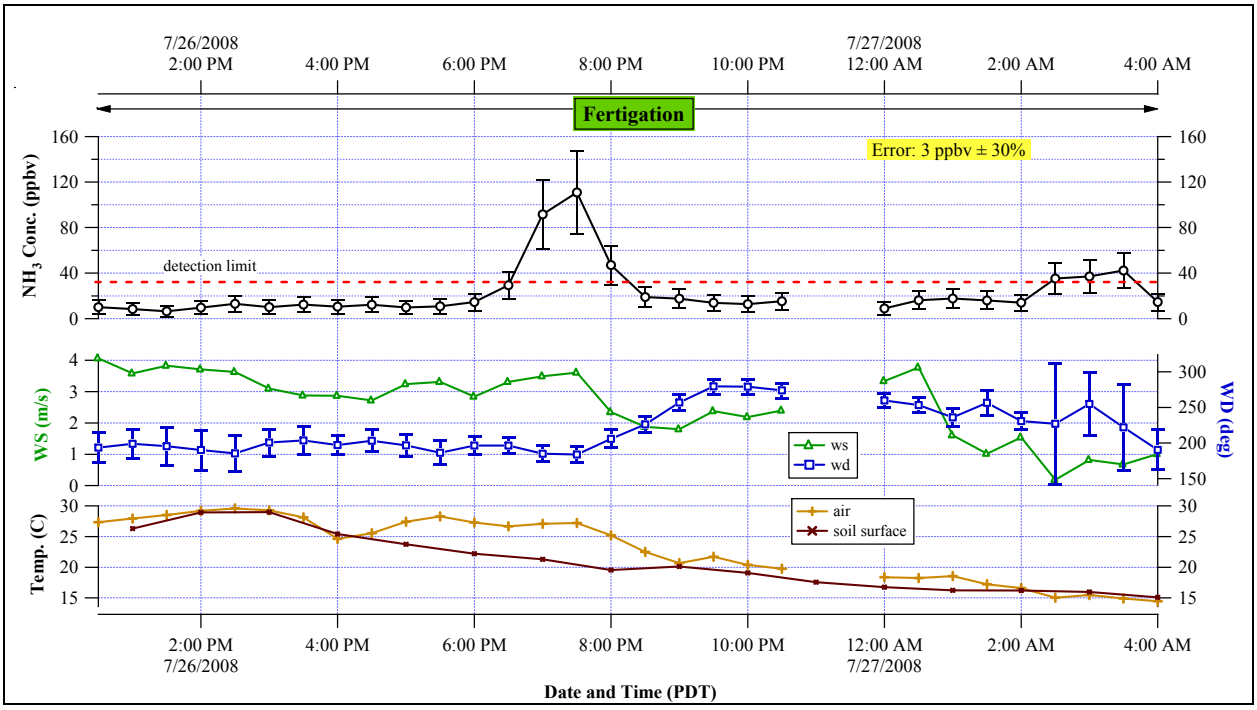

Figure 4.7: Time series plot of measured 30-minute average NH_3 concentration, wind speed, wind direction, air temperature, and soil surface temperature from 07/26/08 12:30 pm to 07/27/08 4 am (PDT). The red line signifies the NH_3 concentration detection limit of 10 ppbv. The bars on the wind direction data represent the 30-minute variation in wind direction (wind direction sigma).

From 12:30 pm to 5:30 pm on 7/26/08, the sprinkler arm was fertigating in the northwest quadrant of the field and west/southwest winds were dominant (Figure 4.8). The average wind speed was ~2.6 m s^{-1}. Since the sprinkler arm was far from the DOAS measurement path, lower

NH_3 concentrations were expected for this period. Measured NH_3 concentrations were only a few ppbv above the detection limit.

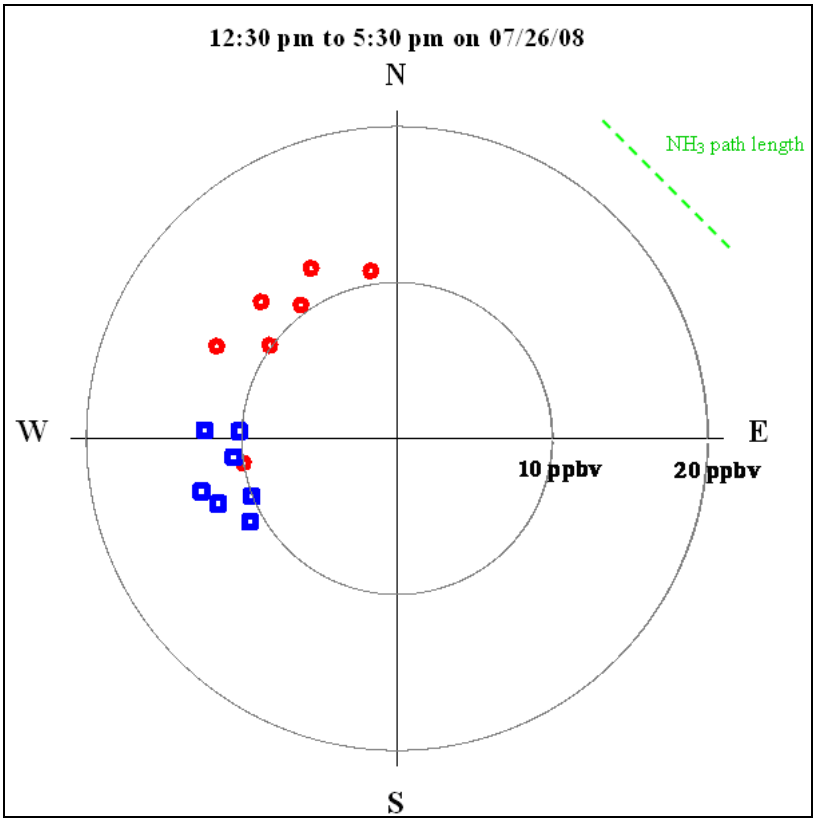

Figure 4.8: Polar plot of NH_3 concentration versus sprinkler arm rotation angle (red circles) and wind direction (blue squares) from 12:30 pm to 5:30 pm on 07/26/08 (PDT). All NH_3 concentrations below the detection limit (10 ppbv) have been omitted.

Measured NH_3 concentrations dramatically increased as the sprinkler arm got closer to the DOAS measurement path (Figure 4.9). The sprinkler arm was in the NE quadrant of the potato field from 6:30 pm to 10:30 pm on 7/26/08 (PDT). The maximum NH_3 concentration measured was ~115 ppbv and occurred around 7:30 pm on 7/26/08 (PDT). At this time, the sprinkler arm was pointed directly towards the DOAS measurement path and winds (~2 m s^{-1}) were coming from the west/southwest.

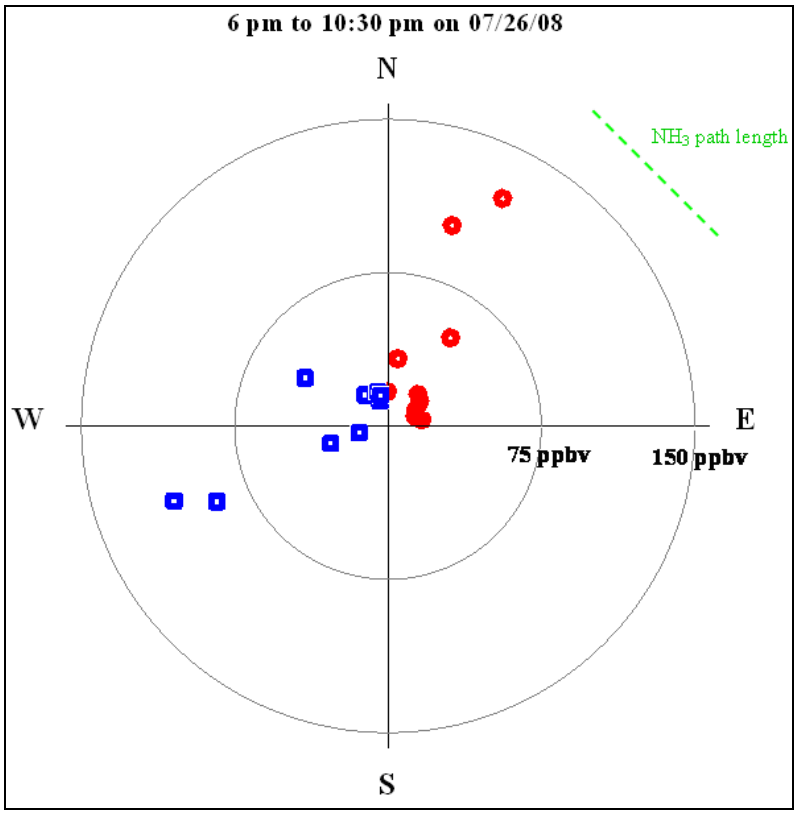

Figure 4.9: Polar plot of NH_3 concentration versus sprinkler arm rotation angle (red circles) and wind direction (blue squares) from 6 pm to 10:30 pm on 07/26/08 (PDT). All NH_3 concentrations below the detection limit (10 ppbv) have been omitted.

Results show that NH_3 concentrations (measured downwind of the potato field) depend on sprinkler arm location, wind speed, and wind direction. The highest NH_3 concentrations measured in the summer of 2007 and the summer of 2008 were ~34 ppbv and ~112 ppbv, respectively. Both peaks occurred during periods of fertigation with the sprinkler arm pointed directly towards the DOAS measurement path and winds greater than 1 m s^{-1} were blowing towards the DOAS measurement path. The field conditions for both days of peak NH_3 measurements are summarized in Table 4.4. The large difference between the two maximum values can be attributed to the greater rate of fertilizer application on 7/26/08 than on 7/18/07. In addition, the measured peak on 7/26/08 occurred at night whereas the measured peak on 7/18/07

occurred during the day. During the day, unstable conditions dominate whereas during the night, conditions are more stable and less mixing occurs.

Table 4.4: Field conditions for peak NH_3 concentrations

Date/Time (PDT)	NH_3 Conc. (ppbv)	N Fertilizer App. Rate ($\mu g\ NH_3\ m^{-2}\ s^{-1}$)	WS ($m\ s^{-1}$)	WD (deg)	DOAS path location	Air Temp. (°C)	Soil Temp. (°C)
7/18/07, 12 pm	~34	950	~3	240	NE quadrant	22.2	21.7
7/26/08, 7:30 pm	~110	1425	~2	251	NE quadrant	27.2	20.4

The relationship between measured NH_3 concentrations normalized by wind speed and the sprinkler arm rotation angle during fertigation periods are shown in Figure 4.10. Only measurements that were above the DOAS instrument detection limit and associated with wind direction variations less than 30 degrees and wind speeds greater than 1.0 $m\ s^{-1}$ are reported. As expected, when the DOAS measurement path was positioned along the SE quadrant of the field, the highest NH_3 concentration was measured when the sprinkler arm rotation angle was 180°, or due south. When the DOAS instrument was positioned along the NE quadrant of the field, the highest NH_3 concentration was measured when the sprinkler arm rotation angle was north-northeast (25°).

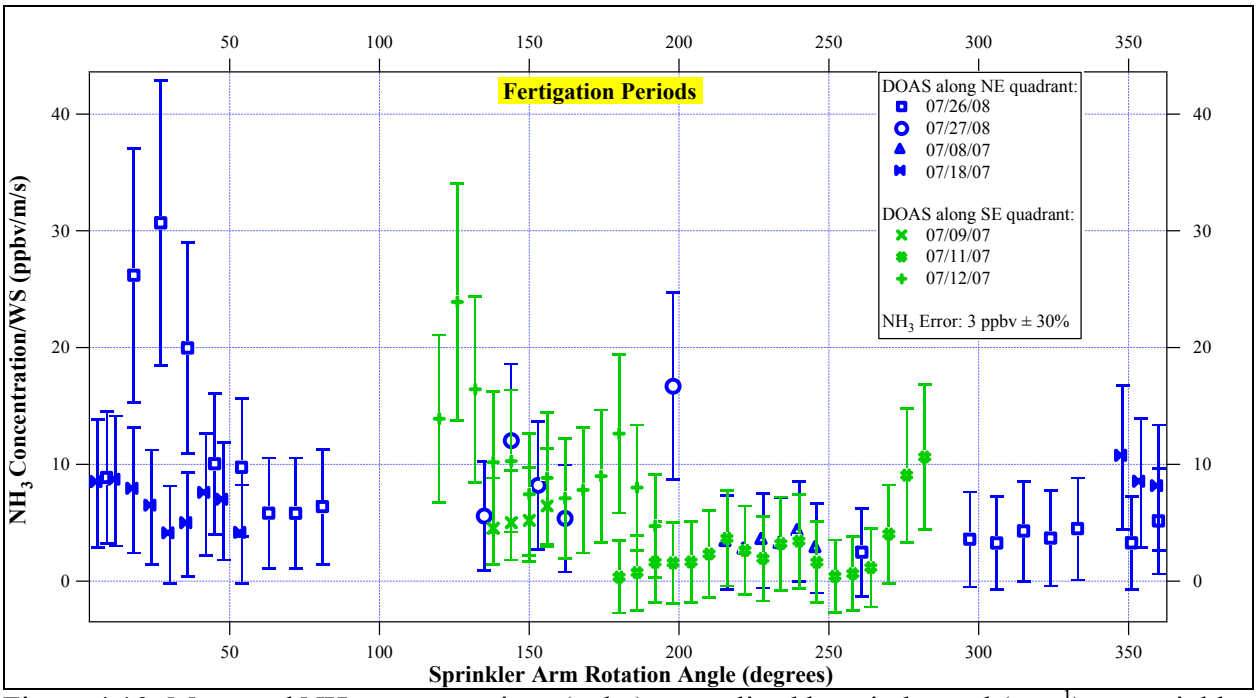

Figure 4.10: Measured NH_3 concentrations (ppbv) normalized by wind speed (m s^{-1}) vs. sprinkler arm rotation angle (degrees) during fertigation periods. The green and blue data points are periods when the DOAS measurement path was positioned along the SE and NE quadrants of the potato field, respectively.

4.4.3 Ammonia Flux Rates

Ammonia measurements were first investigated to determine which periods were suitable for use in estimation of flux rates. Data were separated into periods of fertigation and periods of no irrigation nor fertigation (made 1 day after the sprinkler arm stopped irrigating or fertigating). Fertigation periods were further separated by the position of the sprinkler arm relative to the DOAS measurement path. "Far" and "close" fertigation periods are associated with the sprinkler arm being far or pointed away from and close to or pointed towards the DOAS measurement path, respectively.

Figure 4.11 is a polar plot of 30-minute averaged NH_3 concentrations normalized by wind speed versus sprinkler arm rotation angle. Since wind speeds greatly influenced measurements (section 4.4.2), NH_3 concentrations were normalized by wind speed to remove the effect of the

variable. Ammonia concentrations normalized by wind speed were generally greater for "close" fertigation periods (4 ppbv m^{-1} s^{-1} to 11 ppbv m^{-1} s^{-1}) than for "far" fertigation periods (1.7 ppbv m^{-1} s^{-1} to 3.7 ppbv m^{-1} s^{-1}). The difference between the two groups was expected since point sources that were "close" to the DOAS measurement path dispersed less than "far" point sources. The magnitudes of measured NH_3 concentrations normalized by wind speed for periods of no irrigation/fertigation were comparable to measurements made during "far" fertigation periods.

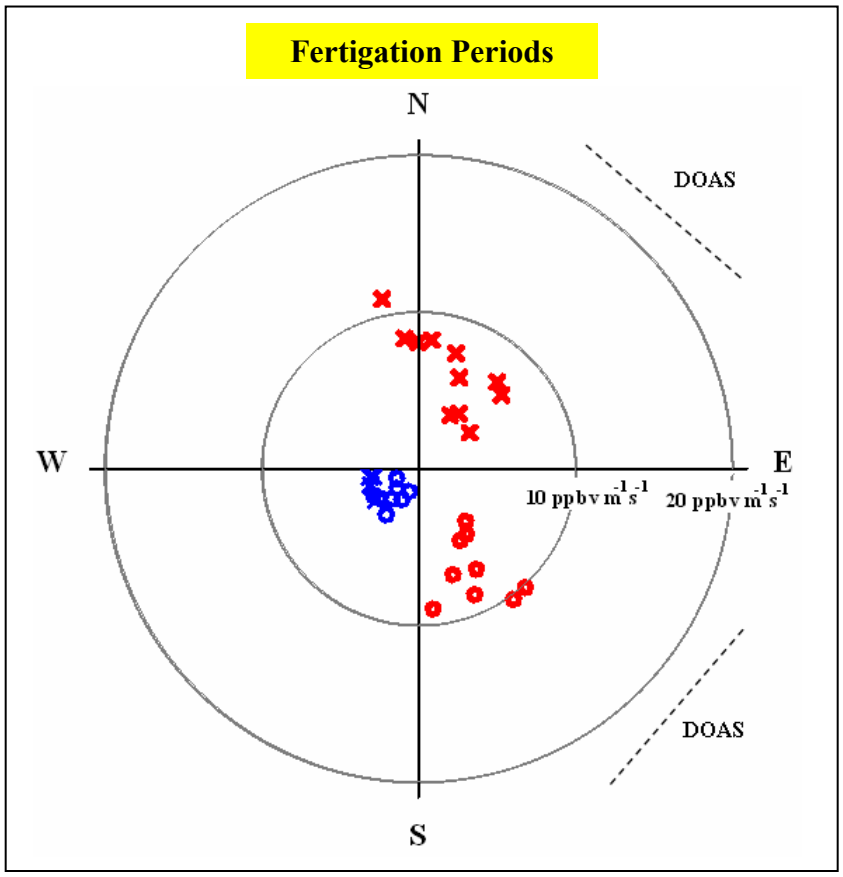

Figure 4.11: Polar plot of 30-min. averaged NH_3 concentrations (ppbv) normalized by wind speed (m s^{-1}) versus sprinkler arm rotation angle (degrees). Measurements made during "far" and "close" fertigation periods are in blue and red, respectively. Measurements made when the DOAS path was along the SE quadrant are marked as circles while measurements made when the DOAS path was along the NE quadrant are marked as x's.

Ammonia flux rates and percent NH_3 loss as a function of wind speed during fertigation periods and periods of fertigation/irrigation are plotted in Figures 4.12 and 4.13, respectively. Similar to NH_3 concentrations (section 4.4.2), NH_3 flux rates and NH_3 loss (ratio of NH_3 emission rate to NH_3 application rate) increased with increasing wind speed.

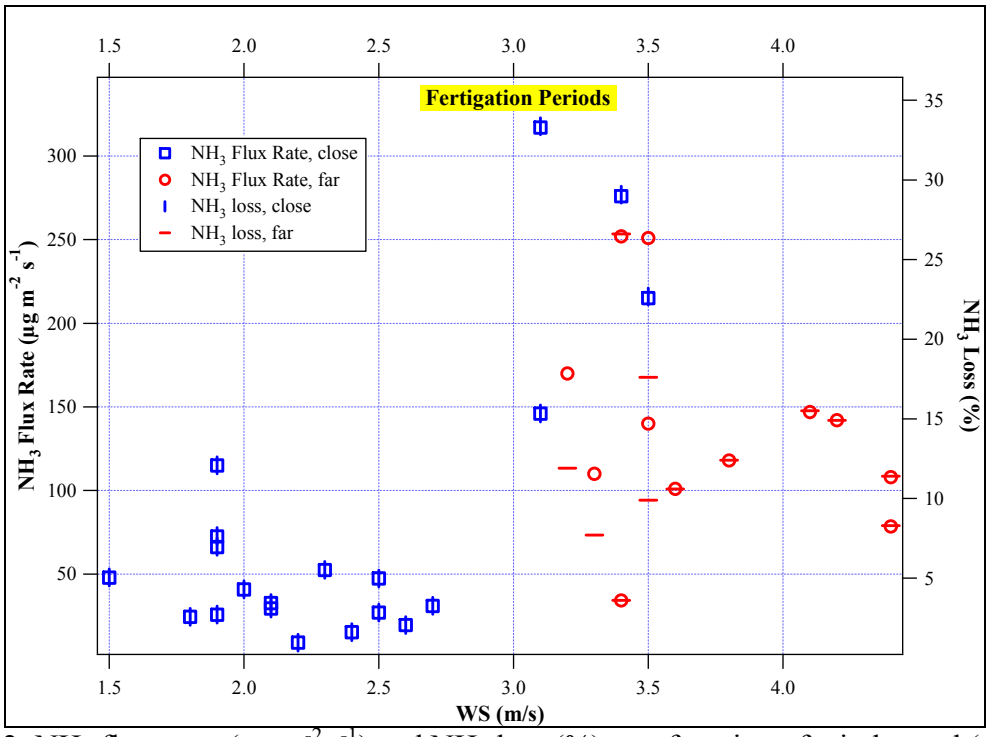

Figure 4.12: NH_3 flux rates (µg m^{-2} s^{-1}) and NH_3 loss (%) as a function of wind speed (m s^{-1}) measured during fertigation periods.

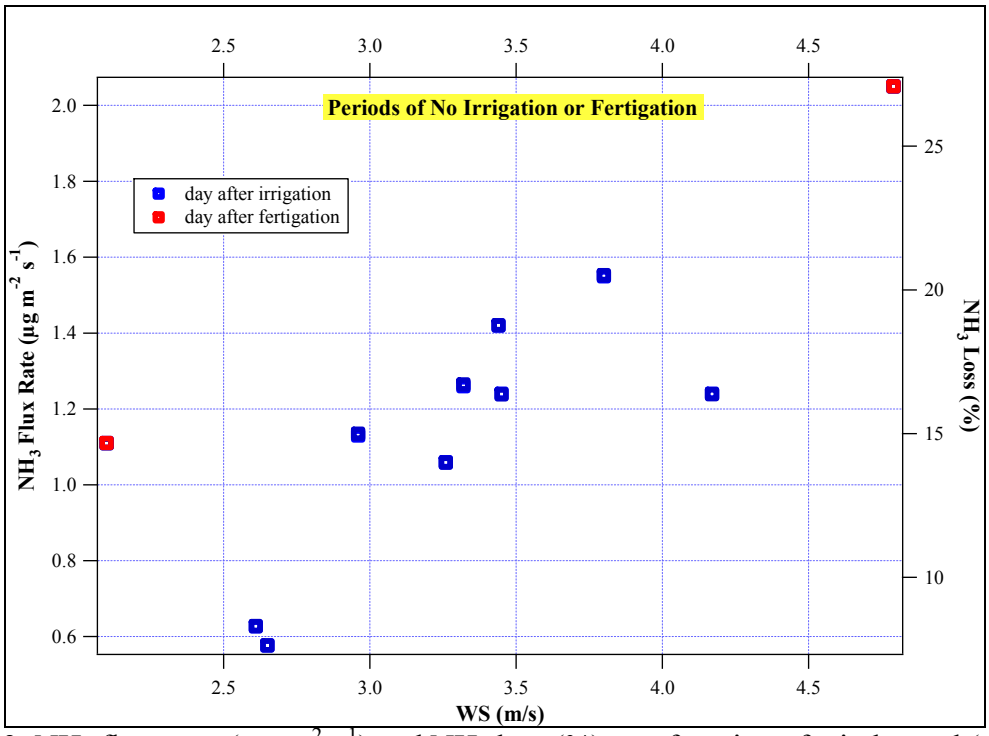

Figure 4.13: NH_3 flux rates (µg m^{-2} s^{-1}) and NH_3 loss (%) as a function of wind speed (m s^{-1}) measured one day after fertigation. Note the scale change from the previous figure.

The relationship between NH_3 flux rates and the portion of plume captured was investigated. The portion of plume captured for each 30-min sampling period was calculated by determining the ratio of the area of the plume measured to the area of the entire plume predicted, assuming both were Gaussian shaped plumes. Figures 4.14 and 4.15 are plots of NH_3 flux rates as a function of portion of the NH_3 plume captured by the DOAS measurement path for all fertigation periods and periods of no irrigation/fertigation, respectively. For "far" fertigation periods, 35% to 80% of the NH_3 plume was captured by the DOAS measurement path while 53% to 99% was captured for "close" fertigation periods. For periods when no irrigation/fertigation was applied, only 34% to 43% of the NH_3 plume was captured. There is no significant dependence of NH_3 flux rates with the percentage of plume captured for all of the periods, however, for fertigation periods, the flux rates tend to decrease with increasing percentage of plume captured. There is currently no plausible explanation for this.

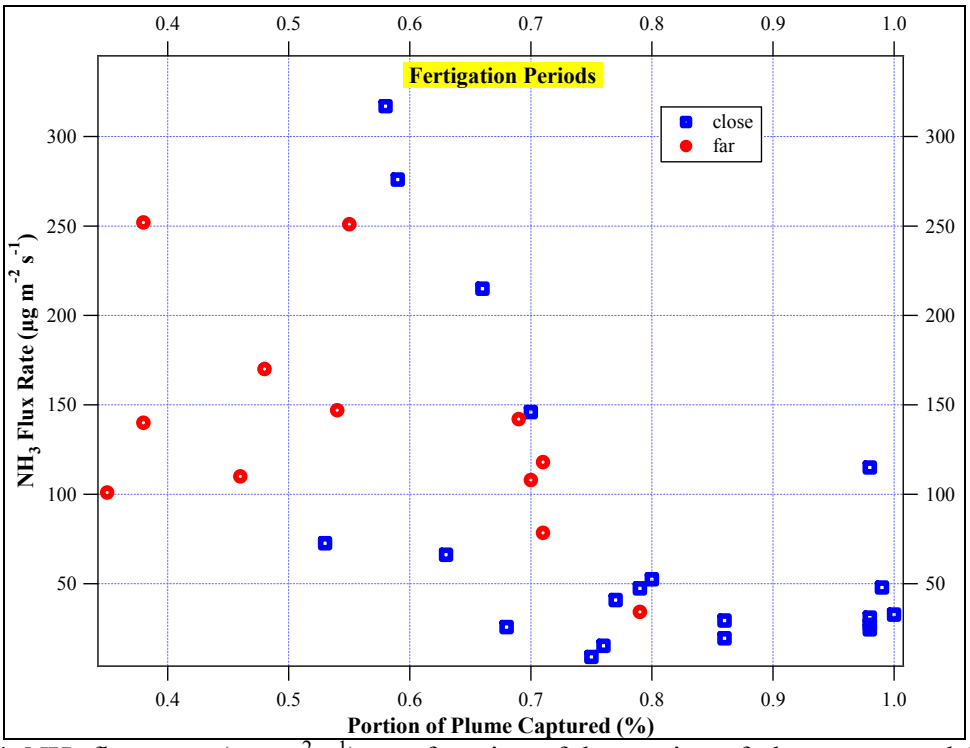

Figure 4.14: NH_3 flux rates (µg m^{-2} s^{-1}) as a function of the portion of plume captured (%) for fertigation periods.

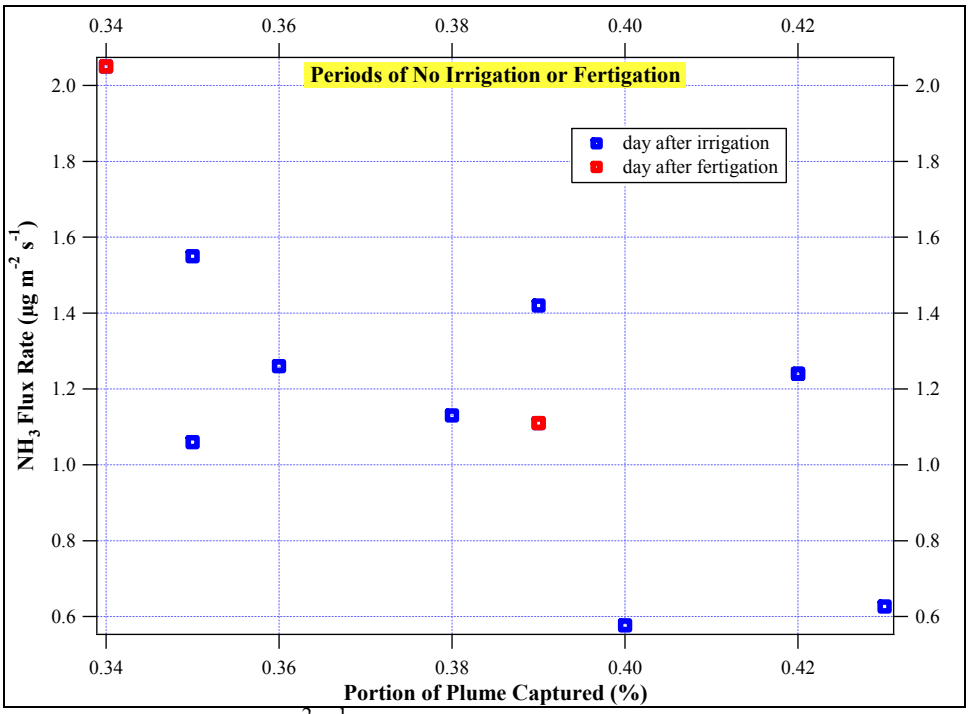

Figure 4.15: NH_3 flux rates (µg m^{-2} s^{-1}) as a function of the portion of plume captured (%) for periods of no irrigation/fertigation.

Other variables were investigated to see if they impacted NH_3 emission rates. The relationship between NH_3 flux rates and solar radiation, soil temperature, air temperature, and the time after the sprinkler arm passed the DOAS measurement path were investigated and no obvious trends were found. Periods used for estimation of NH_3 flux rates occurred between 10 am and 6 pm (PDT), when fluctuations in air and soil temperatures were small. Due to the limited range in air and soil temperatures, there was no obvious relationship between NH_3 concentrations and emissions and soil and air temperatures (see Figures C.21 to C.24 in Appendix C). For "far" fertigation periods, there was no dependence of NH_3 flux rates with the time after the sprinkler passed the DOAS measurement path (Figure 4.16).

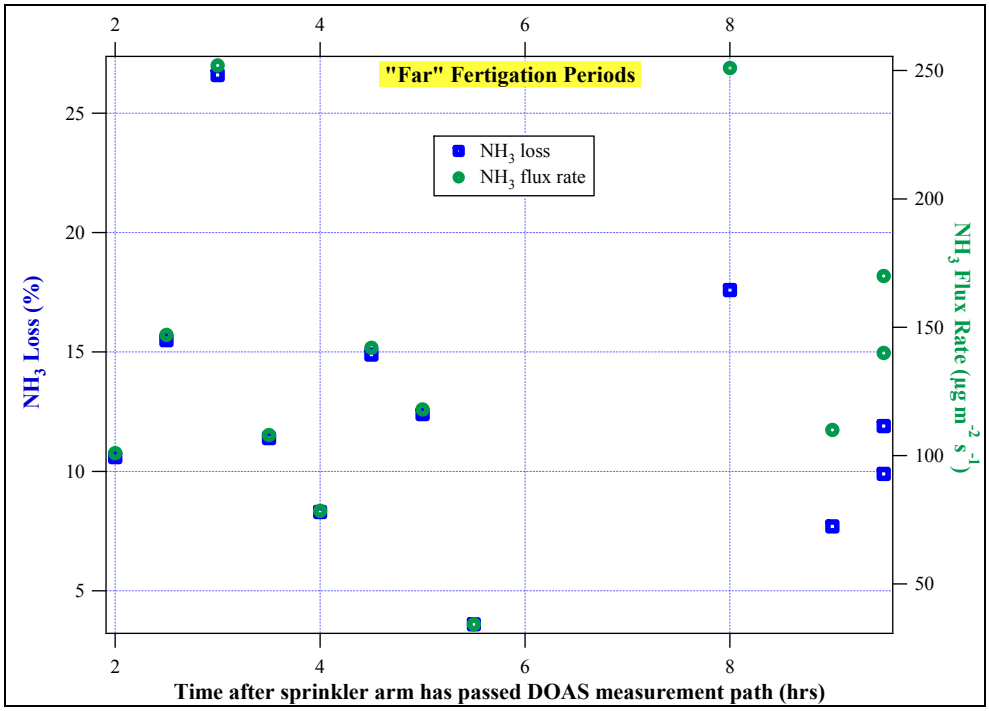

Figure 4.16: NH_3 flux rates and percent loss as a function of time after the sprinkler passed the DOAS measurement path for "far" fertigation periods.

Table 4.5 shows the range of measured NH_3 concentrations, estimated flux rates, and percent of NH_3 lost grouped by application status. The percent of NH_3 lost was calculated by dividing the estimated NH_3 flux rate by the fertilizer application rate. There was no irrigation period that met the criteria parameters and, thus, there are no calculations of flux rates and percent of NH_3 lost for irrigation periods. Estimated NH_3 flux rates ranged from 34 μg NH_3 m^{-2} s^{-1} to 250 μg NH_3 m^{-2} s^{-1} and from 9.1 μg NH_3 m^{-2} s^{-1} to 320 μg NH_3 m^{-2} s^{-1} during fertigation periods when the sprinkler arm was "far" and "close" to the DOAS measurement path, respectively. Higher normalized NH_3 concentrations were observed when the sprinkler arm was closer to the DOAS path. However, in estimating the flux rates, dispersion is taken into account and the variation in calculated flux rates is smaller. When there was no irrigation/fertigation, NH_3 flux rates varied from 0.6 μg NH_3 m^{-2} s^{-1} to 2.1 μg NH_3 m^{-2} s^{-1}.

Table 4.5: Range of measured NH_3 concentrations, estimated flux rates, and percent of NH_3 loss grouped by application status.

Application Status	**Measured NH_3 Conc. (ppbv)**	**Q (μg NH_3 m^{-2} s^{-1})**			**NH_3 Loss (%)**		
		Min	**Average**	**Max**	**Min**	**Avg.**	**Max**
No Irrigation or Fertigation	8.4 to 18.5	0.6	1.2	2.1	--	--	--
Fertigation (spray close to DOAS)	9.9 to 34.0	9.1	80	320	0.95	8.5	34
Fertigation (spray far from DOAS)	5.5 to 13.6	34	140	250	3.6	12.5	26.7

Ammonia loss during fertigation ranged from 0.95% to 48.4% (average of ~8% for "far" periods and ~12% for "close" periods). The frequency distribution of NH_3 flux rates during fertigation are shown in Figure 4.17. The average NH_3 flux rate during all fertigation periods was 100 μg m^{-2} s^{-1}. The standard deviation was ~84 μg m^{-2} s^{-1} and the median was ~75 μg m^{-2} s^{-1}.

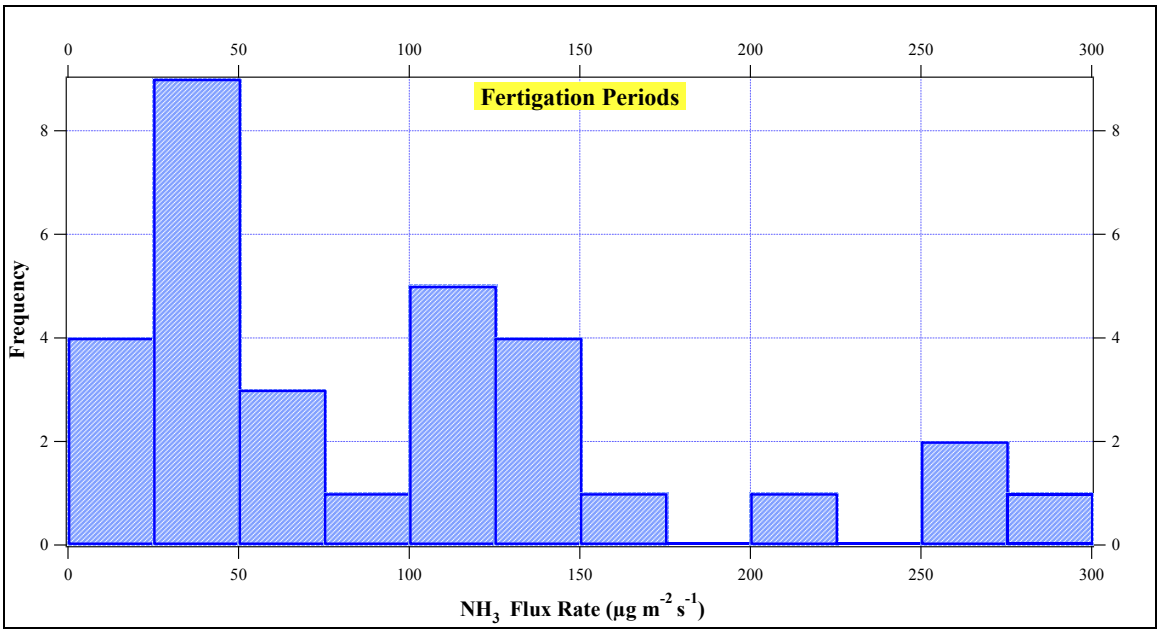

Figure 4.17: Frequency distribution of NH_3 flux rates during fertigation periods.

A total N loss of 47% was estimated for the entire period of heavy N fertigation (month of July). A total of 38% was lost through NH_3 emissions. For N lost as NH_3, the following assumptions were used:

- an average of 2.75 Mg of N (6050 lbs) total was applied to the potato fields
- the average NH_3 flux during irrigation was assumed to be 50% of the average NH_3 flux during fertigation
- the average NH_3 flux during periods of no irrigation nor fertigation was 1 µg m^{-2} s^{-1}
- daytime and nighttime flux rates are the same, even though flux rates were only calculated from daytime measurements
- the emissions during irrigation and fertigation were based on the 400 m by 10 m area underneath the sprinkler arm
- the emissions during periods with no irrigation nor fertigation were constant throughout the month (the decrease of emissions with time after fertigation was not accounted for).

Of the 38% N lost through NH_3 emissions, 27% of the applied N was lost during periods of no fertigation/irrigation while 8% was lost during fertigation and 3% was lost during irrigation. More was lost during no irrigation/fertigation periods than fertigation or irrigation periods because of the greater time period and area of emissions used for that calculation.

Table 4.6: Total N Loss through NH_3 Emissions for the month of July.

Application Status	**# Hours**	**Avg. Emission Rate (Q) ($\mu g\text{-}NH_3\ m^{-2}\ s^{-1}$)**	**Avg. Q ($\mu g\text{-}N\ m^{-2}\ s^{-1}$)**	**July N loss (kg-N)**	**% of Lost N (NH_3 Emissions)**
No Fertigation nor Irrigation	414	1.2	1	749	27%
Fertigation	180	100	84	218	8%
Irrigation	150	50	42	91	3%
				Total	**38%**

A total of 9% was lost through N_2O emissions. For N lost as N_2O the following assumptions were used:

- an average of 2.75 Mg of N (6050 lbs) total was applied to the potato fields
- the average N_2O flux after irrigation was assumed to be 100 $\mu g\ N_2O\ m^{-2}\ s^{-1}$
- the average N_2O flux after fertigation was assumed to be 50 $\mu g\ N_2O\ m^{-2}\ s^{-1}$
- N_2O flux rates on days of no irrigation nor fertigation were assumed negligible
- emission rates were assumed constant (no decrease with time)

Of the 9% N lost through N_2O emissions, 6% of the applied N was lost during fertigation and 3% was lost during irrigation.

Table 4.7: Total N Loss through N_2O Emissions for the month of July.

Application Status	**# Hours**	**Avg. Emission Rate (Q) (µg-N_2O m^{-2} s^{-1})**	**Avg. Q (µg-N m^{-2} s^{-1})**	**July N loss (kg-N)**	**% of Lost N (N_2O Emissions)**
No Fertigation nor Irrigation	414	0	0	0	0%
Fertigation	180	100	32	174	6%
Irrigation	150	50	16	72	3%
				Total	**9%**

4.5 Conclusions

Ammonia results show that as wind speeds increased, so did the measured NH_3 concentrations as well as estimated NH_3 flux rates and percent of NH_3 loss. Wind direction influenced measured NH_3 concentrations and, as a result, calculated flux rates for periods when winds blew towards the DOAS measurement path more accurately represent emission rates from the potato fields. There were no clear relationships between NH_3 emissions and solar radiation, soil and air temperature, and time after the sprinkler arm passed the DOAS measurement path.

Estimated NH_3 flux rates ranged from 9.1 µg NH_3 m^{-2} s^{-1} to 460 µg NH_3 m^{-2} s^{-1} for fertigation periods (average 100 µg NH_3 m^{-2} s^{-1}) and from 0.6 µg NH_3 m^{-2} s^{-1} to 2.1 µg NH_3 m^{-2} s^{-1} (average 1.2 µg NH_3 m^{-2} s^{-1}) for periods of no irrigation/fertigation which indicates that a significant fraction of NH_3 loss from these fields occurs as a result of direct volatilization of NH_3 during fertigation. The estimated NH_3 flux rates from this study are much higher than the standard rate of 0.01 µg NH_3 m^{-2} s^{-1} typically used for all crops when compiling global emission inventories (Bouwman *et al*., 1997), with the flux rate obviously dependent upon quantity of applied N. The amount of NH_3 loss ranged from 0.95% to 48% for fertigation periods (average 10%), which is comparable to reported NH_3 loss from other studies (range from 8 to 18% using micrometeorological methods and from zero to 45% using dynamic flow chambers) (IFA, 2001).

A total N loss of 47% was estimated for the entire period of heavy N fertigation (month of July). Of the 47% N lost, 38% was lost through NH_3 emissions and 9% was lost through N_2O emissions. Previous studies available in literature report similar total N loss in potato plants. Reported N loss under current best management practices has been reported to be ~35% of N applied (Lang *et al.,* 1999) with a mean of 60% (Balasubramanian *et al.,* 2004).

Nitrous oxide flux rates generally peaked between 2.5 and 3.5 hours after irrigation or fertigation and appeared to be a result of denitrification activity (soil WFPS ranged from 68% to 87%). Nitrous oxide flux rates ranged from negligible to 280 μg N_2O m^{-2} s^{-1} and are much higher than reported emission rates by Flessa *et al.* (2002), who reported mean N_2O emissions of 0.02 and 0.03 μg N_2O m^{-2} s^{-1} during the 1997 and 1998 growing periods of two adjacent potato fields in Germany using automated gas sampling chambers.

The average N loss as N_2O ranged from zero to 12% (average ~4%) of the applied N fertilizer which is comparable to documented EF values of 0.1 to 8% (Dobbie and Smith, 2003). The average N loss is much higher than that reported by Haile-Mariam *et al.* (2008), who reported N_2O losses of 0.3% of applied fertilizer in potato fields in central Washington during the 2005 and 2006 growing seasons using static chambers. Similar to the fields used in this study, the fields used by Haile-Mariam *et al.* (2008) were applied with UAN solution 32 through a center pivot irrigation system and aerobic soil conditions dominated in the fields.

CHAPTER 5

ERROR ANALYSIS

5.1 Uncertainties in NH_3 Measurements

There are various errors associated with the measurements of NH_3. Uncertainty in NH_3 measurements result from errors in the absolute NH_3 absorption cross section of ±20% (Mount *et al*., 2002). The error in residual analysis was approximately ±25% and was due to uncontrollable variations in the dark current (electronic noise of the system) caused by the external radiator used for temperature regulation of the CCD detector, which resulted in difficult subtraction of darks during data analysis. Other errors include changes in the spectral output of the Xe lamp which could not be monitored at high frequency and illumination problems on the system optics from atmospheric turbulence. The overall error in the NH_3 concentration data combining all of these uncertainties in quadrature is estimated to be ± 30% ± 3ppbv.

5.2 Uncertainties in NH_3 Flux Rates

The uncertainty in estimated NH_3 emission rates result from errors associated with the estimation of NH_3 concentrations as well as errors in SIMFLUX. SIMFLUX assumes uniform emission rates from all of the point sources within the field. Numerous factors (i.e. environmental factors, soil properties) regulate NH_3 loss from the soil and potato plants and these factors may not have been uniform throughout the field. During fertigation periods, only the area covered by the sprinkler arm was modeled (400 m by 10 m) as an NH_3 source. While other parts of the field contributed to NH_3 emissions, it was difficult to differentiate between direct volatilization from the spray of the sprinkler arm and the entire field.

There are also errors associated with the SF_6 tracer data used to calibrate the dispersion algorithm in SIMFLUX. During SF_6 tracer studies, the sources of error include changes in the SF_6 release rate, GC analysis (uncertainty in the gas standards ±5%), and error in duplicates. When compared with the SF_6 tracer studies, the equations by Martin (1976) for determining dispersion coefficients resulted in an average mean normalized gross error (MNGE) of 41% between predicted and observed SF_6 concentrations (Appendix A). The error in the NH_3 flux estimates is approximately ± 52%.

5.3 Uncertainties in N_2O Measurements

The uncertainty in N_2O measurements are derived from errors in chamber sampling and GC analysis. Errors associated with the GC analysis include the uncertainty in the gas standard utilized for the calibration of the voltage signal from the ECD (±10%) and the error in duplicate measurements (maximum error was ±18%). The total error ranged from ±11% to ±21%.

The errors associated with the chamber sampling cannot be quantified and include the uncertainty in the accuracy of volume measurements inside the chambers since soil surfaces were irregular. In addition, the concentration with time data was noisy and determination of flux rates required disregarding outliers based on judgment. Also, the number of measurements collected was not enough to capture the heterogeneity of N_2O emissions throughout the field. Other errors associated with chamber sampling should be minimal since installation and sampling of chambers were conducted according to the prudent guidelines of the USDA-ARS GRACEnet protocols (USDA-ARS, 2003). All samples were analyzed within a day of collection to prevent error due to leakage and approximately 10% of all the samples were reanalyzed during each analytical period to ensure data quality.

CHAPTER 6

CONCLUSIONS AND FUTURE WORK

There are limited studies that have measured the magnitude of Nitrogen (N) emissions from intensively managed croplands. It is important to understand the magnitude and factors controlling NH_3 and N_2O emissions because they pose negative effects to human health and the environment. In this research, concentrations and fluxes of ammonia (NH_3) and (N_2O) from potato fields in central Washington were measured during the 2007 and 2008 growing seasons (June – August).

Nitrous oxide fluxes were measured using a static chamber method and samples were analyzed using a GC-ECD. The chamber method was useful for investigating the processes controlling N_2O fluxes. However, the method made it difficult to extrapolate measured fluxes to field-scale estimates since there is a wide range of environmental conditions throughout the fields as well as a large variation in the soil properties.

This study is the first field experiment using the DOAS technique to measure NH_3 fluxes from potato fields. The DOAS technique proved to be an appropriate method for measuring NH_3 flux rates from the fields because it did not disturb the soil-plant-atmosphere pathway and it provided measurements integrated over a large area. However, NH_3 measurements were limited by the problems associated with the revised instrument (i.e. misalignment of mirrors, inability of the internal cooler within the CCD detector to regulate temperature), which disrupted data collection and decreased data quality. Correction of those problems will significantly enhance future measurements made by DOAS.

Suggested Future Work:

- Further improvement of the DOAS instrument (i.e. re-aligning of the mirrors, addition of an appropriate cooler to regulate temperature for the CCD detector) will improve future measurement quality and quantity.
- Measurements of NH_3 and other factors influencing emissions need to be made over a sufficiently longer time period so that the relationships between NH_3 emissions and influencing factors can be determined.
- The use of a relaxed-eddy accumulation technique (REA) concurrent with the DOAS technique would allow for continuous NH_3 flux measurements and provide complementary data to the current data set. (Zhu *et al.* (2000) have shown that the REA technique is successful in measuring NH_3 fluxes over a corn field.)
- Measurement of emissions from other potato fields under a different management practice. (The fields used in this study were continuously applied with small amounts of N fertilizer throughout the growing season. Other farmers apply large amounts of N fertilizer at one time only (i.e. at the beginning of the season)).
- Use of an automated system of chambers, which would allow for continuous, long-term measurements of N_2O and provide a better understanding of spatial and temporal variations in N_2O fluxes throughout the fields.

REFERENCES

Arya, S.P., 1999. Air Pollution Micrometeorology and Dispersion. Oxford University Press, Inc., New York, New York.

Balasubramanian, V., Alves, B., Aulakh, M., Bekunda, M., Cai, Z., Drinkwater, L., Mugendi, D., van Kessel, C., Oenema, O., 2004. Crop, Environmental, and Management Factors Affecting Nitrogen Use Efficiency. In: A. Mosier, J. Syers, J. Freney (eds.) Agriculture and the Nitrogen Cycle: Assessing the Impacts of Fertilizer Use on Food Production and the Environment. 19-33. Island Press, Washington.

Benner, R. L., Lamb, B. 1985. A fast response continuous analyzer for halogenated atmospheric tracers. Journal of Atmospheric Oceanic Technology 2, 582–589.

Bouwman, A.F., 1996. Direct Emission of Nitrous Oxide from Agricultural Soils. *Nutrient Cycling in Agroecosystems* 46, 53-70.

Bouwman, A.F., Lee, D.S., Asman, W.A.H., Dentener, F.J., Van Der Hoek, K.W., Olivier, J.G.J., 1997. A global high-resolution emission inventory for ammonia. *Global Biogeochemical Cycles* 11(4), 561-587.

Bouwman, A.F., Boumans, L.J., 2002. Estimation of Global NH_3 Volatilization Loss from Synthetic Fertilizers and Animal Manure Applied to Arable Lands and Grasslands. *Global Biogeochemical Cycles* 16 (2), 8-1 to 8-15.

Briggs, G., 1973. Diffuion Estimation for Small Emissions, ATDL Contribution File No. 79, Atmospheric Turbulence and Diffusion Laboratory.

Chen, J., Vaughan, J. , Avise, J., O'Neill, S., Lamb, B., 2008. Enhancement and evaluation of the AIRPACT ozone and $PM_{2.5}$ forecast system for the Pacific Northwest. *Journal of Geophysical Research* 113, D14305, doi:10.1029/2007JD009554.

Christensen, S., Ambus, P., Arah, J.R.M., Clayton, H., Galle, B., Griffith, D. W. T., Hargreaves, K. J., Klenzedtsson, L., Lind, A., Maag, M., Scott, A., Skiba, U., Smith, K. A., Welling, M., Wienhold, F. G., 1996. Nitrous oxide emission from an agricultural field: Comparison between measurements by flux chamber and micrometerological techniques. *Atmospheric Environment* 30 (24), 4183-4190.

Dobbie, K.E., McTaggart, I.P., Smith, K,A., 1999. Nitrous Oxide Emissions from Intensive Agricultural Systems: Variations between Crops and Seasons, Key Driving Variables, and Mean Emission Factors. *Journal of Geophysical Research-Atmospheres* 104, 26891-26899.

Dobbie, K.E., Smith, K.A., 2003. Nitrous oxide emission factors for agricultural soils in Great Britain: the impact of soil water-filled pore space and other controlling variables. *Global Change Biology* 9, 204-218.

Draxler, R. R., 1976. Determination of Atmospheric Diffusion Parameters. *Atmospheric Environment* 10, 363–372.

EPA, 2003. Particle Pollution and Your Health. Washington, D.C.: United States Environmental Protection Agency. EPA-452/F-03-001. Available at: http://www.airnow.gov/index.cfm?action=particle.cover. Last updated 19 September 2003. Accessed 18 December 2008.

EPA, 2006. Nitrous Oxide: Sources and Emissions. Washington, D.C.: United States Environmental Protection Agency. Available at: http://www.epa.gov/nitrousoxide/sources.html. Last updated 19 October 2006. Accessed 21 October 2008.

EPA, 2007. Environmental Impacts: Ammonia. Washington, D.C.: United States Environmental Protection Agency. Available at: http://www.epa.gov/agriculture/ag101/impactammonia.html. Last updated 11 September 2007. Accessed 21 October 2008.

EPA, 2008. Draft Inventory of U.S. Greenhous Gas Emissions and Sinks: 1990-2006. Retrieved March 14, 2008, from U.S. Environmental Protection Agency Web site: http://epa.gov/climatechange/emissions/usinventoryreport.html. Last updated February 2008. Accessed 18 December 2008.

FAO/IFA, 2001. Global Estimates of Gaseous Emissions of NH_3, NO and N_2O from Agricultural Land. Food and Agriciculture Organization of the United Nations (FAO) / International Fertilizer Industry Association (IFA), Rome.

Flaherty, J., Lamb, B., Allwine, K., Allwine, E., 2007. Vertical Tracer Concentration Profiles Measured during the Joint Urban 2003 Dispersion Study. *Journal of Applied Meteorology* 46, 2019-2037.

Flessa, H., Ruser, R., Schilling, R., Loftfield, N., Munch, J.C., Kaiser, E.A., Beese, F., 2002. N_2O and CH_4 fluxes in potato fields: automated measurement, management effects and temporal variation. *Geoderma* 105, 307-325.

Forster, P., Ramaswamy, V., Artaxo, P., Berntsen, T., Betts, R., Fahey, D.W., Haywood, J., Lean, J., Lowe, D.C., Myhre, G., Nganga, J., Prinn, R., Raga, G., Schulz, M., Van Dorland, R., 2007. Changes in Atmospheric Constituents and in Radiative Forcing. *In: Climate Change 2007: The Physical Science Basis. Contribution of Working Group I to the Fourth Assessment Report of the Intergovernmental Panel on Climate Change* [Solomon, S., D. Qin, M. Manning, Z. Chen, M. Marquis, K.B. Averyt, M.Tignor and H.L. Miller (eds.)]. Cambridge University Press, Cambridge, United Kingdom and New York, NY, USA.

Freney, J.R., Simpson, J.R., 1983. Gaseous Loss of Nitrogen from Plant-Soil Systems. Martinus Nijhoff/Dr. W. Junk Publishers, The Hague, Netherlands.

Galloway, J.N., Dentener, F.J., Capone, D.G., Boyer, E.W., Howarth, R.W., Seitzinger, S.P., Asner, G.P., Cleveland, C.C., Green, P.A., Holland, E.A., Karl, D.M., Michaels, A.F., Porter, J.H., Townsend, A.R., Vorosmarty, C.J., 2004. Nitrogen cycles: Past, present and future. *Biogeochemistry* 70, 153-226.

Haile-Mariam, S., Collins, H. P., Higgins, S. S., 2008. Greenhouse Trace Gas Fluxes from an Irrigated Sweet Corn (Zea mays L.) - Potato (Solanum tuberosum L.) Rotation. *Journal of Environmental Quality* 37, 759-771. DOI: 10.2134/jeq2007.0400

Hanna, S.R., Briggs, G.A., Hosker, R.P., 1982. *Handbook on Atmospheric Diffusion*. DOE/TIC11223, Tech. Information Center, U.S. Dept. of Energy, Oak Ridge, TN Department of Energy, 102. [NTIS DE8-2002-045.]

Haverkort, A.J., MacKerron, D.K.L., 2000. Recommendations and trends in research and practice of application of nitrogen and water to potato crops. In: Haverkort, A.J. & D.K.L. MacKerron (Eds.), Management of nitrogen and water in potato production. Wageningen Pers, Wageningen, 301-310.

Hutchinson, G.L., Mosier, A.R., 1981. Improved soil cover method for field measurements of nitrous oxide fluxes. *Soil Science Society of America Journal* 45, 311–316.

IPCC (Intergovernmental Panel on Climate Change). Climate Change 1995. Impacts, Adaptations and Mitigation of Climate Change: Scientific–Technical Analyses; Watson, R.T., Zinyowera, M.C., Moss, R.H., Eds.; Cambridge University Press: Cambridge, England, 1996; 1–878.

Kaharabata, S.K., Schuepp, P.H., 2000. Estimating Methane Emissions from Dairy Cattle Housed in a Barn and Feedlot using an Atmospheric Tracer. *Environmental Science & Technology* 34 (15), 3296-3302.

Krasnec, J., Demaray, D., Lamb, B., Benner, R., 1984. Automated sequential syringe sampler for atmospheric tracer studies. *Journal of Atmospheric and Oceanic Technology* 1, 372-376.

Lang, N.S., Stevens, R.G., Thornton, R.E., Pan, W.L., Victory, S., 1999. Irrigated potato nutrient management guide for central Washington. WSU Extension Bulletin #241.

Liu, G., Li, Y., Alva, A.K., 2007. Temperature quotients of ammonia emission of different nitrogen sources applied to four agricultural soils. *Soil Science Society of America Journal* 71, 1482-1489.

Livingston, G.P., Hutchinson, G.L., 1995. Enclosure-based measurement of trace gas exchange: applications and sources of error. In. P.A. Matson and R.C. Harriss (eds.) Biogenic Trace Gases: Measuring Emissions from Soil and Water. Methods in Ecology. 14-51. Blackwell Science Cambridge University Press, London.

Martin, D.O., 1976. The change of concentration standard deviation with distance, *Journal of Air Pollution Control Association* 2, 26.

McGinn, S.M., Janzen, H.H., 1997. Ammonia Sources in Agriculture and their Measurement. *Canadian Journal of Soil Science* 78, 139–148.

Mohan, M., Siddiqui, T.A., 1997. An Evaluation of Dispersion Coefficients for Use in Air Quality Models. Boundary Layer Meteorology 84, 177-206.

Mount, G.H., Rumburg, B., Havig, J., Lamb, B., Westberg, H., Yonge, D., Johnson, K., Kinciad, R., 2002. Measurement of atmopsheric ammonia at a dairy using differential optical absorption spectroscopy in the mid-ultraviolet. *Atmospheric Environment* 36, 1799-1810.

Pandis, S.N., Wexler, A.S., Seinfiekld, J.H., 1995. Dynamics of Tropospheric Aerosols. *Journal of Physical Chemistry* 99 (24), 9646-9659. DOI: 10.1021/j100024a003

Poole, C.F., Poole, S.K., 1991. Chromatography Today. Elsevier Scientific. Amsterdam, The Netherlands.

Potter, C., Krauter, C., Klooster, S., 2001. Statewide Inventory Estimates of Ammonia Emissions From Fertilizer Applications in California. Project report to California Air Resources Board, Sacramento, CA. Contract# ID98-76.

Rumburg, B., Mount, G., Yonge, D., Lamb, B., Westberg, H., Filipy, J., Bays, J., Kincaid, R., Johnson, K., 2006. Atmospheric flux of ammonia from sprinkler application of dairy waste. *Atmospheric Environment* 40, 7246-7258.

Seinfeld, J.H., Pandis, S.N., 1998. Atmospheric chemistry and physics: from air pollution to climate change. Wiley-Interscience. USA.

Smith, K.A., McTaggart, I.P., Tsuruta, H., 1997. Emissions of N_2O and NO Associated with nitrogen fertilization in intensive agriculture, and the potential for mitigation. *Soil Use and Management* 13, 296-304.

Sommer, S.G., Schjoerring, J.K., Denmead, O.T., 2004. Ammonia emission from mineral fertilizers and fertilized crops. *Advances in Agronomy* 82, 557-622.

Stockle, C., Martin, S., Campbell, G., 1994. CropSyst, a cropping systems simulation model: Water/nitrogen budgets and crop yield. *Agricultural Systems* 46, 335-359.

Sutton MA., Schjoerring, J.K., Wyers, G.P., Duyzer, J.H., Ineson, P., Powlson, D.S., 1995. Plant-atmosphere exchange of ammonia. *Philosophical Transactions: Physical Sciences and Engineering* 351 (1696), 261-278.

Turnipseed, A., Pressley, S., Karl, T., Lamb, B., Nemitz, E., Allwine, G., Cooper, W., Shertz, S., Guenther, A., 2008. The use of disjunct eddy sampling methods for the determination of ecosystem level fluxes of trace gases. *Atmospheric Chemistry and Physics Discussions* 8, 13413-13451.

USDA-ARS GRACEnet, 2003. Chamber-based Trace Gas Flux Measurement Protocol. U.S. Department of Agriculture- Agricultural Research Service GRACEnet. Available at: http://gracenet.usda.gov/GRACEnetTraceGasProtocol.pdf. 24 April 2003.

Vitousek, P.M., Aber, J.D., Howarth, G.E., Likens, G.E., Watson, P.A., Schindler, D.W., Schlesinger, W.H., Tilman, D.W., 1997. Human alterations of the global nitrogen cycle: sources and consequences. Ecological Applications, 7, 737-750.

Vitousek, P.M., Aber, J.D., Howarth, G.E., Likens, G.E., Watson, P.A., Schindler, D.W., Schlesinger, W.H., Tilman, D.W., 2000. Human alterations of the global nitrogen cycle: Causes and consequences. Human Alteration of the Global Nitrogen Cycle http://esa.sdsc.edu/tilman.html

Zhu, T., Pattey, E., Desjardins, R.L., 2000. Relaxed Eddy-Accumulation Technique for Measuring Ammonia Volatilization. *Environmental Science & Technology*. 34, 199-203. DOI: 10.1021/es980928

APPENDIX A:

COMPARISON OF VARIOUS METHODS
FOR DETERMINING DISPERSION COEFFICIENTS

In this appendix, a brief overview of the various methods for determining the dispersion coefficients and the comparison results are presented.

A.1 Description of Sigma Methods

Critical input parameters to the Gaussian diffusion models are the dispersion coefficients (σ_y and σ_z), which express the spread of the plume in the horizontal and vertical crosswind directions. These coefficients can be determined empirically or theoretically. The methods compared were:

1) Empirical methods:
    i) Martin's equations based on Pasquill-Gifford diffusion curves (Martin, 1976)
    ii) Briggs' equations for open-country conditions based on several field studies (Briggs, 1973)
2) Theoretical method: Taylor's near-field dispersion theory (Mohan and Siddiqui, 1997)
3) Combination of theory and empirical results: Draxler's method (Draxler, 1976)

A.1.1 Empirical Methods

Values of σ_y and σ_z may be obtained from empirical results. Perhaps the most well-known diffusion study is the 1956 Project Prairie Grass in O'Neill, Nebraska. During Project Prairie Grass, sulfur dioxide (SO_2) was used as the tracer gas and released at a height of 0.5 m above ground over a large flat field (Arya, 1999). Concentrations at 1.5 m above ground were measured at distances between 50 and 800 m from the source and were based on 10 min sampling periods (Arya, 1992). This experiment resulted in the Pasquill and Gifford (P–G) dispersion curves. To estimate σ_y and σ_z from the P-G curves, the stability class must first be determined based on simple measurements such as sunshine, cloud cover, and wind speed

measured at 10 meters above ground, as shown in Table 3.2. "Strong" incoming solar radiation corresponds to a solar angle greater than 60° with clear skies, while "slight" incoming solar radiation corresponds to a solar angle less than 35° with clear skies (Arya, 1999). Along with solar angle, cloud cover is also considered when determining the strength of incoming solar radiation. The use of computers for solving the Gaussian dispersion equations make it desirable to convert the P-G curves into analytical equations. The equations of Martin (1976) represent a reasonable fit to the Pasquill and Gifford (P–G) dispersion curves.

Table A.1: Pasquill Stability Classes

Surface Wind Speed	**Daytime Incoming Solar Radiation**			**Nighttime Cloud Cover**	
(m s^{-1})	**Strong**	**Moderate**	**Slight**	**> 50%**	**< 50%**
< 2	A	A-B	B	E	F
2-3	A-B	B	C	E	F
3-5	B	B-C	C	D	E
5-6	C	C-D	D	D	D
> 6	C	D	D	D	D

Note: Class D applies to heavily overcast skies, at any wind speed day or night

The following equations were developed by Martin for calculating the dispersion coefficients:

$$\sigma_y = ax^{0.894} \qquad \text{A.1}$$

$$\sigma_z = cx^d + f \qquad \text{A.2}$$

where the constants *a, c, d,* and *f* are given in Table A.2. The values of σ_y and σ_z are in meters when the value of the downwind distance *x* of the receptor from the source is given in kilometers.

Table A.2: Values of a, c, d, and f for use in Martin's equation

Stability	*a*	$x < 1$ km			$x > 1$ km		
		c	*d*	*f*	*c*	*d*	*f*
A	213	440.8	1.041	9.27	459.7	2.094	-9.6
B	156	106.6	1.149	3.3	108.2	1.098	2.0
C	104	61.0	0.911	0.0	61.0	0.911	0.0
D	68	33.2	0.725	-1.7	44.5	0.516	-13.0
E	50.5	22.8	0.675	-1.3	55.4	0.305	-34.0
F	34	14.35	0.740	-0.35	62.6	0.180	-48.6

In addition to Project Prairie Grass, a number of other diffusion experiments have been conducted to empirically estimate the dispersion coefficients. For rural situations, the three main diffusion experiments are the 1956 Project Prairie Grass, the Brookhaven National Laboratory (BNL) experiments, and the Tennessee Valley Authority (TVA) experiment. Results from Project Prairie Grass are for non-buoyant, near ground level releases at downwind distances less than 1km. The BNL experiment results reflect effects of elevated releases (~108 m above ground) over a rougher surface at downwind distances extending to tens of kilometers (Arya, 1999). The TVA results reflect effects of highly buoyant releases from higher elevations over gently rolling terrain (Arya, 1999). In 1973, Briggs synthesized the results from Project Prairie Grass, BNL, and TVA to produce a set of formulas for open country situations, which are shown in Table A.3 (Arya, 1999). Briggs' formulas use the Pasquill stability classes.

Table A.3: Briggs' (1973) Interpolation Formulas for Open Country

Stability	σ_y (m)	σ_z (m)
A	$0.22x(1 + 0.0001x)^{-.5}$	.20x
B	$0.16x(1 + 0.0001x)^{-.5}$	.12x
C	$0.11x(1 + 0.0001x)^{-.5}$	$.08x(1 + 0.0002x)^{-.5}$
D	$0.08x(1 + 0.0001x)^{-.5}$	$.06x(1 + 0.0015x)^{-.5}$
E	$0.06x(1 + 0.0001x)^{-.5}$	$.03x(1 + 0.0003x)^{-1}$
F	$0.04x(1 + 0.0001x)^{-.5}$	$.016x(1 + 0.0003x)^{-1}$

A.1.2 Theoretical Methods

Another way of determining the dispersion coefficients is through Taylor's (1921) theory of diffusion. This theory considers one-dimensional diffusion of a cloud of particles released from the same point in a stationary and homogeneous turbulent flow using a frame of reference moving with the mean flow (Arya, 1999). Taylor's theory is difficult to use since it requires exact knowledge of the behavior of the Lagrangian autocorrelation $R(\xi)$ at different times which is often very difficult to obtain (Mohan *et al.*, 1997). Several methods have been suggested for determining σ_y and σ_z which do not require the autocorrelation function but still retain the essential features of Taylor's theory. Pasquill suggested the following relationships, which are more applicable for use with readily measured Eulerian quantities (Mohan *et al.*, 1997):

$$\sigma_y = \sigma_v t F_y \qquad \text{A.3}$$

$$\sigma_z = \sigma_w t F_z \qquad \text{A.4}$$

where σ_v and σ_w are the standard deviation of velocity fluctuations in the y and z directions, t is the travel time, and F_y and F_z are universal functions of a set of parameters that specify the characteristics of the atmospheric boundary layer. For this application, measurements of wind components u, v, and w were measured at 10 Hertz frequency using a sonic anemometer. A coordinate rotation was applied to the u and v components so that the u component is along the mean wind direction and the mean v component of the wind is zero. The w component was not used in the coordinate conversion since its magnitude is small compared to the other two components. The standard deviation of the v and w wind components were calculated for every 30-min period to get the σ_v and σ_w, respectively.

For receptors close to the emission source, the suggested relationships above can be reduced to:

$$\sigma_{y,z} = \sigma_{v,w} t\,, \quad t = \frac{x}{u} \tag{A.5}$$

where x is the downwind distance of receptor from source in meters and u is the wind speed in meters per second. Since the field data used for this project utilized receptors that were relatively close to the source (~400 m downwind), use of the relationship above is appropriate.

A.1.3 Combination of Theory and Empirical Results

In 1975, Draxler combined Taylor's theory with empirical data from various field experiments including Project Prairie Grass and others (Draxler, 1976). Draxler's equations are:

$$\sigma_{y,z} = \sigma_{\theta,\phi} x f_{1,2}\left(\frac{T}{T_i}\right) \tag{A.6}$$

$$f_{1,2}(T/T_i) = \frac{1}{\left[1 + 0.9\left(\frac{T}{T_{\mathrm{i}}}\right)^{0.5}\right]} \tag{A.7}$$

where $\sigma_{\theta,\phi}$ are the standard deviations of vertical and horizontal wind direction fluctuations, x is the downwind distance of receptor from source in meters, and T_i is a time scale proportional to the Langrangian scale (Draxler, 1976). Values of T_i for different stabilities and source heights for use in f_1 and f_2 are given in Table A.4 (Draxler, 1976). Values of *Ti* are mean values from each category of experiments.

Table A.4: Values of T_i for use in f_1 and f_2 in Draxler's Method

	Surface Sources		**Elevated Sources**	
Std Dev	Stable	Unstable	Stable	Unstable
Horizontal	300	300	1000	1000
Vertical	50	100	100	500

A.2 Results

The various methods described were used to simulate eight 30-minute periods of sulfur hexafluoride (SF_6) tracer diffusion data collected from the potato fields (see Table A.5). This section presents the results from the various σ_y and σ_z schemes for the eight 30-minute periods of SF_6 tracer diffusion data. Predicted and observed SF_6 concentrations are compared graphically and statistically.

Table A.5: Periods of diffusion data used for comparing various diffusion schemes

Date	Time (PST)
7/19/07	11:30 am to 12:00 pm
7/19/07	12:30 pm to 1:00 pm
7/19/07	1:00 pm to 1:30 pm
7/19/07	1:30 pm to 2:00 pm
7/19/07	2:30 pm to 3:00 pm
7/29/08	9:20 am to 9:50 am
7/29/08	11:20 am to 11:50 am
7/29/08	11:50 am to 12:20 pm

A.2.1 Comparison graphs

Concentration distributions obtained from using various σ_y and σ_z schemes for 7/19/07 (12:30 pm to 1:00 pm PST) and 7/29/08 (11:50 am to 12:20 pm PST) are shown in Figures A.1-A.2. Results for other periods are given in figures and tables at the end of this appendix. The receptor position represents the location of each syringe sampler employed during the SF_6 tracer studies. For all eight sampling periods, Martin's, Briggs', and Draxler's methods performed well in terms of predicting the shape of the measured concentration distributions while Taylor's method did not. In addition, Taylor's method severely underestimated the maximum observed values and overestimates the outside concentrations.

One to one ratio comparisons (Figures A.3 and A.4) provide another way of evaluating the accuracy of each method. For four out of the eight sampling periods, Martin's method

yielded the best results in terms of accurately predicting observed concentration values at every receptor. For three out of the eight sampling periods, Brigg's method closely predicted measured concentrations for every receptor.

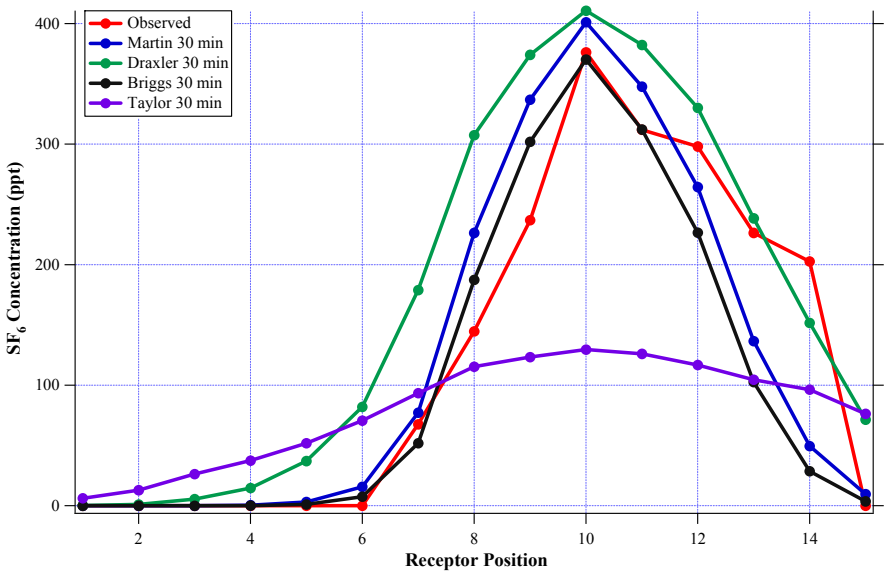

Figure A.1: Predicted and observed SF_6 concentration distribution from 12:30 pm to 1:00 pm on 7/19/07 (PST).

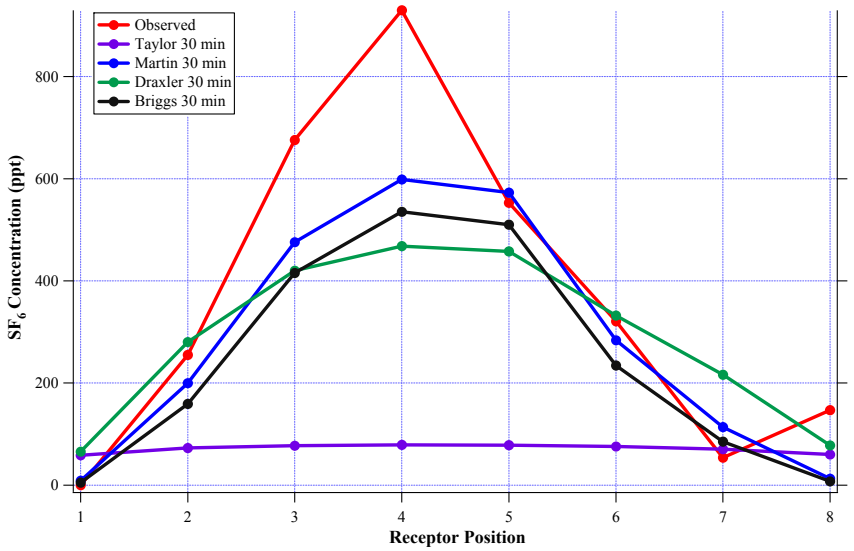

Figure A.2: Predicted and observed SF_6 concentration distribution from 11:50 am to 12:20 pm on 7/29/08 (PST).

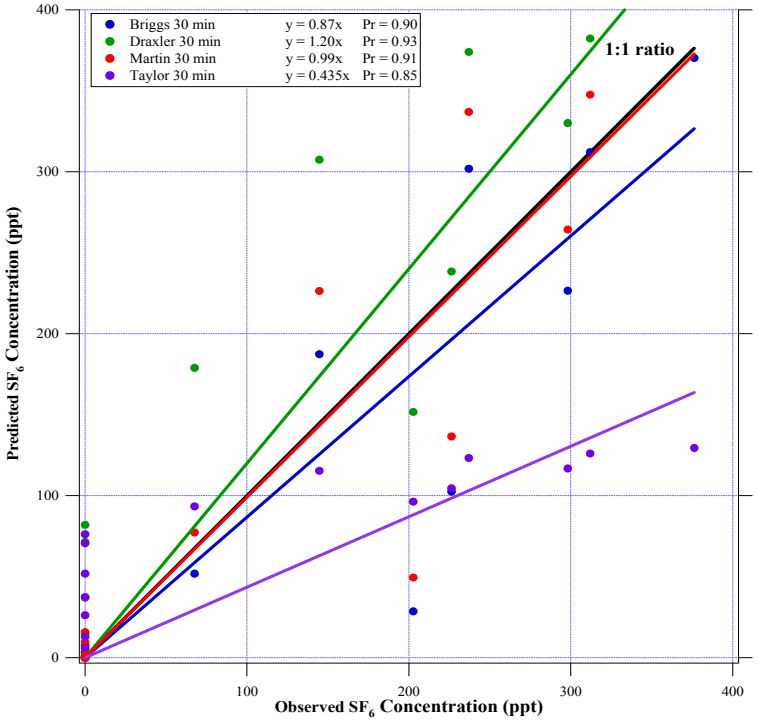

Figure A.3: A 1:1 comparison of observed vs. predicted SF_6 concentrations from 12:30 pm to 1:00 pm on 7/19/07 (PST).

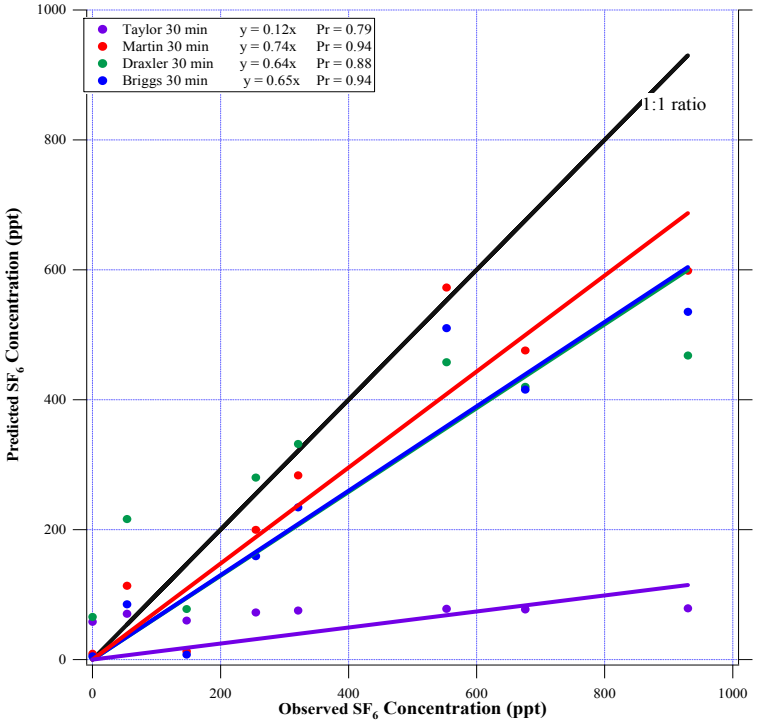

Figure A.4: A 1:1 comparison of observed vs. predicted SF_6 concentrations from 11:50 am to 12:20 pm on 7/29/08 (PST).

A.2.2 Statistical Analysis

Various statistical measures were calculated for further analysis of each method. The statistical measures were: Fractional Bias (FB), Unpaired Peak Prediction Error (UPPE), and Mean Normalized Gross Error (MNGE). These statistical measures were performed for all measured SF_6 concentrations greater than 50 pptv. The FB, UPPE, and MNGE are defined as:

$$\text{Fractional Bias (FB)} = \frac{\frac{1}{N}\sum_{i=1}^{N}\left[C_p(x,t_i) - C_o(x,t_i)\right]}{\frac{\left[C_p(x,t_i) + C_o(x,t_i)\right]}{2}}$$

$$\text{Unpaired Peak Prediction Error (UPPE)} = \frac{C_p(x,t')_{\max} - C_o(x,t')_{mzx}}{C_o(x,t')_{mzx}}$$

$$\text{Mean Normalized Gross Error (MNGE)} = \frac{1}{N}\sum_{i=1}^{N}\frac{\left|C_p(x,t_i) - C_o(x,t_i)\right|}{C_o(x,t_i)} * 100\%$$

where N is the number of concentrations at a given receptor location, $C_o(x,t_i)$ and $C_p(x,t_i)$ are the observed and predicted concentrations at the receptor location at x for hour t_i, respectively, and $C_o(x,t')_{\max}$ and $C_p(x,t')_{\max}$ are the observed and predicted maximum concentrations at a specific receptor location, respectively. The statistical measures for all sampling periods were averaged and are given in Table A.6. The lowest value in each category is highlighted in yellow.

Table A.6: Average Values of Statistical Measures for Various Methods

Method	FB	UPPE	MNGE
Martin	-0.06	0	41 %
Briggs	-0.11	-0.08	43 %
Draxler	0.04	-0.06	60 %
Taylor	-0.17	-0.7	53 %

Bias statistics measure the tendency of a model to over or under predict observed values. FB equally weighs positive and negative bias estimates. An FB of zero is ideal. Draxler's

method resulted in the lowest average FB values while Taylor's method yielded the highest. Martin's method resulted in the second lowest average FB.

Error is a measure of the extent that the model deviates from the observations. The UPPE compares the maximum observed and maximum predicted concentrations at a single sampling period. For the MNGE, a value of zero would indicate that the model exactly matches the observed values at all points in space/time. Martin's method resulted in the lowest average UPPE and MNGE values.

A.2.3 Conclusions

Several methods (Martin, Briggs, Taylor, and Draxler) for determining σ_y and σ_z have been compared with real diffusion data. Through analysis of comparison plots between predicted and observed SF6 values as well as statistical measures including FB, FGE, and UPPE, Martin's method yielded the best results. The average UPPE was zero for Martin's method, showing that maximum observed and maximum predicted concentrations closely matched at every period. The average FB and MNGE for all sampling periods were -0.06 and 41 % for Martin's method. Thus, Martin's method was used for estimating the diffusion coefficients for SIMFLUX to simulate NH_3 and N_2O emission rates from potato fields.

A.3 Additional Results

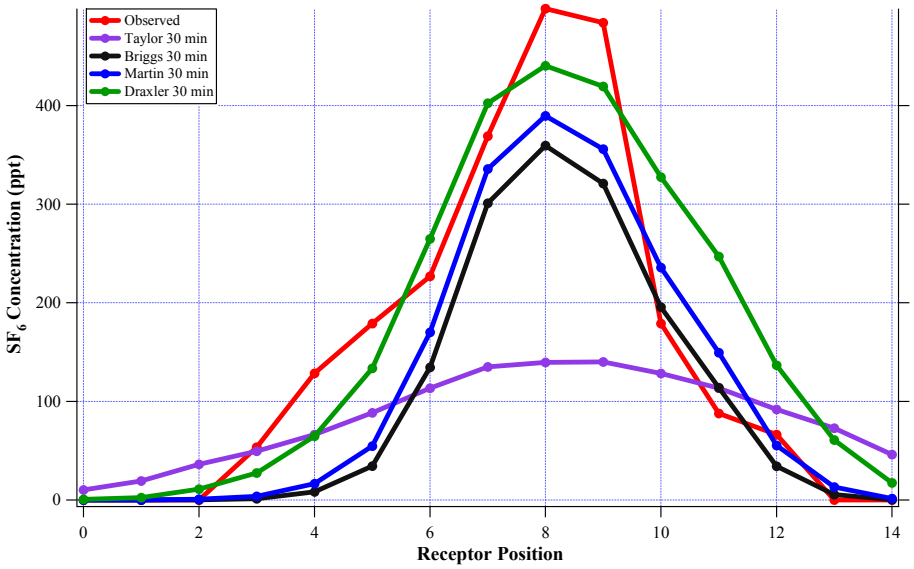

Figure A.5: Predicted and observed SF_6 concentration distribution for Tracer 7/19/07 (Syringe #2, 11:30 am to 12:00 pm PST)

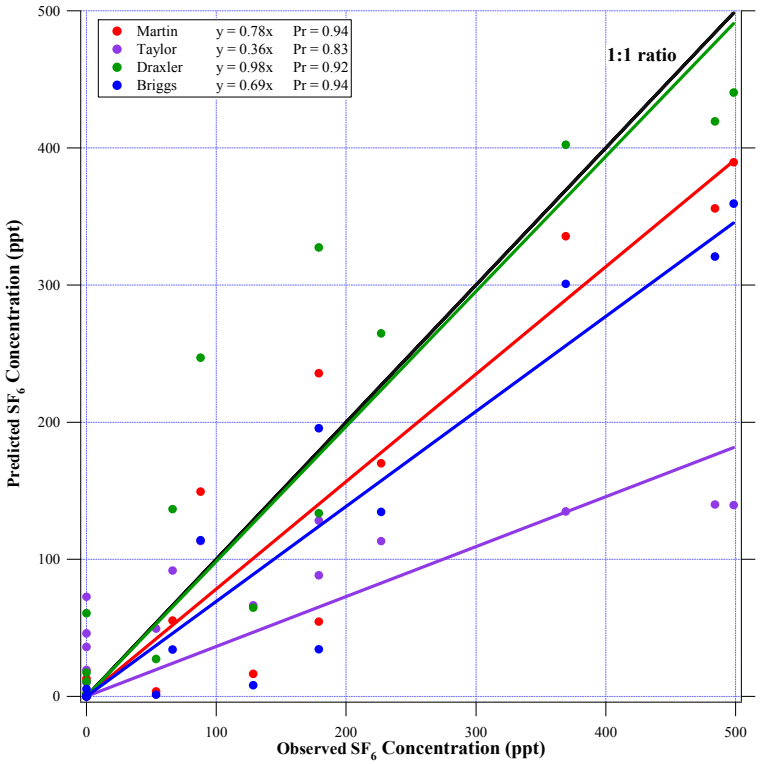

Figure A.6: A 1:1 comparison of observed vs. predicted SF_6 concentrations for Tracer 7/19/07 (Syringe #2, 11:30 am to 12:00 pm PST)

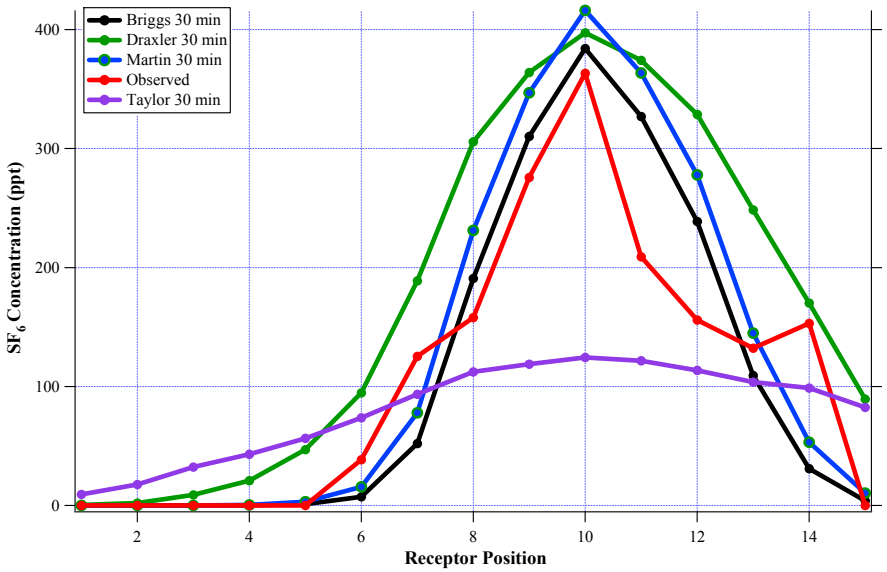

Figure A.7: Predicted and observed SF_6 concentration distribution for Tracer 7/19/07 (Syringe #5, 1:00 pm to 1:30 pm PST)

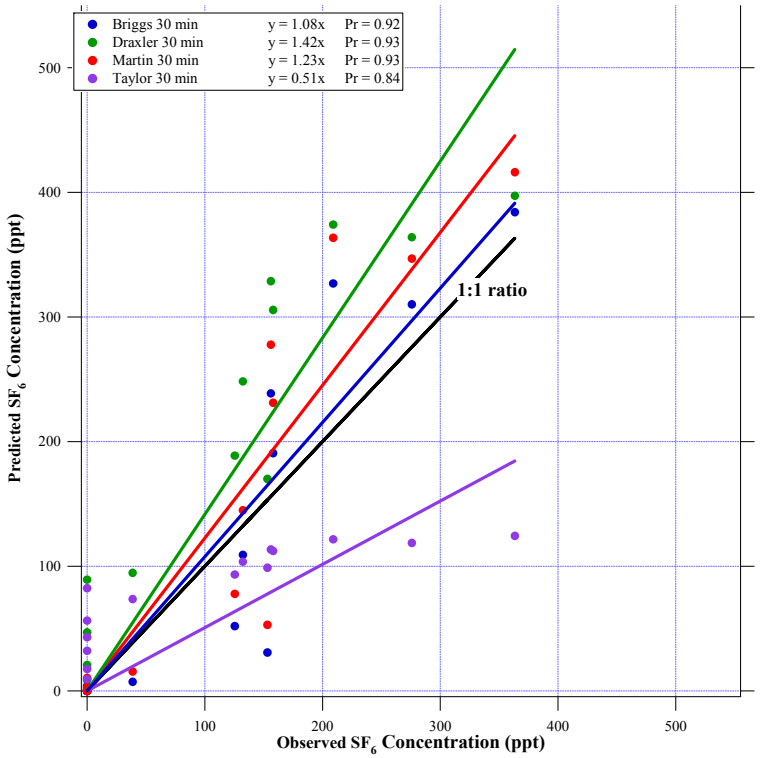

Figure A.8: A 1:1 comparison of observed vs. predicted SF_6 concentrations for Tracer 7/19/07 (Syringe #5, 1:00 pm to 1:30 pm PST)

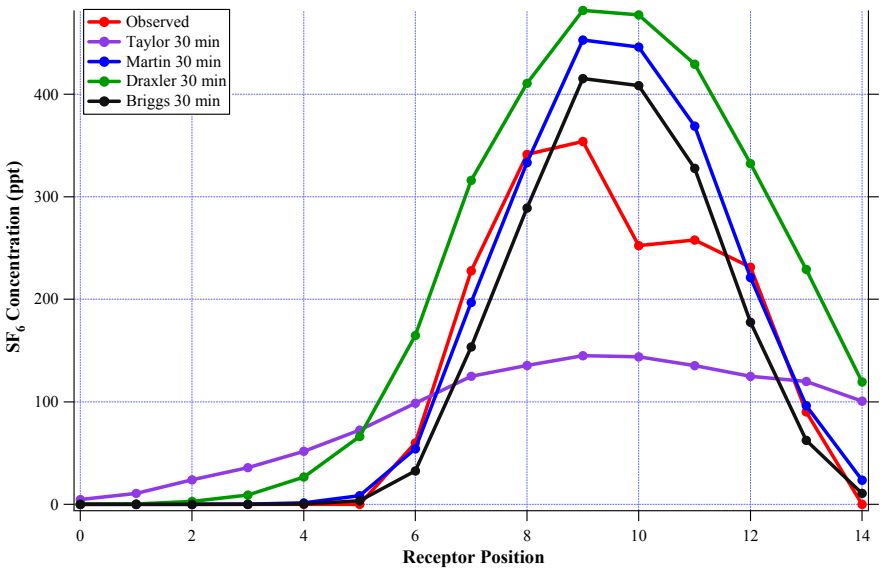

Figure A.9: Predicted and observed SF_6 concentration distribution for Tracer 7/19/07 (Syringe #6, 1:30 pm to 2:00 pm PST)

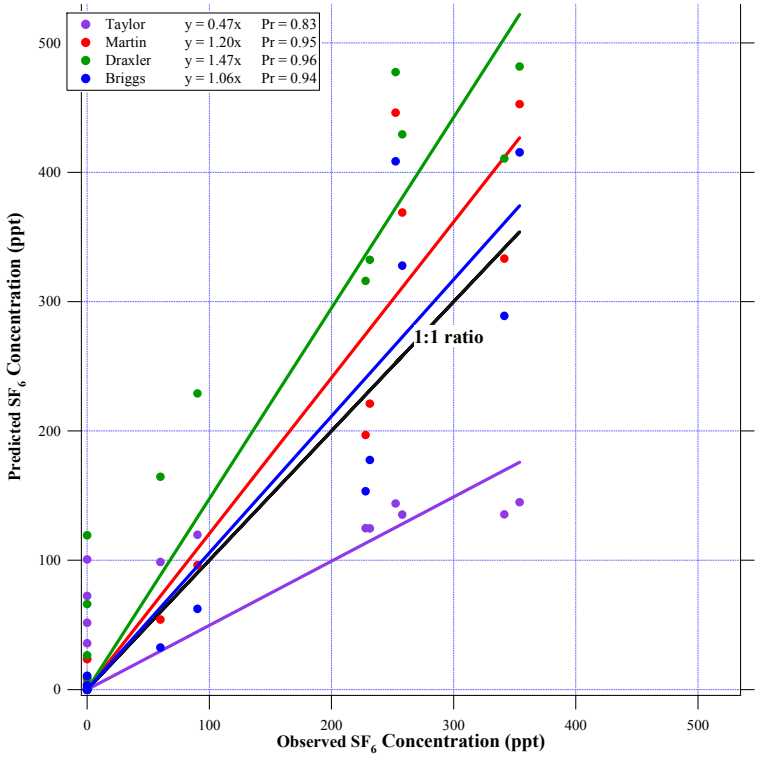

Figure A.10: A 1:1 comparison of observed vs. predicted SF_6 concentrations for Tracer 7/19/07 (Syringe #6, 1:30 pm to 2:00 pm PST)

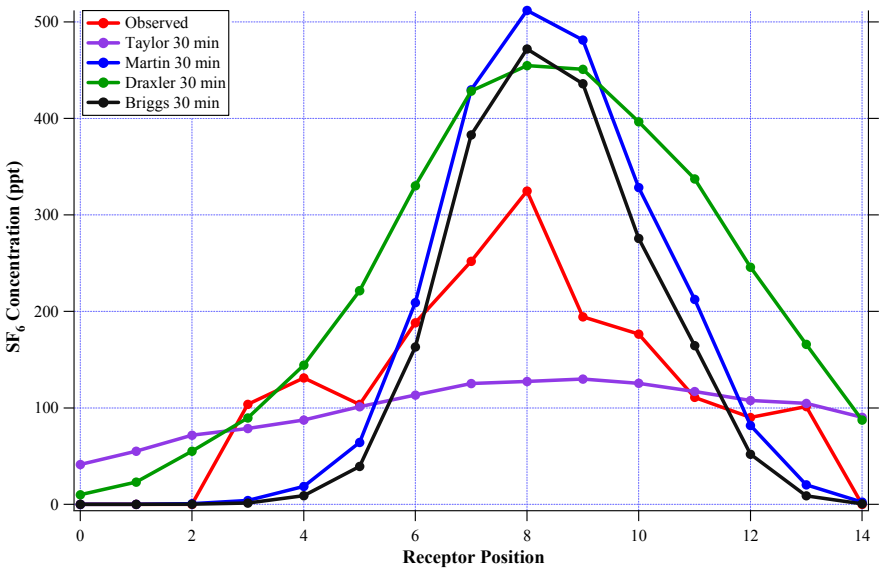

Figure A.11: Predicted and observed SF_6 concentration distribution for Tracer 7/19/07 (Syringe #8, 2:30 pm to 3:00 pm PST)

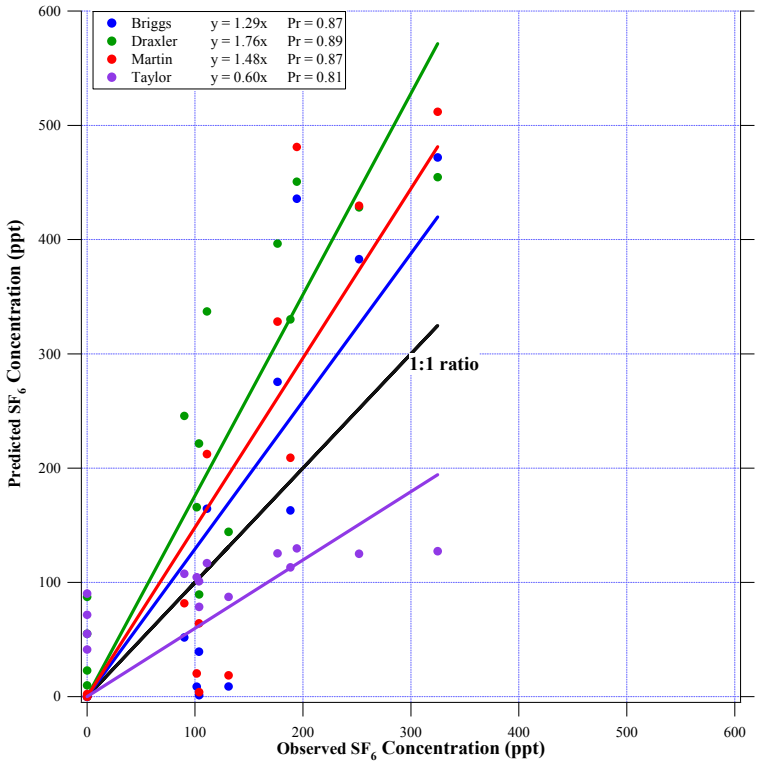

Figure A.12: A 1:1 comparison of observed vs. predicted SF_6 concentrations for Tracer 7/19/07 (Syringe #8, 2:30 pm to 3:00 pm PST)

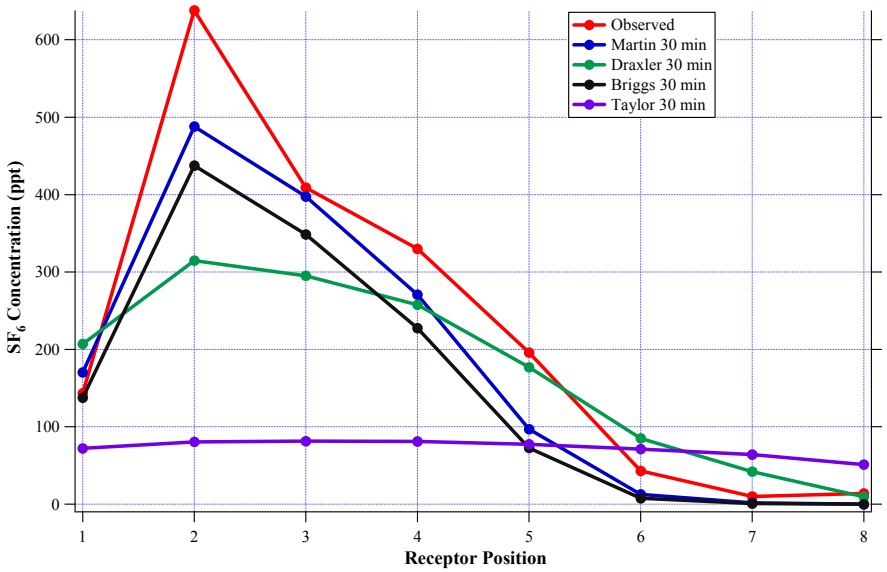

Figure A.13: Predicted and observed SF_6 concentration distribution for Tracer 7/29/08 (Syringe #4, 9:20 am to 9:50 am PST)

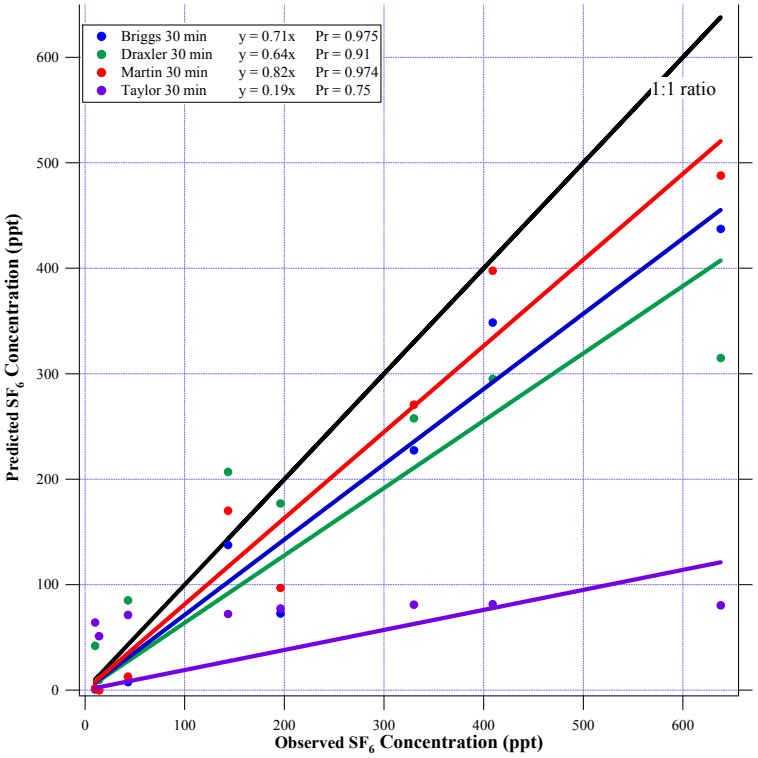

Figure A.14: A 1:1 comparison of observed vs. predicted SF_6 concentrations for Tracer 7/29/08 (Syringe #4, 9:20 am to 9:50 am PST)

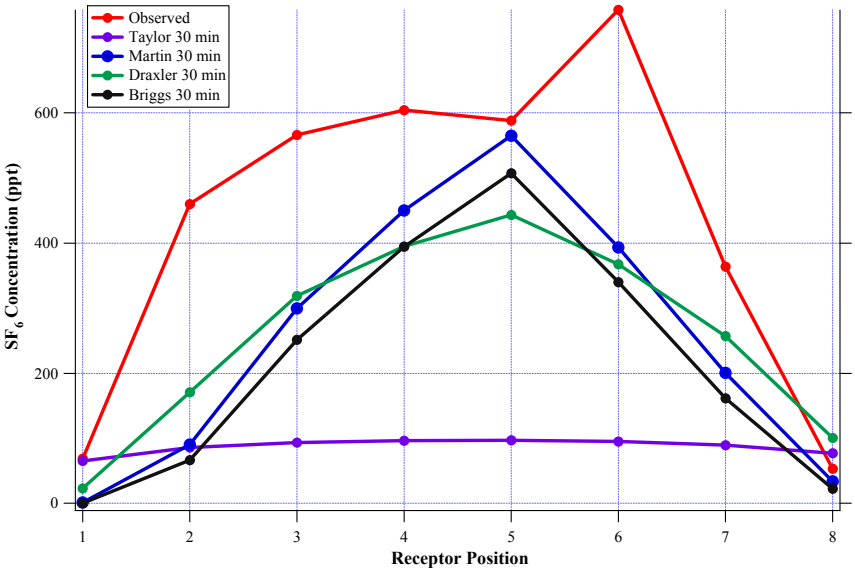

Figure A.15: Predicted and observed SF_6 concentration distribution for Tracer 7/29/08 (Syringe #8, 11:20 am to 11:50 am PST)

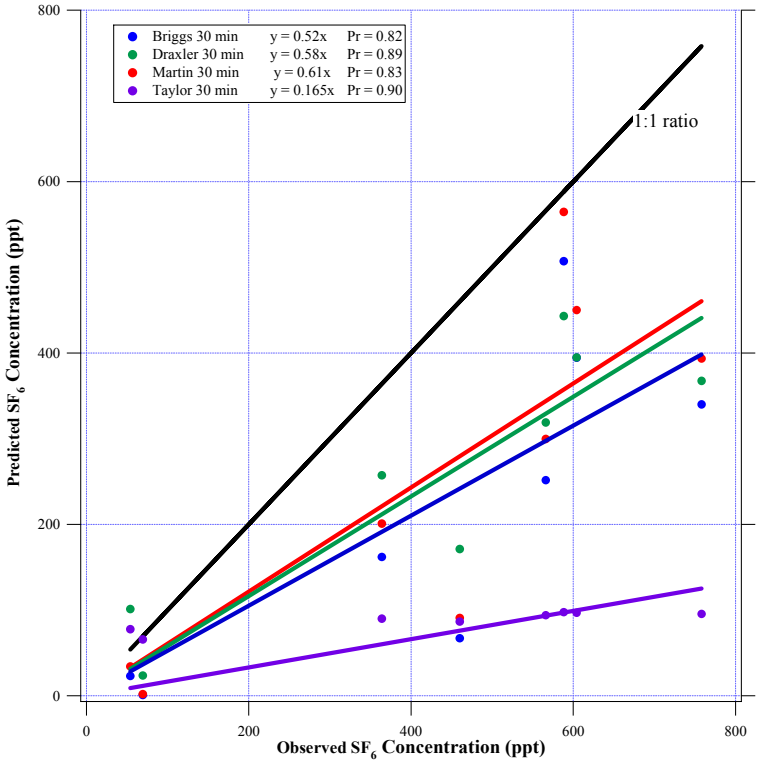

Figure A.16: A 1:1 comparison of observed vs. predicted SF_6 concentrations for Tracer 7/29/08 (Syringe #8, 11:20 am to 11:50 am PST)

Table A.7: Values of Statistical Measures for Various Sigma Methods for Tracer 7/19/07 (Syringe #2, 11:30 am to 12:00 pm PST)

Method	FB	MNB	MAE	MNGE	UPPE
Martin	-0.12	-25%	74.24	45%	-0.22
Briggs	-0.17	-40%	85.44	48%	-0.28
Draxler	0.02	25%	70.70	54%	-0.12
Taylor	-0.12	-32%	130.88	46%	-0.72

Table A.8: Values of Statistical Measures for Various Sigma Methods for Tracer 7/19/07 (Syringe #5, 1:00 pm to 1:30 pm PST)

Method	FB	MNB	MAE	MNGE	UPPE
Martin	0.02	18%	79.25	44%	0.15
Briggs	-0.04	-1%	63.44	38%	0.06
Draxler	0.11	59%	100.59	59%	0.09
Taylor	-0.12	-38%	85.71	38%	-0.66

Table A.9: Values of Statistical Measures for Various Sigma Methods for Tracer 7/19/07 (Syringe #6, 1:30 pm to 2:00 pm PST)

Method	FB	MNB	MAE	MNGE	UPPE
Martin	0.03	16%	58.05	23%	0.28
Briggs	-0.03	-5%	65.36	32%	0.17
Draxler	0.13	78%	128.32	78%	0.36
Taylor	-0.10	-25%	115.45	50%	-0.59

Table A.10: Values of Statistical Measures for Various Sigma Methods for Tracer 7/19/07 (Syringe #8, 2:30 pm to 3:00 pm PST)

Method	FB	MNB	MAE	MNGE	UPPE
Martin	-0.05	14%	115.18	70%	0.58
Briggs	-0.10	-7%	101.55	66%	0.45
Draxler	0.14	90%	137.90	93%	0.40
Taylor	-0.07	-22%	55.70	27%	-0.33

Table A.11: Values of Statistical Measures for Various Sigma Methods for Tracer 7/29/08 (Syringe #4, 9:20 am to 9:50 am PST)

Method	FB	MNB	MAE	MNGE	UPPE
Martin	-0.05	-15%	69.36	23%	-0.24
Briggs	-0.09	-29%	98.61	29%	-0.24
Draxler	-0.05	-13%	118.44	31%	-0.51
Taylor	-0.28	-71%	264.82	71%	-0.87

Table A.12: Values of Statistical Measures for Various Sigma Methods for Tracer 7/29/08 (Syringe #8, 11:20 am to 11:50 am PST)

Method	FB	MNB	MAE	MNGE	UPPE
Martin	-0.18	-48%	178.40	48%	-0.26
Briggs	-0.22	-57%	214.62	57%	-0.33
Draxler	-0.11	-28%	184.98	50%	-0.27
Taylor	-0.25	-57%	350.85	68%	-0.84

APPENDIX B:
ADDITIONAL N_2O RESULTS

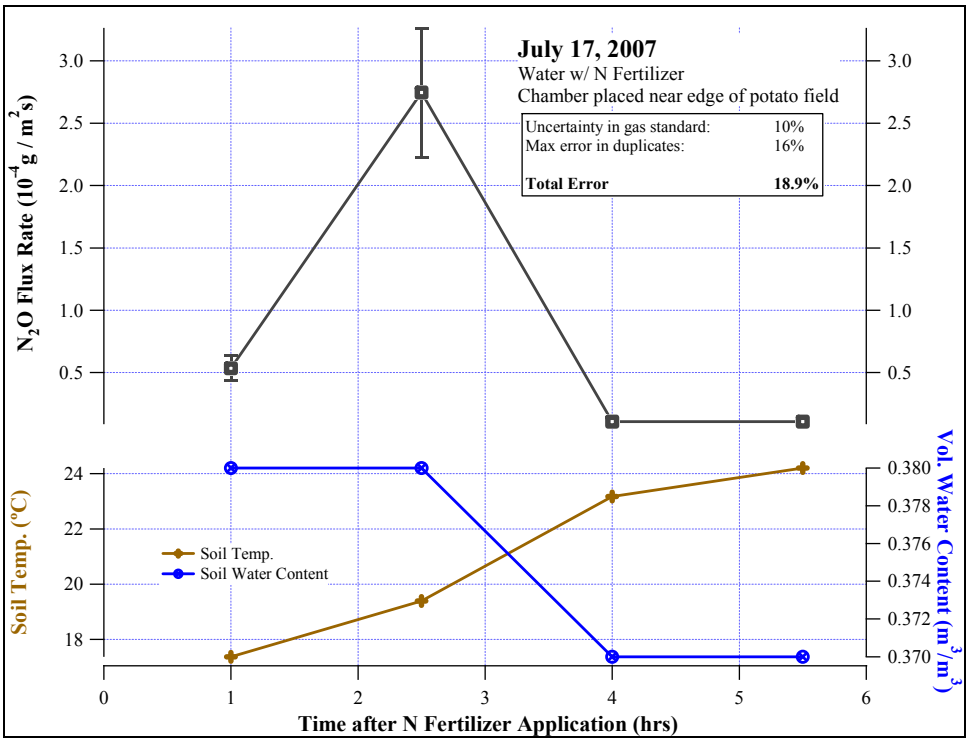

Figure B.1: N_2O flux rate, soil temperature, and soil volumetric water content (0-10 inches below the soil surface) as a function of time after fertigation from 9:15 am to 2:45 pm on 07/17/07 (PDT).

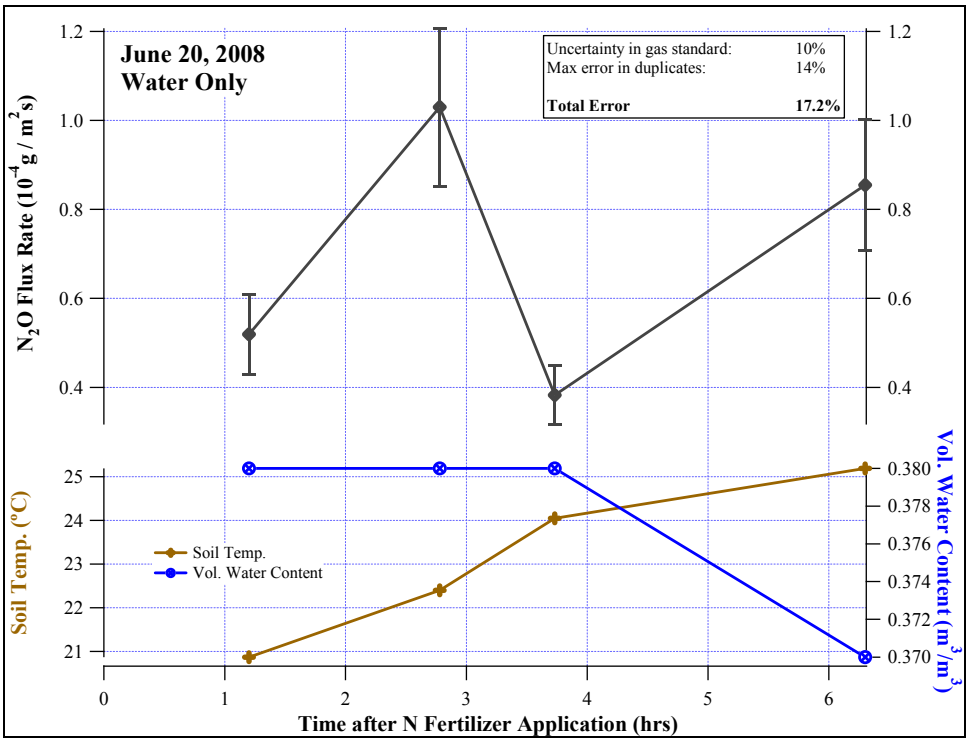

Figure B.2: N_2O flux rate, soil temperature, and soil volumetric water content (0-10 inches below the soil surface) as a function of time after fertigation from 12:10 pm to 5:10 pm on 06/20/08 (PDT).

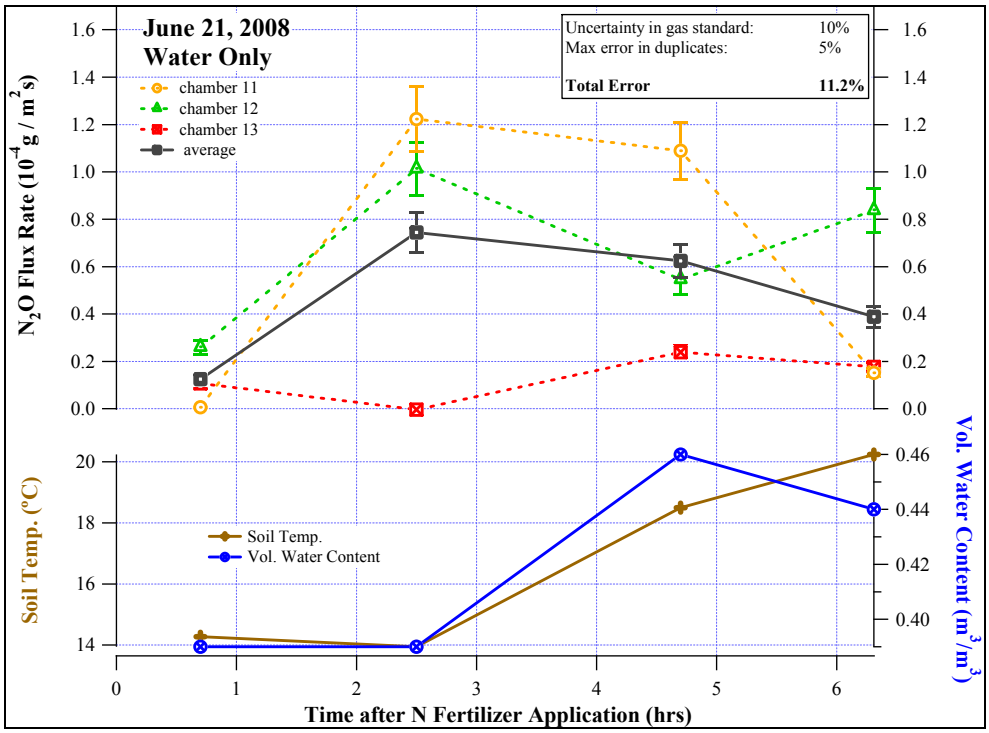

Figure B.3: N_2O flux rate, soil temperature, and soil volumetric water content (0-10 inches below the soil surface) as a function of time after fertigation from 9:45 pm to 3:15 pm on 06/21/08 (PDT).

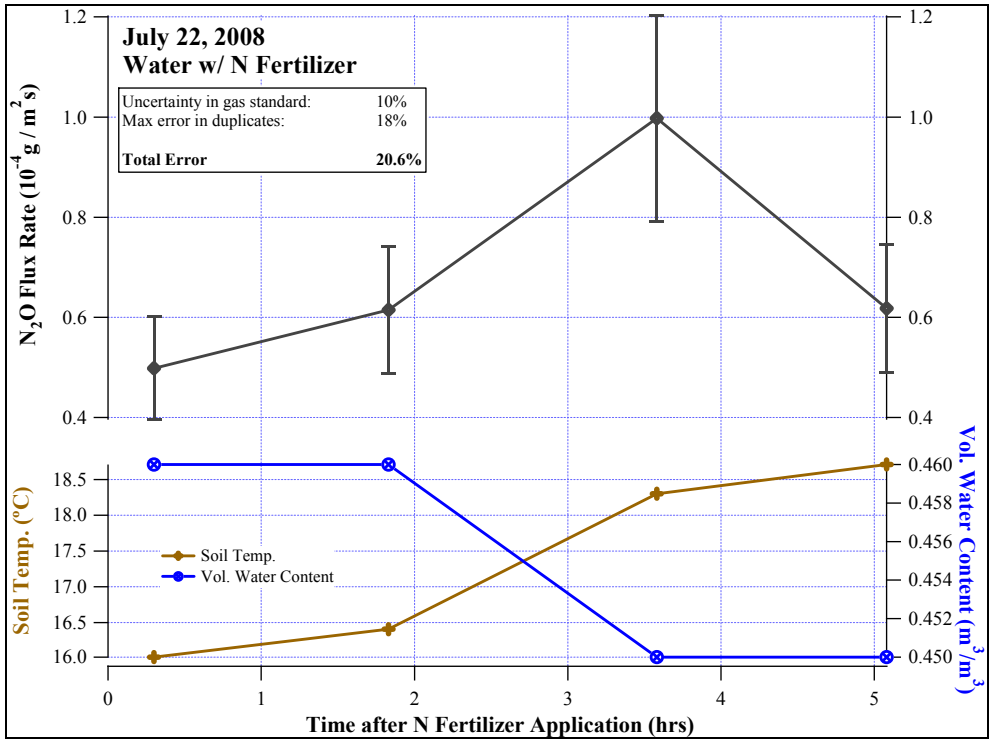

Figure B.4: N_2O flux rate, soil temperature, and soil volumetric water content (0-10 inches below the soil surface) as a function of time after fertigation from 9:45 am to 2:30 pm on 07/22/08 (PDT).

APPENDIX C:

ADDITIONAL NH_3 RESULTS

C.1 Application Rates Calculations:

N application rate (12 deg hr^{-1} sprinkler arm rotation rate):

$$6\frac{\text{lbsN}}{\text{acre}*\text{rotation}}*124.2\text{acres}*\frac{1\text{rotation}}{360\text{deg}}*\frac{6\text{deg}}{30\text{min}}*\frac{1\text{min}}{60\text{s}}*\frac{453.6\text{g}}{1\text{lb}}*\frac{1}{10\text{m}*400\text{m}}=7.8\text{E}-4\frac{\text{gN}}{\text{m}^2\text{s}}$$

N application rate (18 deg hr^{-1} sprinkler arm rotation rate):

$$6\frac{\text{lbsN}}{\text{acre}*\text{rotation}}*124.2\text{acres}*\frac{1\text{rotation}}{360\text{deg}}*\frac{9\text{deg}}{30\text{min}}*\frac{1\text{min}}{60\text{s}}*\frac{453.6\text{g}}{1\text{lb}}*\frac{1}{10\text{m}*400\text{m}}=11.7\text{E}-4\frac{\text{gN}}{\text{m}^2\text{s}}$$

NH_3 application rate by sprinkler arm (400 m by 10 m) (12 deg hr^{-1} sprinkler arm rotation rate):

$$6\frac{\text{lbsN}}{\text{acre}*\text{rotation}}*124.2\text{acres}*\frac{1\text{rotation}}{360\text{deg}}*\frac{6\text{deg}}{30\text{min}}*\frac{1\text{min}}{60\text{s}}*\frac{453.6\text{g}}{1\text{lb}}*\frac{1}{10\text{m}*400\text{m}}*\frac{17g/molNH_3}{14g/molN}=9.5\text{E}-4\frac{\text{gNH}_3}{\text{m}^2\text{s}}$$

NH_3 application rate by sprinkler arm (400 m by 10 m) (18 deg hr^{-1} sprinkler arm rotation rate):

$$6\frac{\text{lbsN}}{\text{acre}*\text{rotation}}*124.2\text{acres}*\frac{1\text{rotation}}{360\text{deg}}*\frac{9\text{deg}}{30\text{min}}*\frac{1\text{min}}{60\text{s}}*\frac{453.6\text{g}}{1\text{lb}}*\frac{1}{10\text{m}*400\text{m}}*\frac{17g/molNH_3}{14g/molN}=14.25\text{E}-4\frac{\text{gNH}_3}{\text{m}^2\text{s}}$$

C.2 Additional NH_3 Concentrations Results

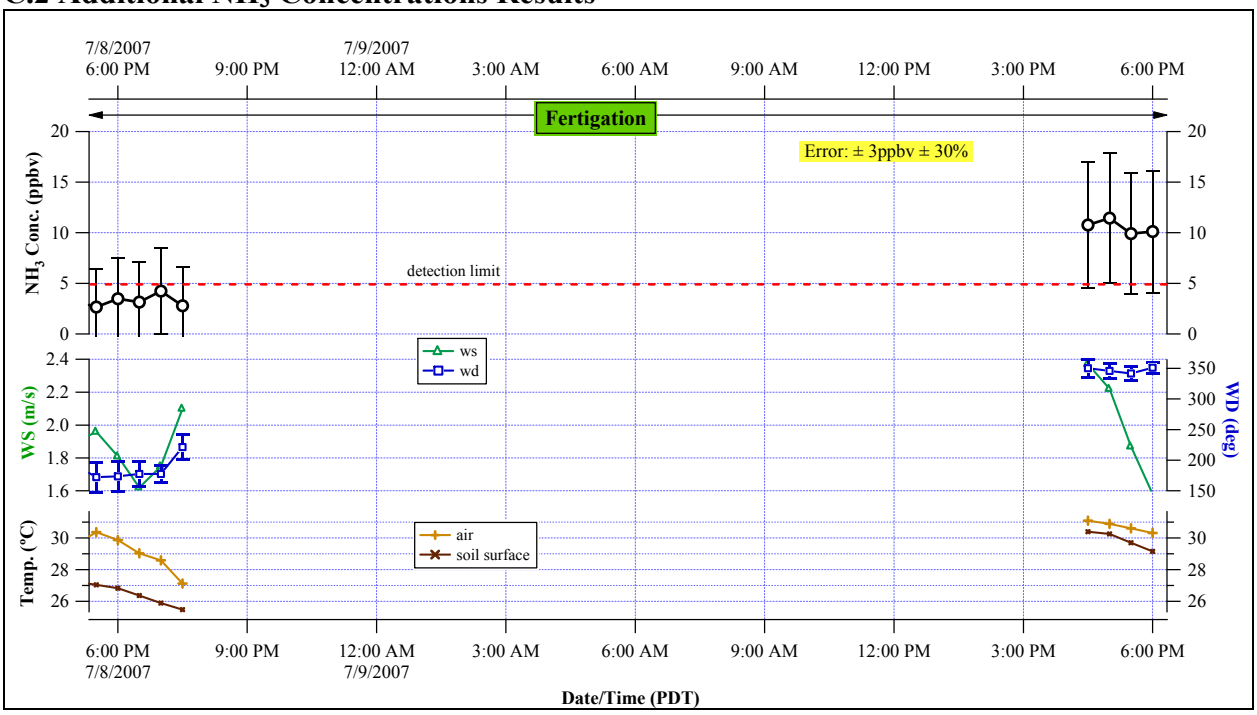

Figure C.1: Time series plot of measured 30-minute average NH_3 concentration, wind speed, wind direction, air temperature, and soil surface temperature from 5 pm on 07/08/07 to 6 pm on 07/09/07.

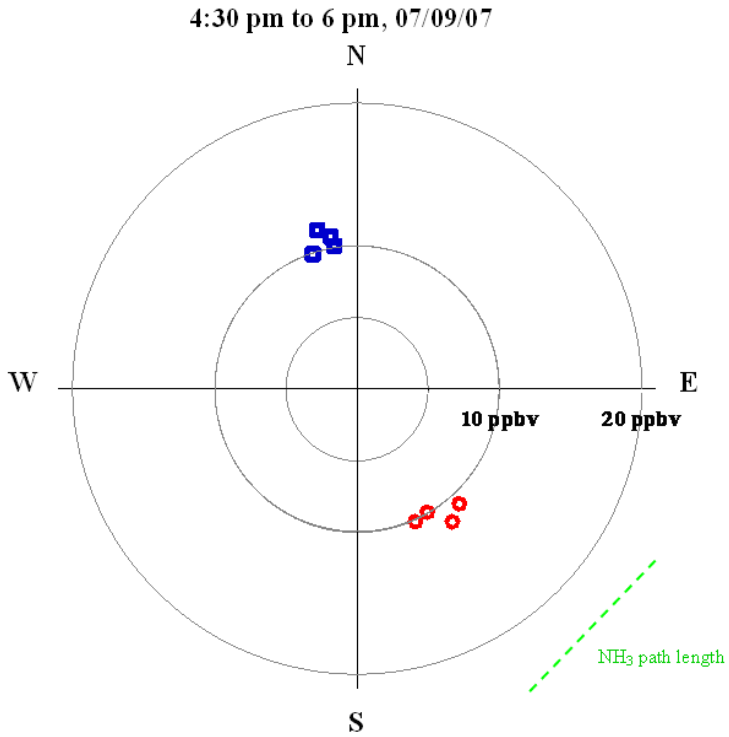

Figure C.2: Polar plot of NH_3 concentration versus sprinkler arm rotation angle (red circles) and wind direction (blue squares) for 4:30 pm to 6 pm 07/09/07 (PDT).

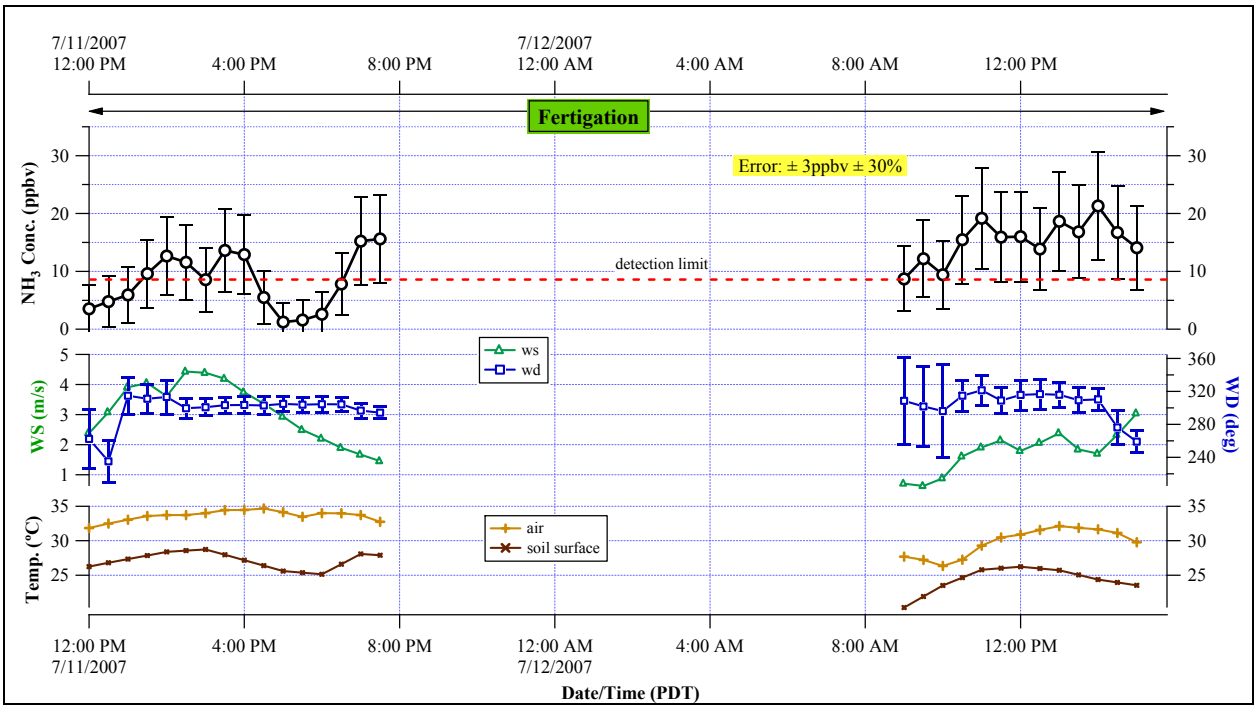

Figure C.3: Time series plot of measured 30-minute average NH_3 concentration, wind speed, wind direction, air temperature, and soil surface temperature from 11 am on 07/11/07 to 3 pm 07/12/07.

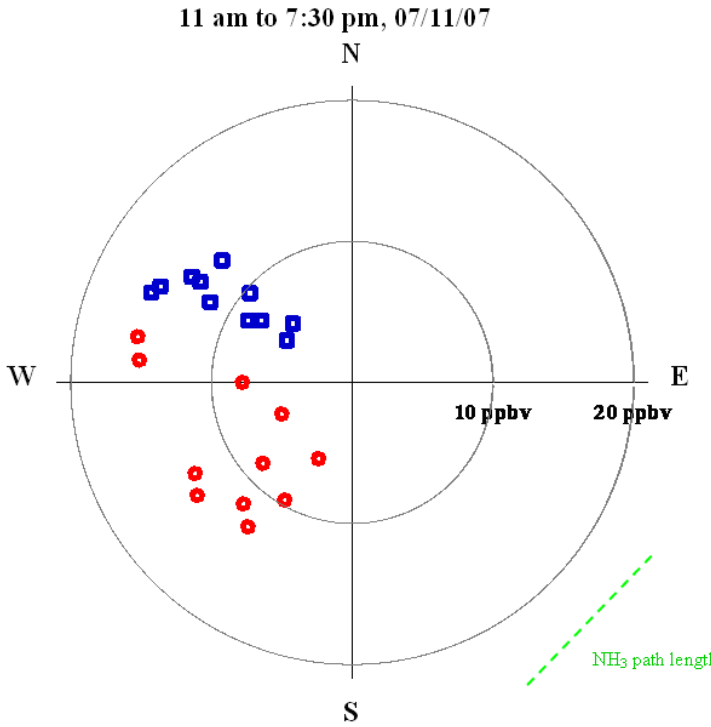

Figure C.4: Polar plot of NH_3 concentration versus sprinkler arm rotation angle (red circles) and wind direction (blue squares) for 11 am to 7:30 pm 07/11/07 (PDT).

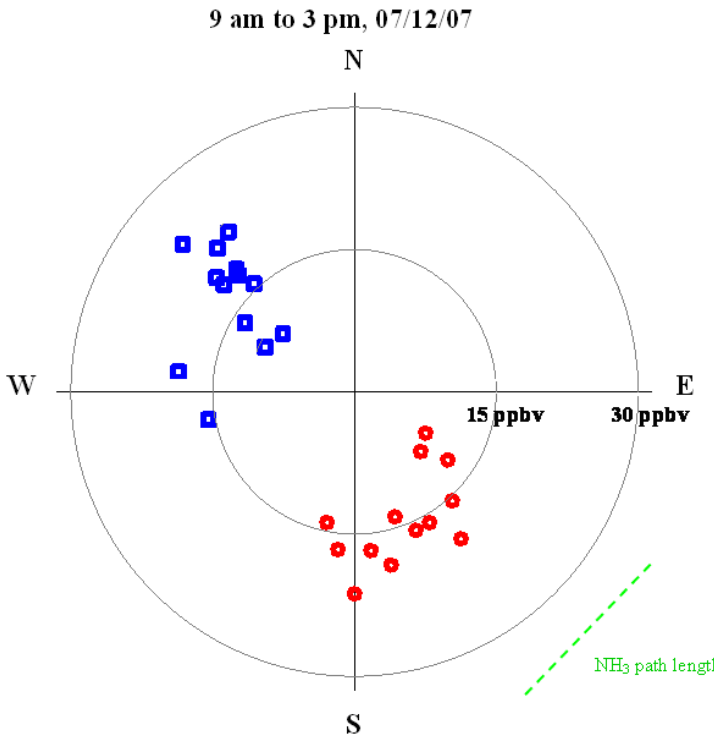

Figure C.5: Polar plot of NH_3 concentration versus sprinkler arm rotation angle (red circles) and wind direction (blue squares) for 9 am to 3 pm on 07/12/07 (PDT).

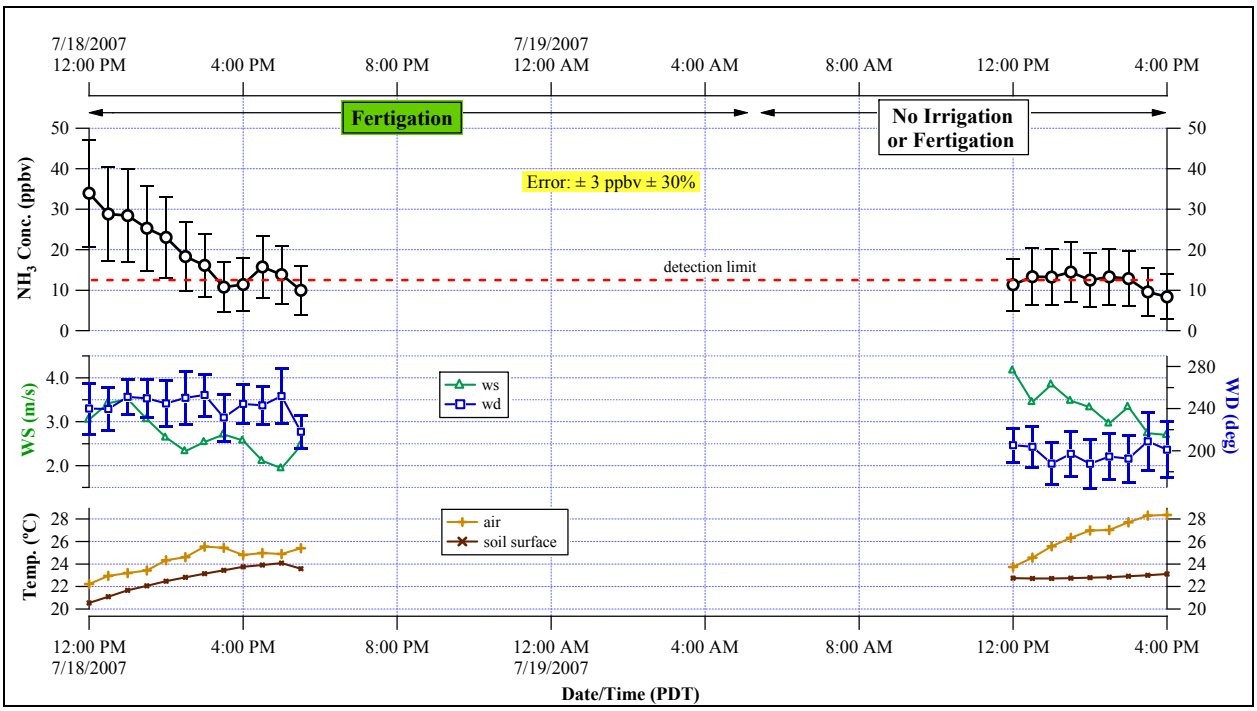

Figure C.6: Time series plot of measured 30-minute average NH_3 concentration, wind speed, wind direction, air temperature, and soil surface temperature from 12 pm on 07/18/07 to 4 pm on 07/19/07.

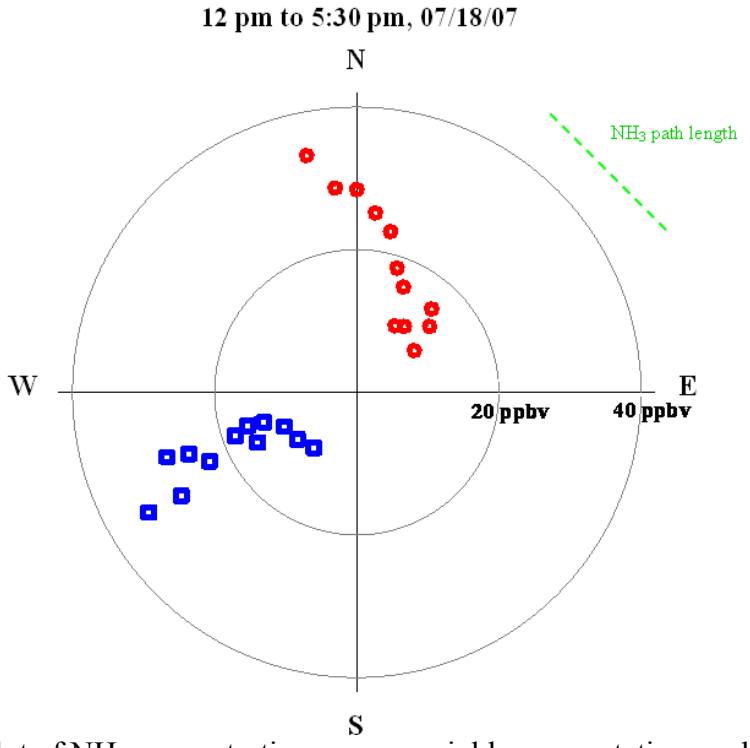

Figure C.7: Polar plot of NH_3 concentration versus sprinkler arm rotation angle (red circles) and wind direction (blue squares) for 12 pm to 5:30 pm on 07/18/07 (PDT).

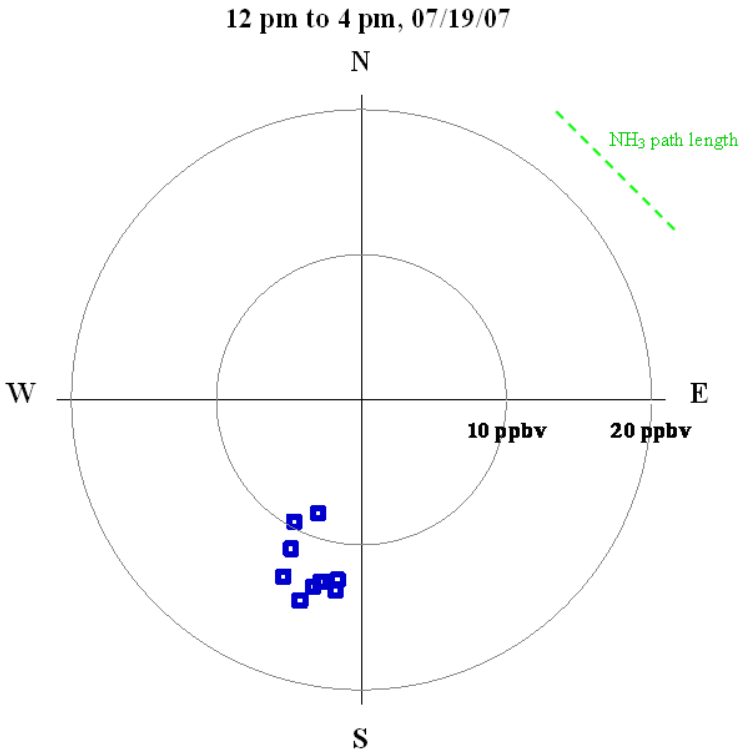

Figure C.8: Polar plot of NH_3 concentration versus sprinkler arm rotation angle (red circles) and wind direction (blue squares) for 12 pm to 4 pm on 07/19/07 (PDT).

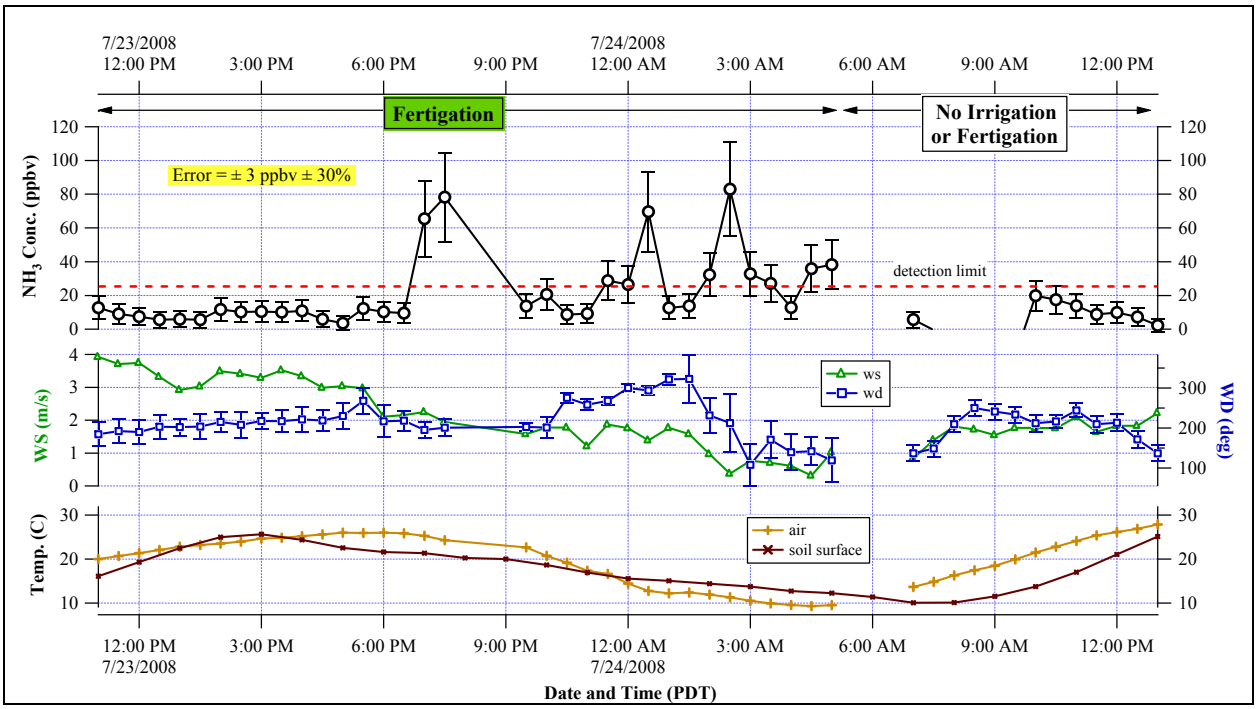

Figure C.9: Time series plot of measured 30-minute average NH_3 concentration, wind speed, wind direction, air temperature, and soil surface temperature from 11 am on 07/23/08 to 1 pm on 07/24/08.

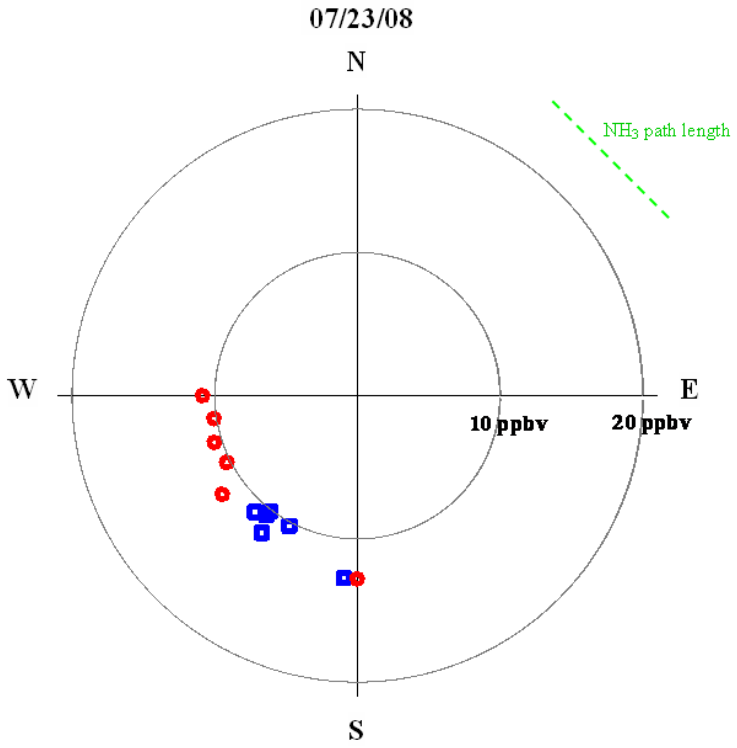

Figure C.10: Polar plot of NH_3 concentration versus sprinkler arm rotation angle (red circles) and wind direction (blue squares) for 11 am to 4 pm on 07/23/08 (PDT).

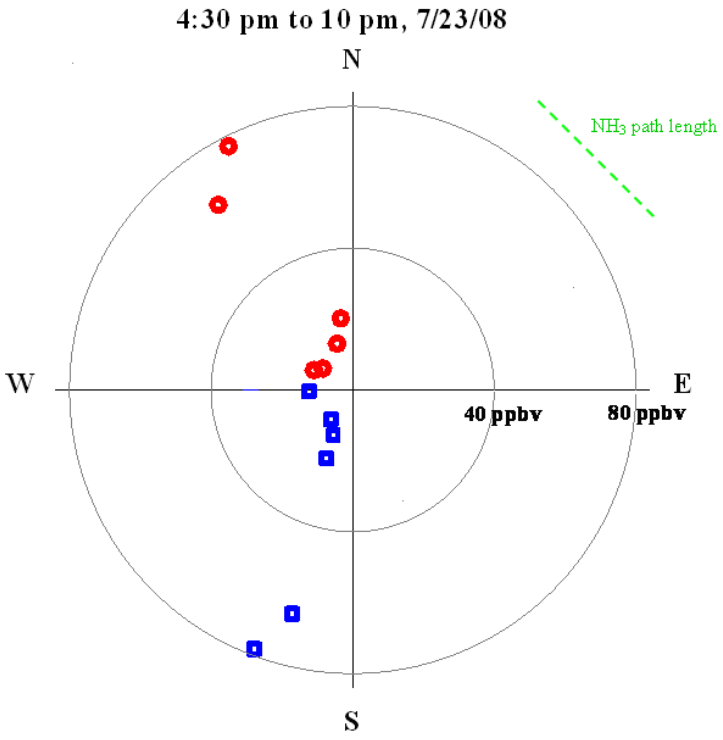

Figure C.11: Polar plot of NH_3 concentration versus sprinkler arm rotation angle (red circles) and wind direction (blue squares) for 4:30 pm to 11:30 pm on 07/23/08 (PDT).

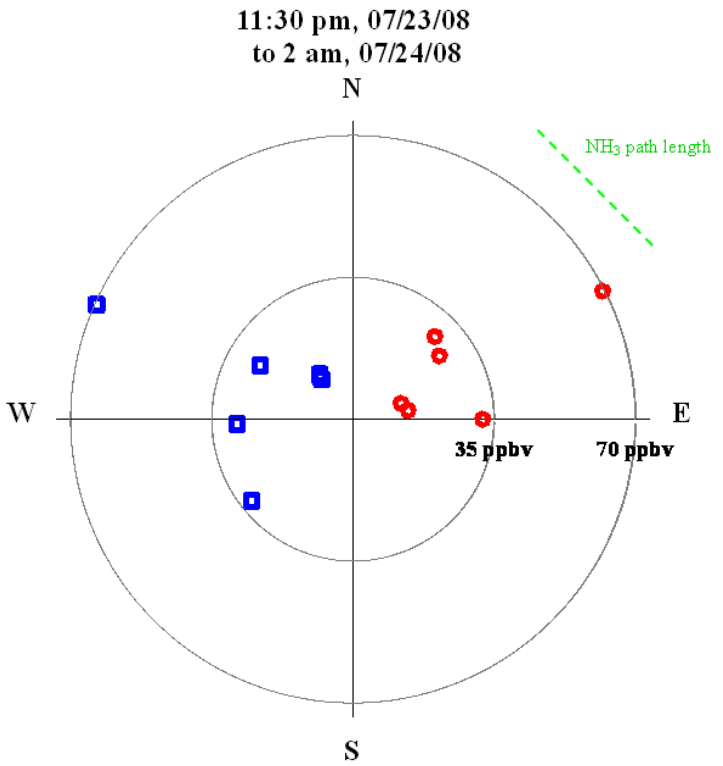

Figure C.12: Polar plot of NH_3 concentration versus sprinkler arm rotation angle (red circles) and wind direction (blue squares) for 11:30 pm on 7/23/08 to 2 am on 07/24/08 (PDT).

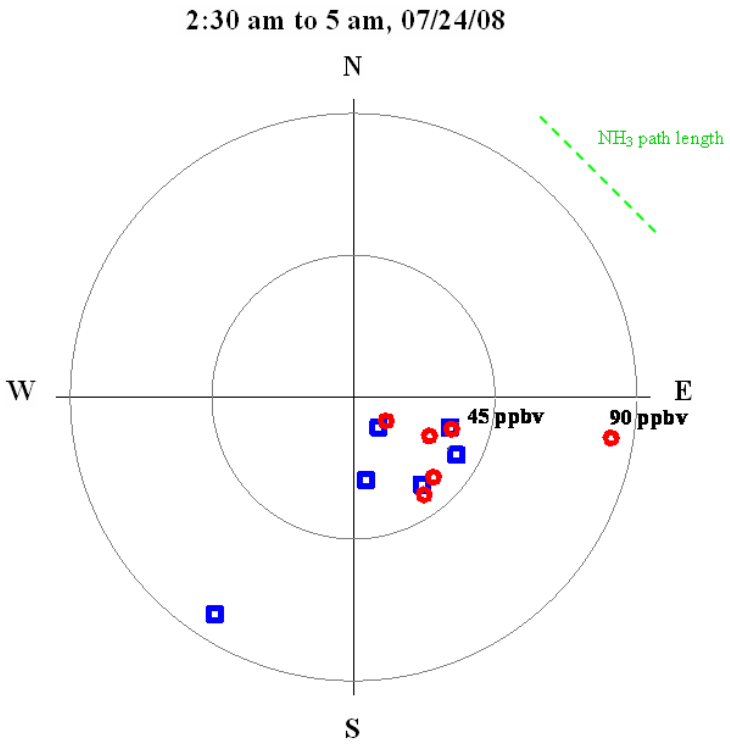

Figure C.13: Polar plot of NH_3 concentration versus sprinkler arm rotation angle (red circles) and wind direction (blue squares) for 2:30 am to 5 am on 07/24/08 (PDT).

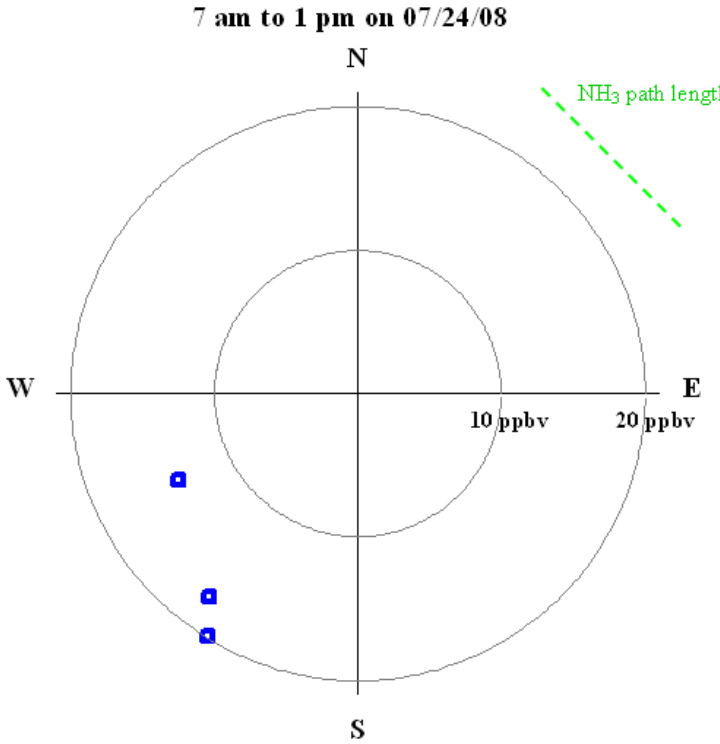

Figure C.14: Polar plot of NH_3 concentration versus sprinkler arm rotation angle (red circles) and wind direction (blue squares) for 7 am to 1 pm on 07/24/08 (PDT).

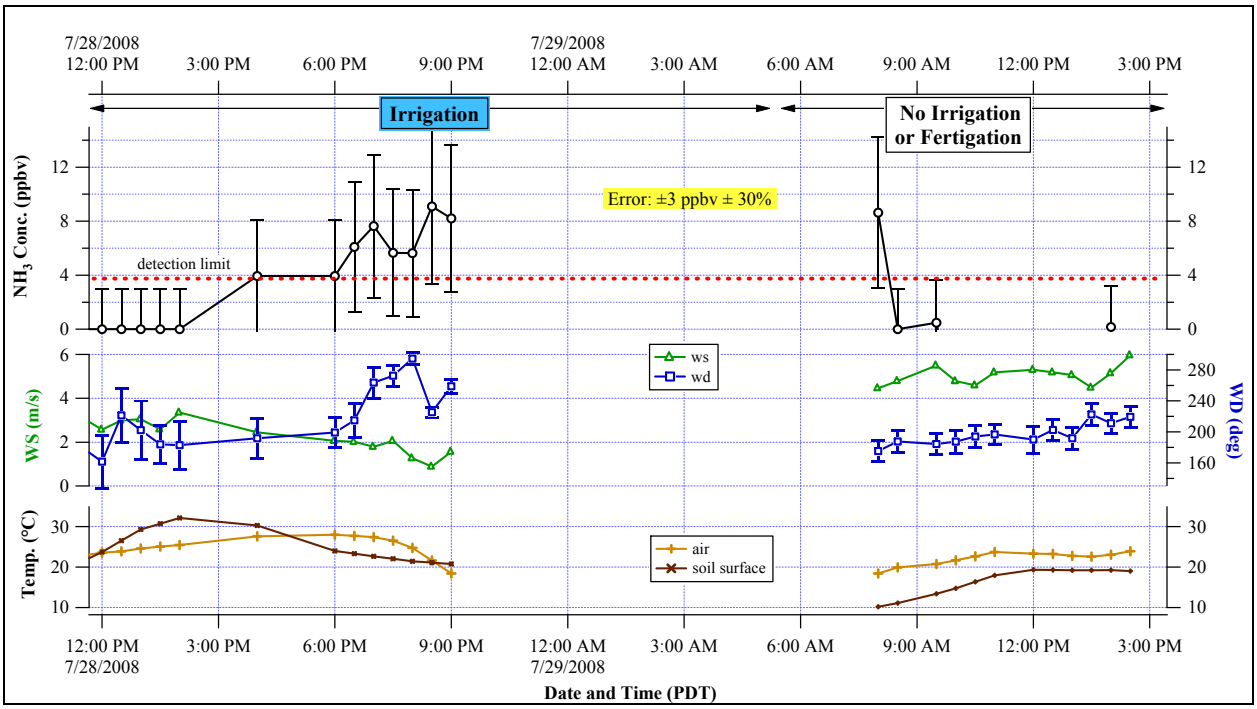

Figure C.15: Time series plot of measured 30-minute average NH_3 concentration, wind speed, wind direction, air temperature, and soil surface temperature from 10 am on 07/28/08 to 2:30 pm on 07/29/08.

C.3 Additional NH_3 Flux Rates Results

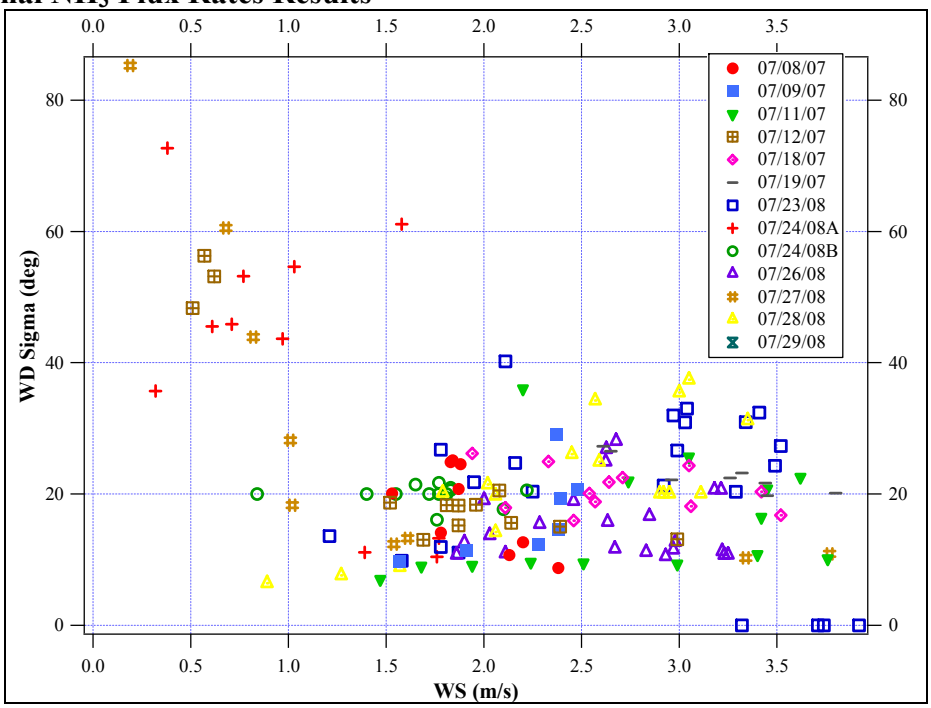

Figure C.16: Wind speed vs. wind direction sigma (given in 30-min averages) for all days of NH_3 measurement. Low wind speeds are associated with large variation in wind direction. Periods with large variation in wind direction (greater than 30 deg) and low wind speeds (less than 1 m s^{-1}) should not be included in determining NH_3 flux rates since the theoretical basis of the Gaussian plume dispersion model becomes invalid.

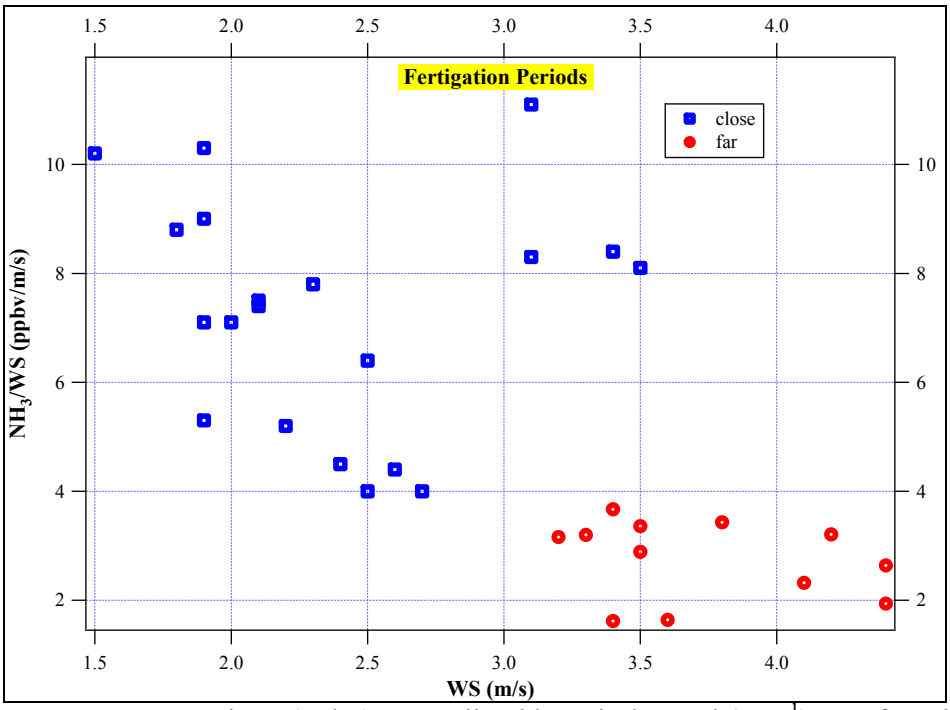

Figure C.17: NH_3 concentrations (ppbv) normalized by wind speed (m s^{-1}) as a function of wind speed (m s^{-1}).

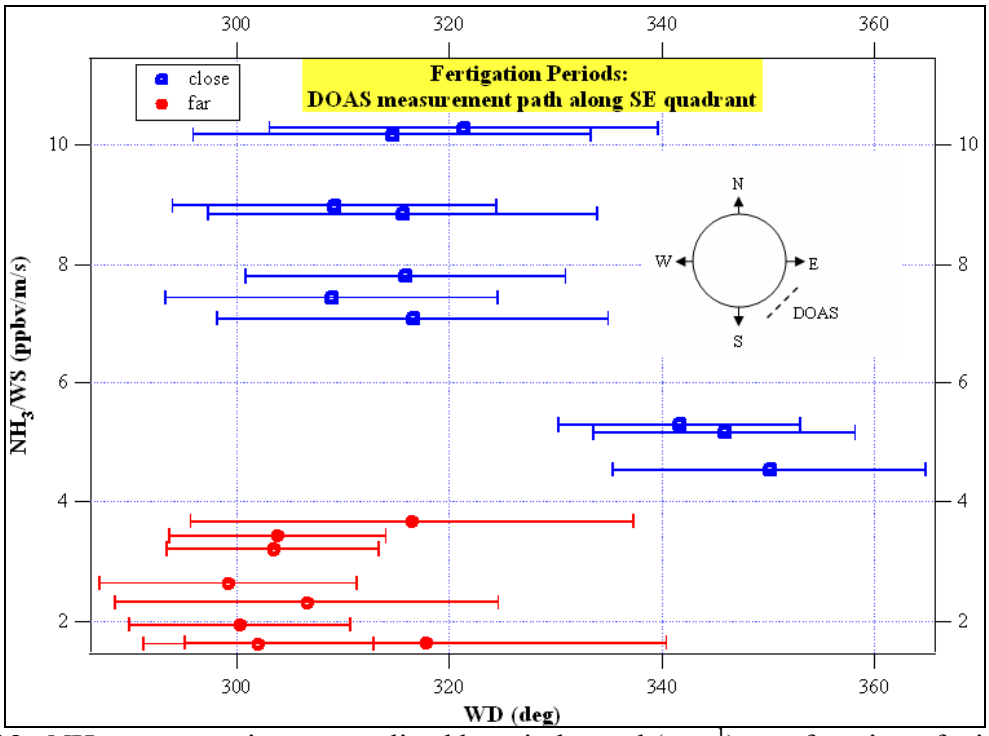

Figure C.18: NH_3 concentrations normalized by wind speed (m s^{-1}) as a function of wind direction (deg) for fertigation periods when the DOAS measurement path was in the SE quadrant of the potato fields

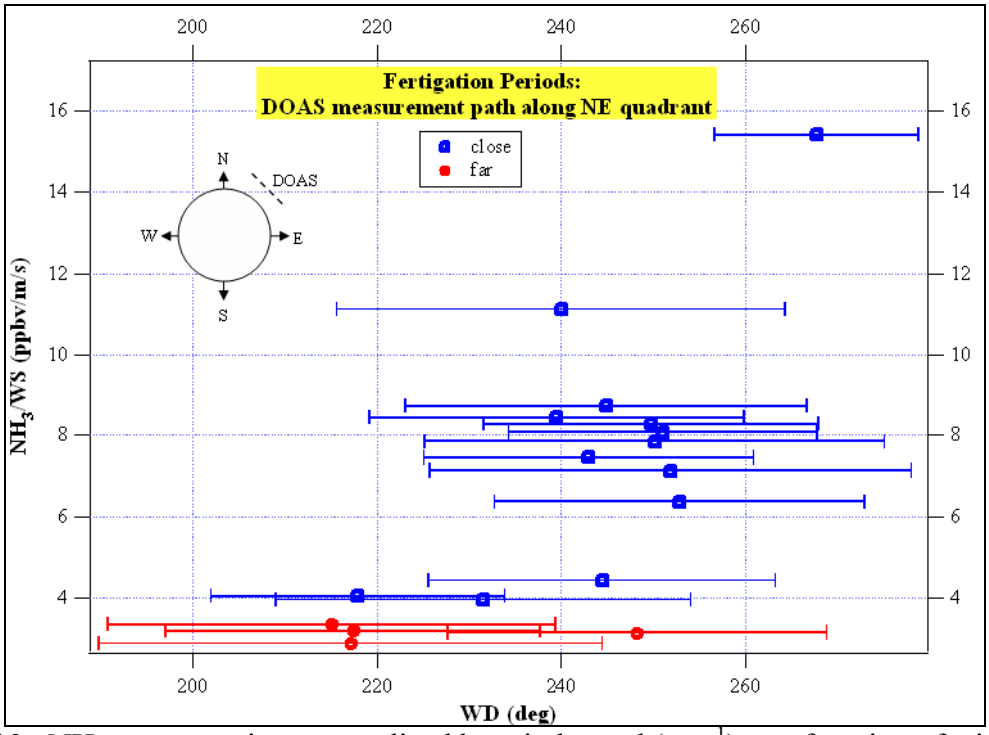

Figure C.19: NH_3 concentrations normalized by wind speed (m s^{-1}) as a function of wind direction (deg) for fertigation periods when the DOAS measurement path was in the NE quadrant of the potato fields.

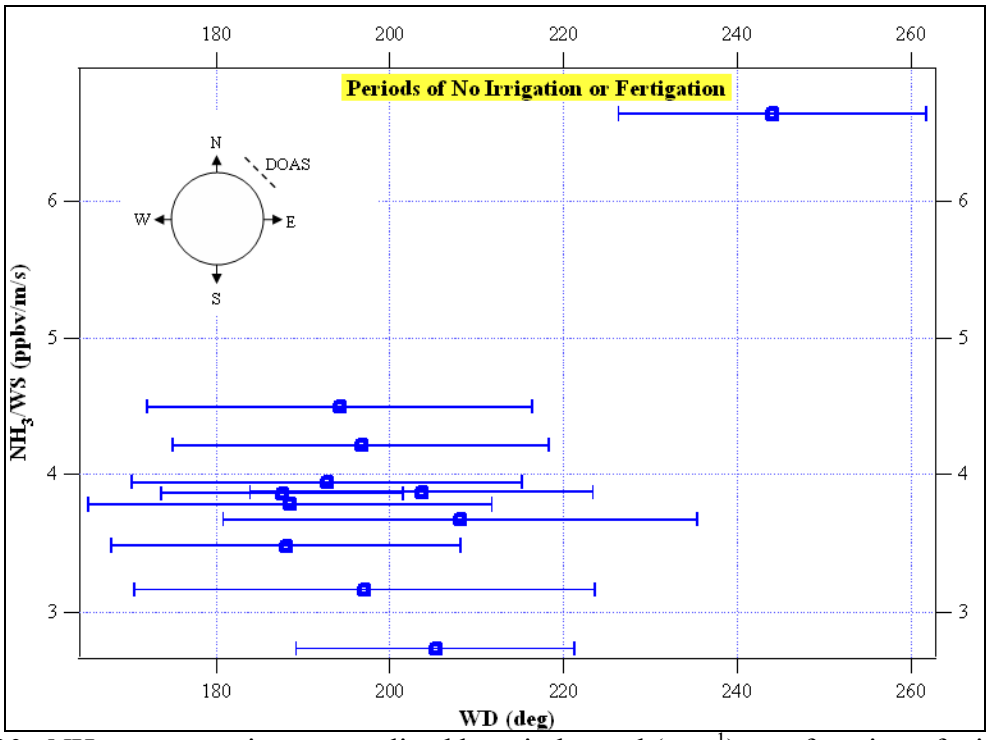

Figure C.20: NH_3 concentrations normalized by wind speed (m s^{-1}) as a function of wind direction (deg) for periods of no irrigation or fertigation.

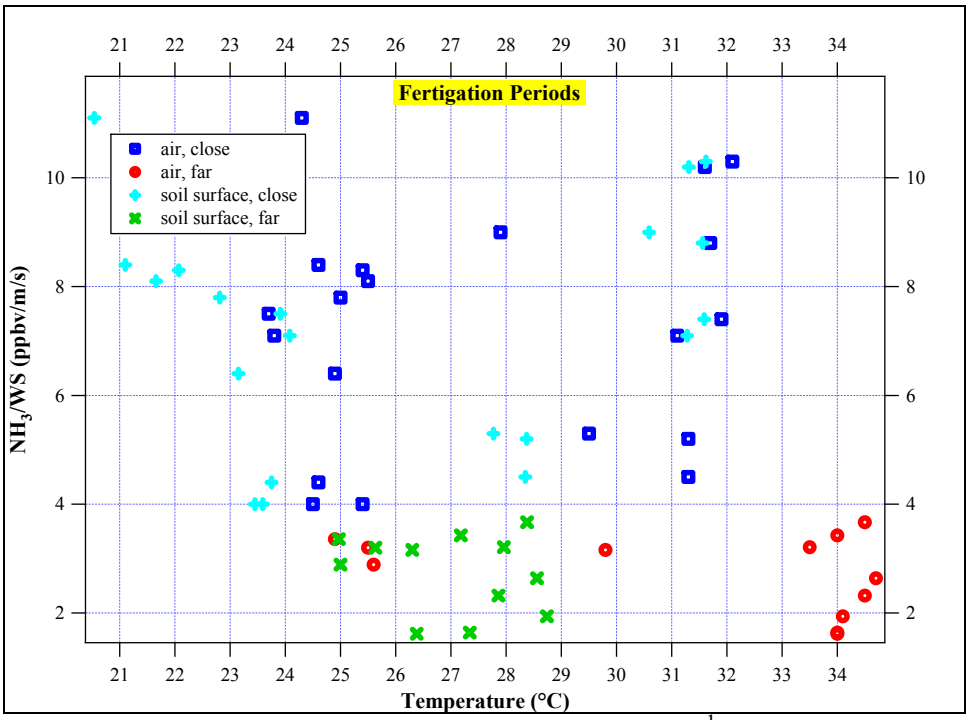

Figure C.21: NH_3 concentrations normalized by wind speed (m s^{-1}) as a function of soil surface and air temperature (°C) for fertigation periods.

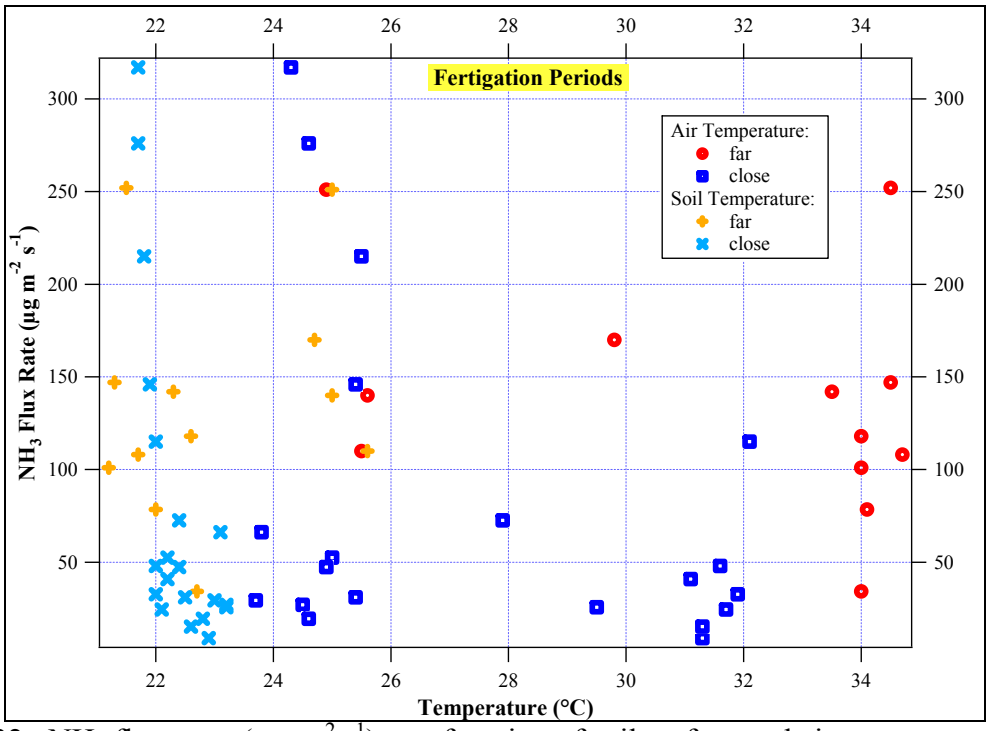

Figure C.22: NH_3 flux rates (µg $m^{-2}s^{-1}$) as a function of soil surface and air temperature (°C) for fertigation periods.

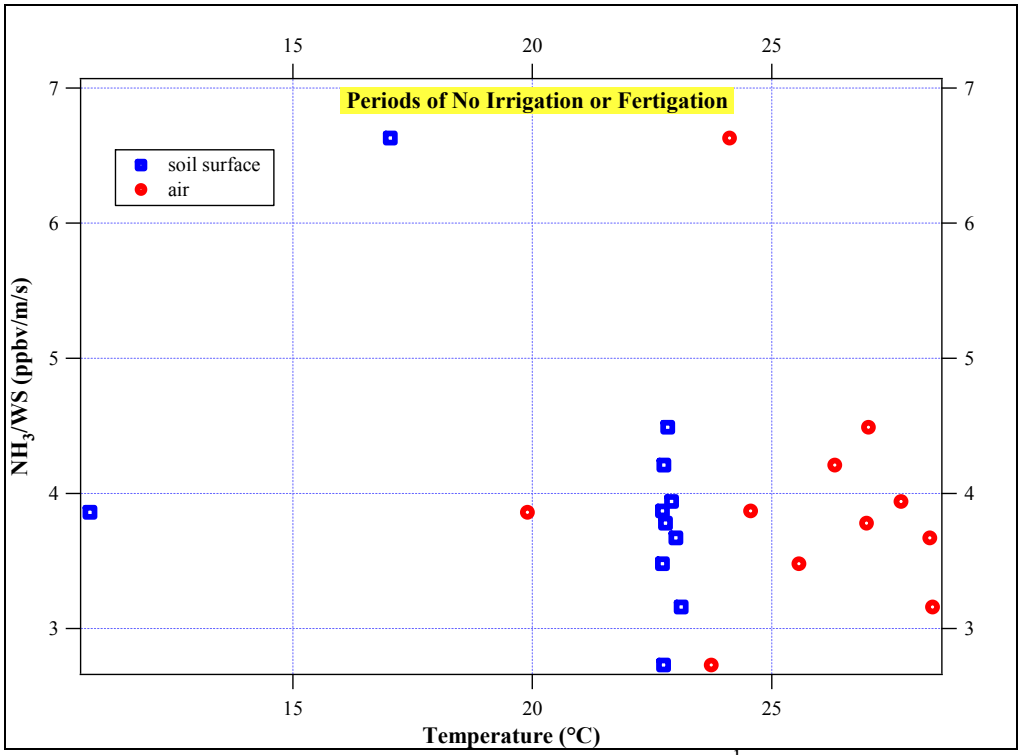

Figure C.23: NH_3 concentrations normalized by wind speed (m s^{-1}) as a function of soil surface and air temperature (°C) for periods of no irrigation or fertigation.

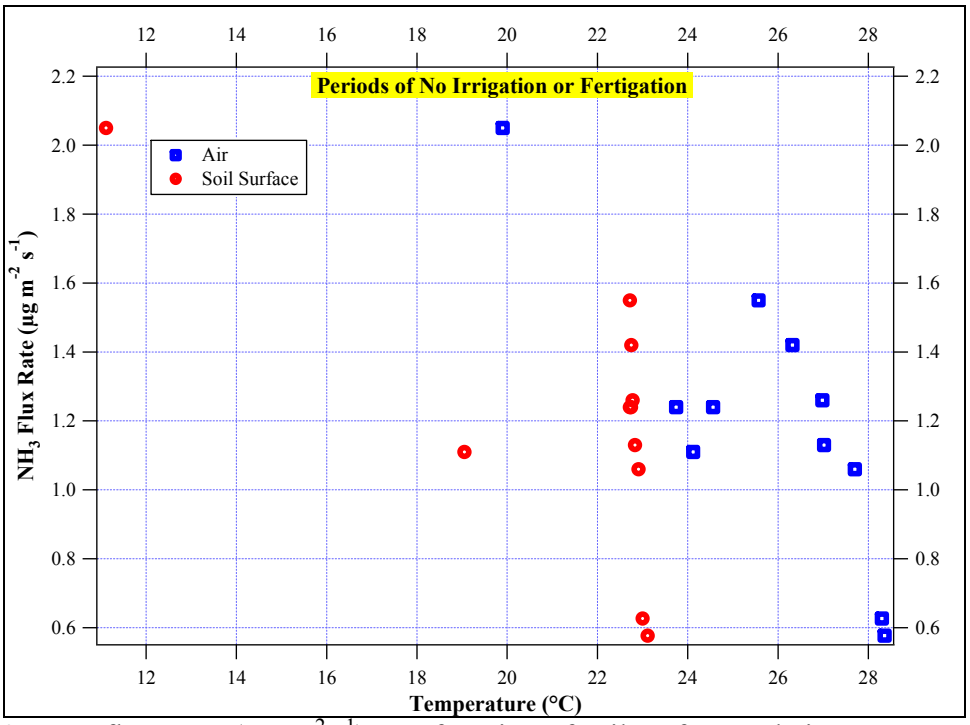

Figure C.24: NH_3 flux rates (µg $m^{-2}s^{-1}$) as a function of soil surface and air temperature (°C) for periods of no irrigation or fertigation.

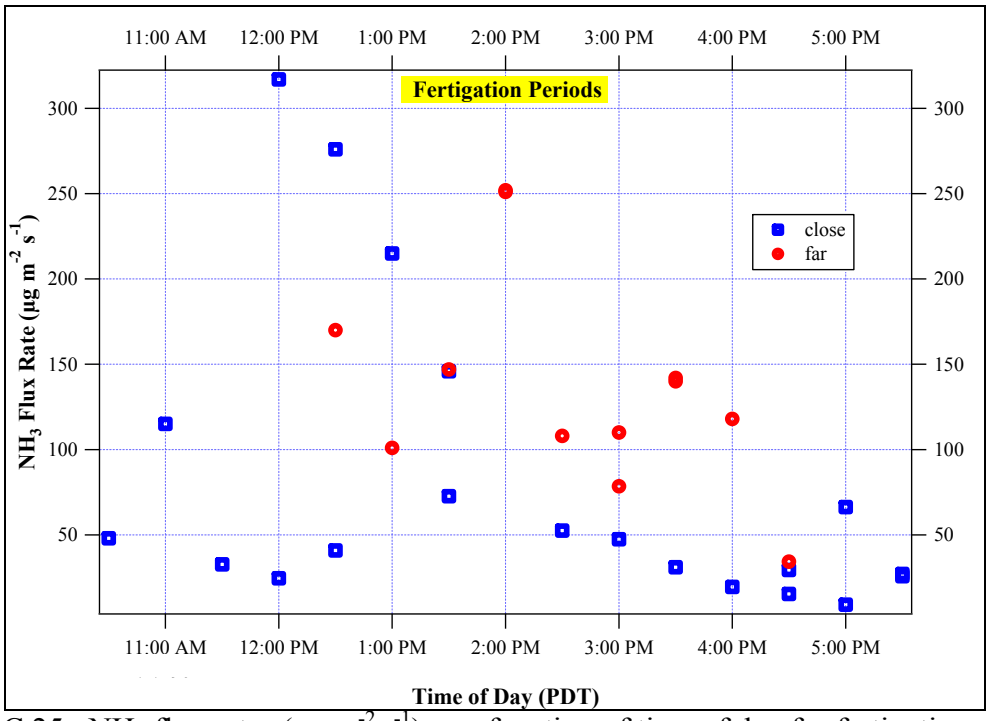

Figure C.25: NH_3 flux rates (µg m^{-2} s^{-1}) as a function of time of day for fertigation periods.

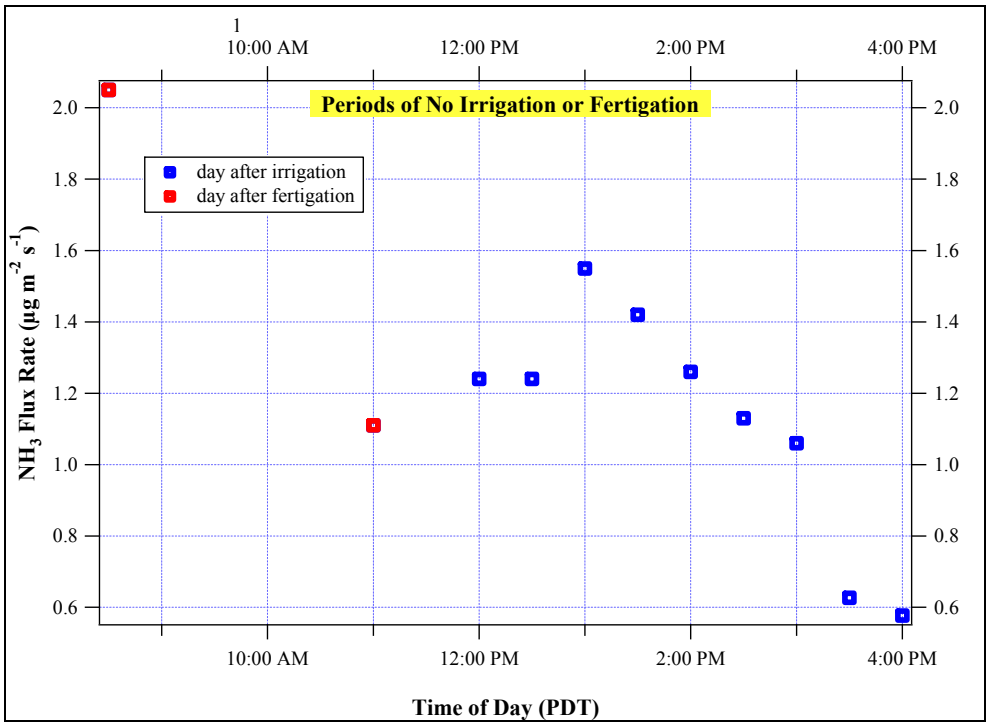

Figure C.26: Temperature (°C) as a function of time of day (PDT) for periods of no irrigation or fertigation

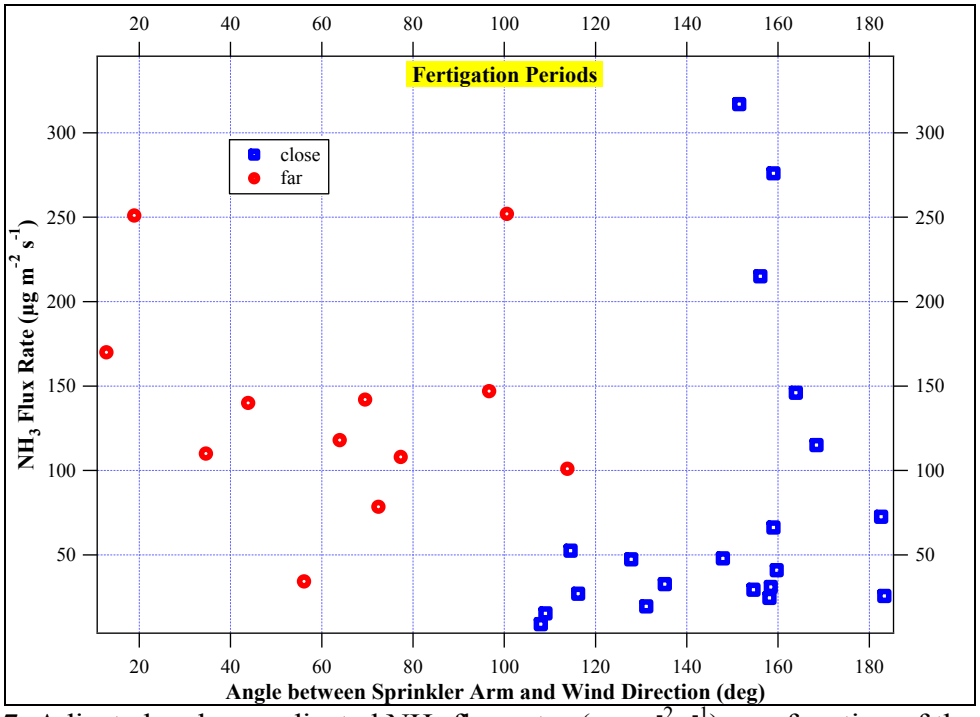

Figure C.27: Adjusted and non-adjusted NH_3 flux rates (µg m^{-2} s^{-1}) as a function of the angle between the sprinkler arm and wind direction (deg).

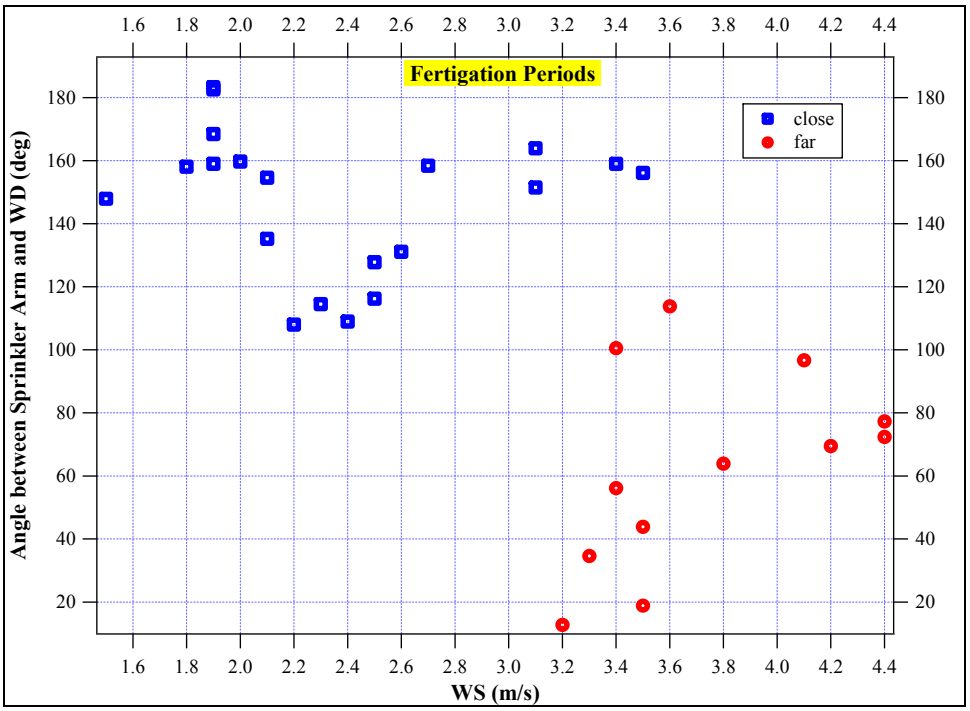

Figure C.28: Angle between sprinkler arm and wind direction (deg) as a function of wind speed (m s^{-1}).